Dissertation

RAdar Multi-Sensor (RAMS) Quantitative Precipitation Estimation (QPE)

Submitted by

Delbert Darrell Willie

Department of Electrical and Computer Engineering

In partial fulfillment of the requirements

For the Degree of Doctor of Philosophy

Colorado State University

Fort Collins, Colorado

Summer 2015

Doctoral Committee:

Advisor: V. Chandrasekar

Paul Mielke
Anura P. Jayasumana
Branislav Notaros

Abstract

RAdar Multi-Sensor (RAMS) Quantitative Precipitation Estimation (QPE)

Quantitative precipitation estimation (QPE) continues to be one of the principal objectives for weather researchers and forecasters. The ability of radar to measure over broad spatial areas in short temporal successions encourages its application in the pursuit of accurate rainfall estimation, where radar reflectivity-rainfall (Z-R) relations have been traditionally used to derive quantitative precipitation estimation. The purpose of this research is to present the development of a regional dual polarization QPE process known as the **RA**dar **M**ulti-**S**ensor QPE (RAMS QPE). This scheme applies the dual polarization radar rain rate estimation algorithms developed at Colorado State University into an adaptable QPE system. The methodologies used to combine individual radar scans, and then merge them into a mosaic are described. The implementation and evaluation is performed over a domain that occurs over a complex terrain environment, such that local radar coverage is compromised by blockage. This area of interest is concentrated around the Pigeon River Basin near Asheville, NC. In this mountainous locale, beam blockage, beam overshooting, orographic enhancement, and the unique climactic conditions complicate the development of reliable QPE's from radar. The QPE precipitation fields evaluated in this analysis will stem from the dual polarization radar data obtained from the local NWS WSR-88DP radars as well as the NASA NPOL research radar.

Acknowledgements

First of all, I would like to acknowledge Dr. Chandrasekar for advising me throughout this work, and Dr. Robert Cifelli at NOAA for providing insight into the challenges associated with obtaining QPE in complex environments. The contributions and assistance from the Radar Group at CSU as will as the co-workers at NOAA in which this work would not be possible. Furthermore, I want to acknowledge my committee: Dr. Notaros, Dr. Jayasumana, and Dr. Mielke. And last but not least, my wife for supporting me throughout this entire process.

Table of Contents

List of Tables

List of Figures

CHAPTER 1

Introduction

The estimation of rainfall rate and accumulation is an essential application of weather sensing radars (Bringi and Chandrasekar 2001; Cifelli and Chandrasekar 2013). The establishment of quantitative precipitation estimation (QPE) continues to be one of the primary purposes for weather researchers, where radar has the ability to measure wide spatial areas in short time periods, and therefore it is highly desirable to implement this into the pursuit of accurate rainfall estimation. However, the radar's physical scanning ability must be comprehended, so as to realize it limitations and how it is affected by factors such as beam width widening at far range, scanning elevation heights, and range resolution. Operating in flat unobstructed topography, radars can observe precipitation and measure QPE very effectively. In effort to obtain reliable QPE, the best choice is to be able scan as close to the ground and as frequently as possible. In complex terrain that encompasses high mountains and valleys, this ability becomes even more challenging. In regards to measuring QPE, traditionally radar has relied upon reflectivity measurements to determine rainfall amount. Due to variations in climate and rainfall microphysics, the use of reflectivity sometimes requires well researched reflectivity-rainfall rate (Z-R) relations to better relate to ground measurements. The accuracy of rain rate estimates is also dependent upon other factors that affect reflectivity measurements, such as radar calibration, ground clutter, vertical profile of reflectivity (VPR), signal attenuation, beam blockages, bright bands and anomalous propagation, etc. (Kitchen et al. 1994; Fulton et al. 1998; Kitzmiller et al. 2011). The National Weather Service (NWS) maintains a network or radars referred to as the Next Generation Weather Radar (NEXRAD), which are comprised of S-band Weather Surveillance Radars

with Doppler capability and was introduced in 1988 (WSR-88D). Depending upon the region of interest for QPE, the NWS NEXRAD coverage over certain areas is not possible (Maddox et al. 2002). Where in certain locales, it can be advantageous to employ existing gap-filling non-NEXRAD radars for the purposes of improving quantitative precipitation estimation in areas of poor radar coverage.

When single radar coverage is compromised due to beam blockage, it is advantageous to seek the use of multiple radars in determining QPE, since overlapping scanning regions may permit at least one radar to have a unobstructed low level elevation scanning view, especially in areas that contain complex terrain. A multi-radar QPE system has several advantages over single radar, where some of the characteristics are listed:

- Better estimates of rainfall rate versus single radar
- Provide quantitative precipitation estimation (QPE) using the best rainfall estimation equations
- Able to ingest both NEXRAD and Non-NEXRAD radars
- Operate in both real-time or retroactive mode
- Provide QPE coverage over various domains including complex terrain
- Adaptable to a multi-sensor system with ability to ingest data from gauges, satellite and other sensors

Quantitative precipitation estimation from radar is a continuously evolving science, which is dependent uon the current state-of-the-art weather measurement radar technology. Since the introduction of dual polarization weather sensing radar measurements (Seliga and Bringi 1976) provides additional capacities that can be used to further improve estimates of rainfall rate and accumulation versus traditional reflectivity methods, which is discussed in detail in Bringi and Chandrasekar (2001). Therefore the objective of this work is to discuss the

development of a multi-radar QPE system that is geared toward regional application and draws upon dual polarization rain rate relations. This QPE system will be referred to as the RAdar Multi-Sensor QPE (RAMS QPE) that integrates these abilities into more accurate rainfall amounts. The design of the RAM QPE system will have many similarities to other QPE systems. However it is unique in the sense that it is built exclusively upon dual polarimetric algorithms, and that its domain is optimized to operate on a regional scale. The architecture and the implementation methodology are presented. The evaluation is performed within a domain defined over a region that includes complex terrain with poor NEXRAD radar coverage and where the relative performance of QPE is hindered. This region resides in an area encompassing and surrounding the Pigeon River basin located in North Carolina near Asheville, NC and which is located within the Southern Appalachian Mountains.

1.1. Problem Statement

In generating QPE, the use of radar reflectivity is still prevalent in the pursuit of rainfall estimation and has been the case since the introduction of radar for weather applications. The achievement of accurate measurements is dependent upon an unobstructed view of rainfall, which is determined by the position of the radar and the location of mountains or blockage more generally. For QPE in complex terrain, it is nearly impossible for single scanning radar to make low level measurements over these areas when there are issues of partial to complete beam blockage. The National Severe Storms Laboratories (NSSL) in Norman, OK has established a multi-radar QPE system package that combines the existing

NEXRAD WSR-88D radar measurements along with gauge measurements to create a multi-sensor approach to rainfall estimation. This QPE system is called the Multi-Radar Multi-Sensor (MRMS) system (Zhang et al. 2011), and is summarized below:

- Reflectivity based QPE system (currently upgrading to dual-polarization QPE)
- Designed to cover the entire continental U.S
- Radar reflectivity requires much clutter filtering
- Scans above the melting layer require reflectivity correction
- Developed to work with NEXRAD
- Integrates gauge, satellite and other sensors into QPE

The WSR-88D radars are positioned to scan the entire continental U.S. and have a range up to 300 km, where if placed on a map would appear to give near complete coverage as shown in Figure 1.1. The reality is that the effectiveness of the radar beams passing through rain decreases with increasing distance from the radar. This is attributed to the increasing height of the beam, the curvature of the earth, and the increasing beam width at far ranges. The more distant a storm event occurs from the radar, the higher above the ground and into the cloud tops the radar tends to scan. This leads to adjusting rainfall-reflectivity (Z-R) relations or applying corrections to account for measurements at higher altitudes that contain ice or melting ice. Storms are dynamic and evolve in structure and intensity and this also has to be taken into account to try and give the best estimation based upon reflectivity. Given the multitude of variables that make QPE difficult at far ranges and high altitudes, the presence of mountains demands that radars scan at higher elevations to avoid blockage, which in turn means that algorithms need to be intelligent to decipher rainfall amounts from these high altitude measurements. Furthermore, the climate in mountainous regions

is much different than flat land areas; therefore in order to effectively measure rainfall, the methodologies used to quantify rain needs to be further investigated for these regimes.

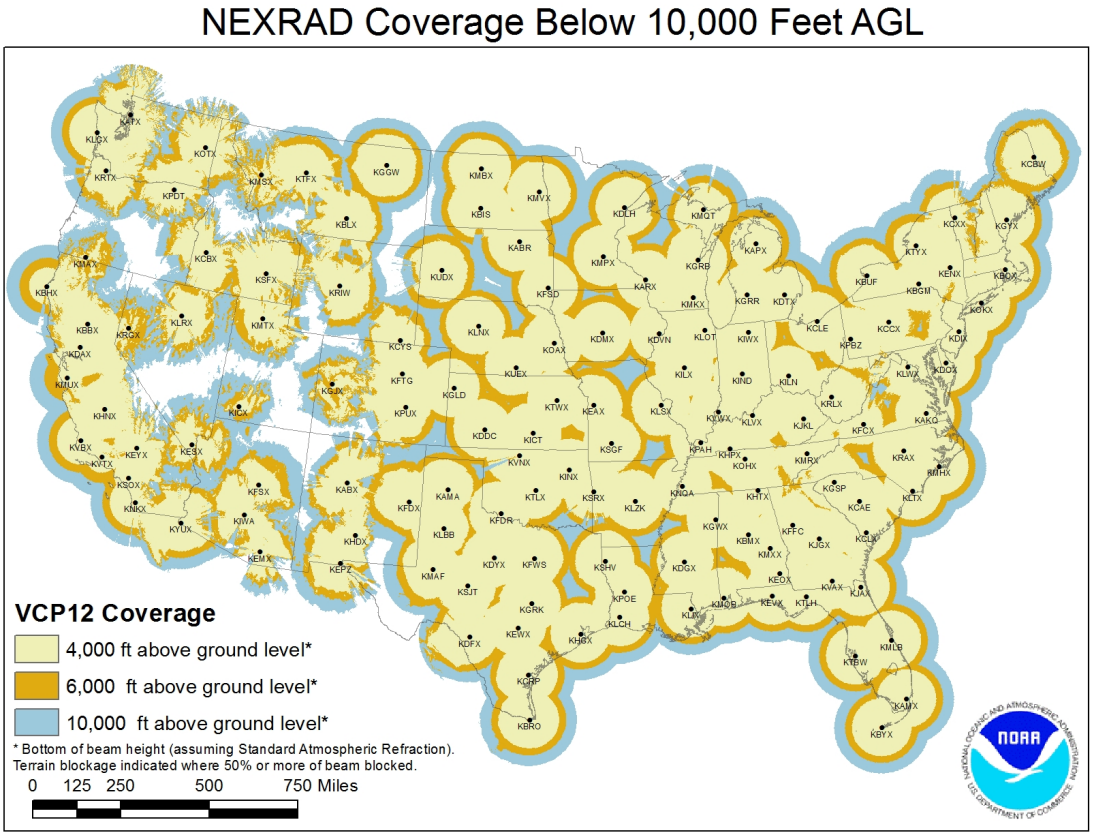

FIGURE 1.1. NEXRAD radar coverage over the continental US indicating the unblocked scan heights up to 10,000 ft above ground level.

1.2. Objective of the Research

This research aims to develop a RAdar Multi-Sensor QPE (RAMS QPE) methodology based upon dual polarization measurements from scanning radars for regional application. To begin with, it is necessary to evaluate the performance of the existing Multi-Radar Multi-Sensor (MRMS also known as NMQ) QPE algorithm package (Zhang et al. 2011) within a complex terrain area in order to assess the effectiveness of this system in this type of region. This is important, since the development of the techniques used to derive the MRMS QPE

system was primarily derived from an environment in which the radar scanning operations are performed over an unobstructed flat surface of land, and it is helpful to asses the performance of the MRMS QPE system within a mountainous locale. In this type of environment, radar measurements needed to quantify rainfall are difficult to impossible to obtain, since there is blockage and the ability to scan over particular areas requires higher radar elevation scanning. Further the structure and development of storms is very different in mountainous terrain as opposed to that seen over flat land, and storms also differ from region to region, where the presence of mountains or high elevation alters storm evolution and the behavior of precipitation. Therefore the NSSL MRMS is assessed over the Russian River basin north of San Francisco, CA, which is situated within the National Oceanic and Atmospheric Administration (NOAA) Hydrometeorology Testbed (HMT) West. In this coastal mountainous environment, the challenge of obtaining reliable QPE's is deterred by blockage and beam overshooting (Maddox et al. 2002), as well as orographic enhancement (Kitchen et al. 1994). In this evaluation, the effectiveness of several local radars, which include four National Weather Service WSR-88D radars and a gap filling C-band TV station radar, are considered in deriving QPE over this region.

Although a significant amount of research and development has gone into producing the MRMS QPE algorithms used to estimate accurate rainfall radar measurements. This system was initally built upon reflectivity measurements and the implementation of several reflectivity-rain rate (Z-R) relationships used to calculate rainfall amounts. The reliance on reflectivity for this system is a reflection of the evolution of radar technology, where reflectivity is fundamentally the echo from targets seen by the radar. Currently MRMS is in the process of implementing and evaluating dual polarization QPE methods into its operational version.

As radars have advanced, the concept of dual polarized radar created additional ability to measure precipitation, where the electromagnetic waves are orthogonal to each other and are transmitted essentially at the same time. This scheme created the capability to measure differences between the two waves as it propagated through hydrometeors. Given the complexities associated with the use of reflectivity in the generation of rainfall estimation. A new QPE system referred to as the RAMS QPE will be established that operates equivalently to the NSSL MRMS QPE, such that MRMS system relies upon the default NEXRAD dual polarimetric techniques. The RAMS QPE system also employs dual polarimetric QPE algorithms which are more robust and tunable to specific regional domains. The RAMS QPE will also have the ability to consider input from the surrounding NEXRAD radars as well as other radar types such as NASA NPOL radar and NASA D3R radar, which may operate at attenuating frequencies. This RAMS QPE will look to integrate the dual polarization algorithms developed by Colorado State University into its rainfall estimation and is summarized as follows:

- Dual polarization based QPE system
- A multi-radar QPE system that operates an a regional scale
- Adaptable to complex terrain environments
- Ingest of NEXRAD and other radar networks
- Planned ability to incorporate gauge, and other sensor data

The evaluation of the RAMS QPE will be done in conjunction with the MRMS QPE system in area referred to as NOAA HMT Southeast. This is another testbed established that encompasses complex terrain. Specifically this domain is defined over a region that includes the Pigeon River basin and Catawba River basin located in North Carolina near Ashville, NC. This area was selected, since it coincided with the Integrated Precipitation and

Hydrology Experiment (IPHEx) Ground Validation Field Campaign (GVFG) centered in the Southern Appalachians and spanning into the Piedmont and Coastal Plain regions of North Carolina, where the primary purpose is to provide intensive ground based measurements for purpose of validating the National Aeronautics and Space Administration (NASA) Global Precipitation Measurement (GPM) satellite. The partnership with other agencies in this mission aims to share efforts in recording and collaborate research efforts using data. In order to equivalently evaluate the QPE systems in this region, both the MRMS and RAMS systems will be modified to generate QPE over these mountainous areas using only the surrounding NEXRAD(s).

1.3. Dissertation Outline

The organization of this proposal follows as:

Chapter 2

An overview of the challenges in determining QPE from radar based measurements from the perspective of radar operation and the challenges associated with complex terrain. In respect to the radar operational characteristics, the problems of beam widening and height of the beam at far distance from the radar make QPE unreliable at far range. QPE is also problematic in areas of complex terrain where mountains create beam blockage and the environment in these areas have orographic enhancement, which complicates precipitation estimation.

The operational aspects of the MRMS system are briefly introduced such as to illustrate the aspects that affect the methodology in how QPE is derived from the various data inputs. These are mosaicking of the radar data from multiple radar input as well as the use of VPR correction to handle the effects of bright band on reflectivity measurements.

Chapter 3

This section gives the details within MRMS in terms of the methodologies used in the generation of reflectivity-based QPE products. This begins with going through the steps used to quality control the raw reflectivity data for clutter and other non-precipitation echoes. If the height of the beam occurs within the melting layer or above, the use of VPR to correct for bright band is performed. Next the steps used for hydrometeor identification are reviewed. Once the rainfall estimation is done, then a mosaicking scheme is applied to combine multiple radar reflectivity regions, and finallly some of the MRMS QPE products of interest are examined.

Chapter 4

This chapter discusses the performance of the MRMS QPE system in the Russian River basin near Santa Rosa, CA. The results provide an indication into the complexities associated with operating within a complex domain. The radars used for this particular study are the local NEXRAD radar as well as a non-NEXRAD C-band TV station radar. In this region, stratiform rain is the prevailing storm type with the existence of a bright band. The results are reported based upon radar measurements that occur below the bright band.

Chapter 5

The architecture of the RAMS QPE system will be presented and discussed to illustrate the flow and data processing required. Briefly these are, to first evaluate the radar data source and then reformat the data to be ingested into RAMS QPE process. Once the radar data is conditioned for input, the single radar QPE is determined via existing CSU hydrometeor identification and dual polarization techniques. Next, individual radar scans are gridded into a common domain, then the lowest level scans are combined to create a single radar hybrid scan dual polarization (HSDP). To merge the radars, the combination of

available single radar HSDP is performed to construct a mosaicked QPE over the common radar coverage area.

Chapter 6

Specifics on the single radar QPE processing are examined in detail in this chapter. Radar data is examined for the availability of proper dual polarization measurements. As well as an assessment of the individual radar dual pole measurement biases. Operating in complex terrain, radar beam blockage is expected and therefore an estimate of the amount of occlusion is evaluated to establish which scanning angles are best fitted to the region. Using the reliable elevation scanning angles for QPE, the rainfall is derived using CSU Dual Polarization Product System algorithms referred to as DROPS which first identifies hydrometeor type and then calculates rainfall rate based upon this information. This is completed for the lowest level elevation scans. In addition to the DROPS QPE, reflectivity-based QPE is calculated. Once single radar QPE is established for the lowest elevation scans, a technique to combine multiple tilts to formulate a hybrid scan dual polarization (HSDP) is discussed. This methodology is then evaluated using radar data from the NOAA HMT East testbed near Asheville North Caroline using hourly rain gauge measurements.

Chapter 7

The availability of multiple radar scans over complex terrain is beneficial in improving the QPE when there exists beam blockage. This section will examine the details into the merging of single radar data as well as the mosaic of multiple radar scans over a particular region. This is done using simple methods such as the the mean or the max of common pixels. For the region under consideration, the merging will be done considering combinations of the local NEXRAD WSR-88DP, NASA and NPOL radars.

Chapter 8

This chapter will assess the performance of the MRMS QPE system and the RAMS QPE system over the Pigeon River basin located near Asheville, NC, which exists within a complex terrain. This domain is chosen since it is an intensive area of study for satellite ground validation and has many rainfall measuring devices deployed for this campaign. The evaluation will compare the radar-only QPE maps from both systems using an independent set of validation gauges.

Chapter 9

This will be the summary and future work chapter.

CHAPTER 2

Challenges of QPE in Complex Terrain

The use of radar for QPE has the advantage of covering wide areas in shorter timeframes in comparison to QPE derived from gauges only. However for the purpose of rainfall estimation, the preferred radar measurements should occur as close to the ground as possible. In complex terrain, the major impediment is the existence of mountains that deter the ability of radars to perform low level scans. As the scanning distance from the radar increases, there are added complications stemming from the beam broadening and the height of the beam. These are such that the beam scans into the bright band or in the ice regions that require changes in rainfall rates based upon these hydrometeor types. Furthermore, the beam broadening effect at far ranges can result in non-uniform beam filling. The other considerations are climate and storm structure within complex terrain. The climates in these regions typically have the occurrence of orographic rainfall, which often involves collision-coalscence microphysical processes at low levels and leads to enhancement of rainfall on the windward sides of mountains and drier conditions on the leeward. Mountainous locals usually have much cooler temperatures and unique humidity conditions and require rainfall algorithms that are based upon the unique climactic environment, such that the application of broad based rainfall relations do not apply well to these regions. Storm structure can occur either as convective or stratiform depending on the season, but in mountainous areas in the cold season, the case is most likely stratiform. The radar beam depending upon the location and range will encounter these storms at various heights and the resulting hydrometeors will differ and need to be accounted for in rainfall estimation.

2.1. Radar Operation and Terrain Effects on QPE

The ability of radar to effectively scan is determined by the physics of system. In terms of using a radar system to measure rainfall, there are several elements that need to be comprehended as this applies to this effort. The radar transmit frequency first of all is inherently related to the size of the radar antenna which for S-band is approximately 10 meters, and the diameter reduces for higher frequencies where the diameter for X-band is about 2 meters and about 4 meters for C-band. The National Weather Service (NWS) Weather Surveillance Radar-1998 Doppler (WSR-88D) network was developed at the S-band frequency (Crum and Alberty 1993). S-band is considered a non-attenuating frequency in regards to scanning through rainfall, however it can experience some attenuation in the presence of severe storms (Ryzhkov and Zrnic 1995). For weather radars operating at higher frequencies such as C-band and X-band, the attenuation of the signal through rainfall becomes an issue and a correction scheme is needed to account for this physical characteristic. Other aspects to consider are the operational scanning patterns of weather radars. Scanning is typically performed at various incremental constant elevation angles, while the radar dish rotates a full 360 degrees. Depending upon the radar's operational transmit frequency, the effective range can be limited. Even though S-band is un-attenuated, the effective range for NEXRAD radars is set to 300 km, since the beam height at these far distances becomes greater in height to the point of becoming ineffective to measure rainfall, such that the beam can well over shoot the storm due to the curvature of the earth (Figure 2.1). For higher frequencies that experience attenuation, the effective range is approximately 100 km for C-band, and 40 km for X-band, where these ranges can be shorter in the presence of intense rainfall.

In addition to the increase in beam height at far ranges, the other aspect is that the beam width becomes wider as the distance from radar increases. When the measurements are taken

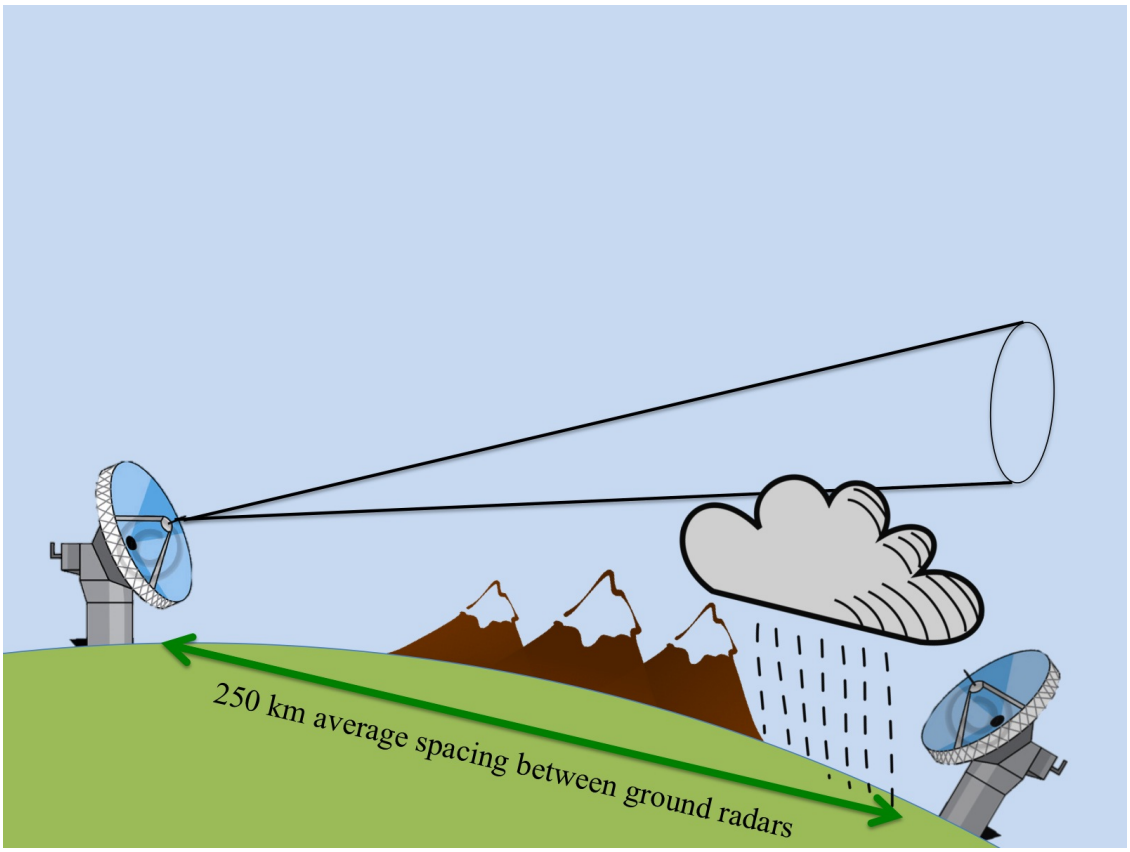

FIGURE 2.1. Earth curvature prevents radars from scanning 72% of the troposphere below 1 km.

at a distance of 100 km, the beam width is approximately 1.6 km wide and expands to around 5 km at a range of 300 km leading to the radar beam encompassing larger and larger volumes (see Figure 2.2). With electromagnetic wave propagation within the atmosphere, the radar beam path can encounter several conditions, such as ground clutter, anomalous propagation, radar artifacts, clear-air returns, and biological contamination, which then lead to erroneous precipitation estimation, and therefore an identification of non-precipitation echoes from the raw radar scans is applied to remove these unwanted echoes.

Beyond the physical characteristics and concerns from the radar system operation and measurement, the type and layout of the terrain in which the radar is placed does play a significant role in the scanning capabilities especially in mountainous locale where these areas

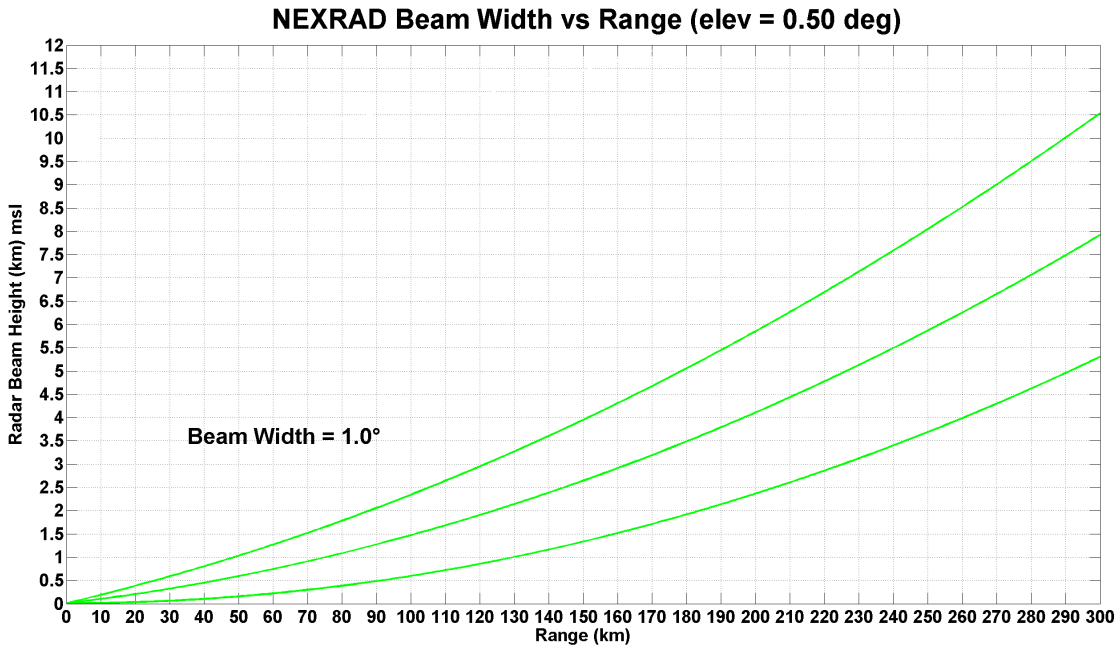

FIGURE 2.2. NEXRAD beam height and beam width at 0.5 degree elevation angle up to a range of 300 km.

are prone to beam blockage. As an added hindrance, the combination of far range scanning and beam blockage in complex terrain creates a challenge for QPE as is depicted in Figure 2.3. The beam can overshoot the storm event or miss the storm due to blocking by mountainous terrain. Furthermore, the climate associated within these regions exhibit unique features in term of weather dynamics such as orographic effects and the possible presence of a melting layer, where the former can result in increased rainfall on the windward slope and very little on the leeward. If there is a melting layer, this height needs to be resolved, so as to delineate between liquid rain or ice and then apply appropriate rainfall estimation relationships.

Given the scanning radars ability to encounter weather phenomenon, the type of storm event needs to be identified either as convective or stratiform in order to resolve the correct application of rainfall equations. Convective storms can be described as events exhibiting intense rainfall with the presence of hail and in which ground lightning strikes occur and where storm occurance is brief. Stratiform storm events on the other hand are designated

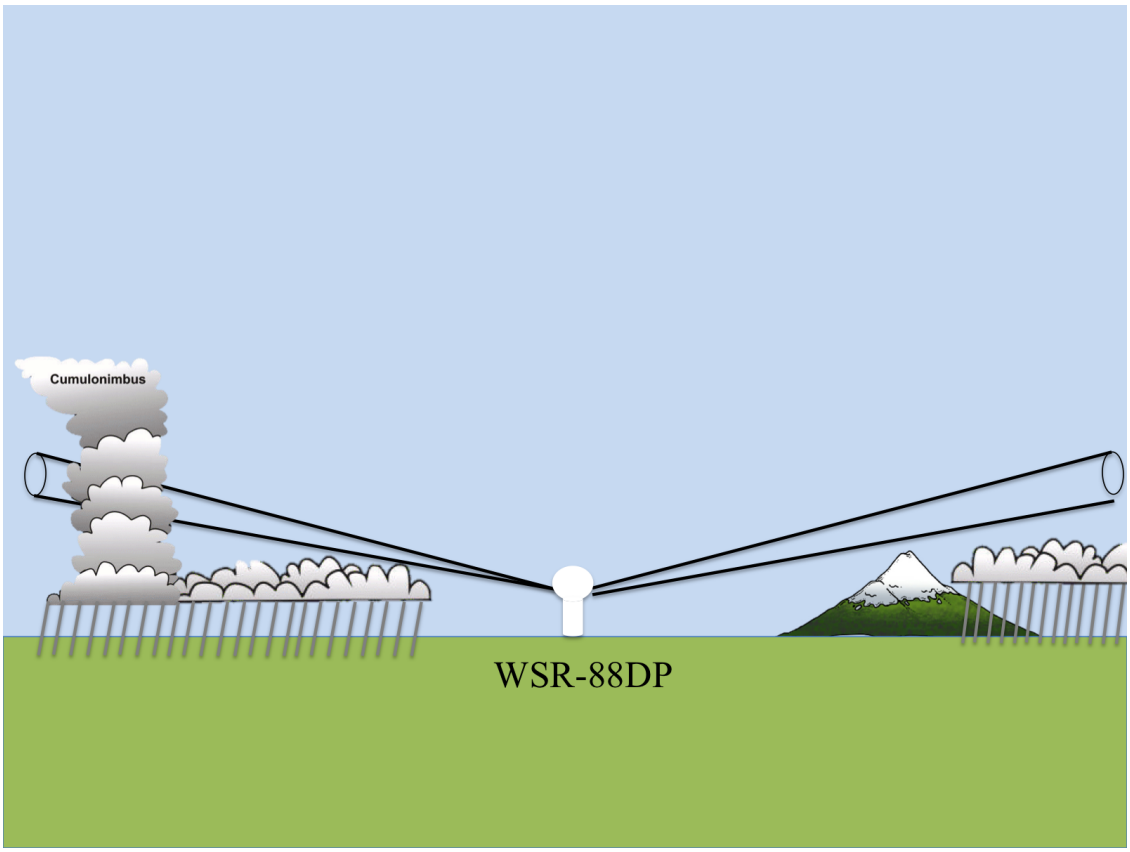

FIGURE 2.3. Beam blockage due to mountain and beam overshooting of storm.

when the rainfall is light and constant, and these storms are slow moving and usually are accompanied by the presence of a bright band, also these events can last much longer as opposed to the convective type. Within these structures, the drop size distribution (DSD) can vary depending upon storm dynamics especially if there are updrafts and downdrafts such as in the case of convective types of events, where updrafts can force super cooled liquid water higher into the storm cell, so that as it comes in contact with ice, it will continually enlarge to form a hail particle. In less dynamic situations as is the case with stratiform, water forms into ice particles at high alititudes and evenutally falls towards the earth as snow. If it encounters warmer air, it begins melting into liquid drops as the ice falls through the melting layer. Once water is in liquid form usually at lower altitudes, it will undergo collision-coalescence process, where the raindrops can increase in diameter up

to a certain width at which they tend to break apart into smaller droplets. The structure of both these type of events are identified from a combination of current climactic conditions and radar measurements. The bright band is an interesting physical aspect of stratiform rain, which occurs near the freezing level in which ice at high altitude transitions into snow and causes an enhanced reflectivity reading, which can be misinterpreted as intense rainfall. This phenomenon requires techniques to correct for it, so as to give reliable QPE estimates.

2.2. Radar Scan Strategy

The scanning possibilities of radars in regard to elevation and range are countless, and therefore creating the necessity to determine specific scanning parameters especially in the presence of precipitation. Taking into account an effective range and beam width, the number of elevation scans within a volume are optimized to encompass as much space within a timely manner taking into account the speed and motion in which the radar can operate where the volume is taken to be the space surrounding the radar. In the occurrence of precipitation, the ideal approach would be to scan as frequently as possible and as close to the ground as possible. There are several operational scan strategies used by the NWS WSR-88D as shown in Table 2.1, and the beam center heights for ranges up to 230 km are displayed in Figure 2.4. For complex terrain environments, the surrounding mountains obstructs the uniform radar scanning ability at low elevation angles, and higher elevation scans are required to clear these obstacles resulting in beams that reach high into the atmosphere. The NEXRAD scan strategies were mainly defined for the ideal scanning scenario, which is without the presence of mountains. When these radars are place near mountains, the scan strategies remain the same and the blockage is noted. The other situation that affects the scanning height is the radar positioning, which in mountainous setting can sometimes occur at the

top of a mountain. This reduces the amount of blockage, but also eliminates the possibility of measuring close to the ground.

TABLE 2.1. WSR-88D volume scan strategies

VCP ID	Tilts	Scan Cycle	Elevation Angles (deg)	Description
11	14	5	0.5, 1.45, 2.4, 3.35, 4.3, 5.25, 6.2, 7.5, 8.7, 10.0, 12.0, 14.0, 16.7, 19.5	Convective storm close to radar
21	9	6	0.5, 1.45, 2.4, 3.35, 4.3, 6.0, 9.9, 14.6, 19.5	Convective storm
31	5	10	0.5, 1.5, 2.5, 3.5, 4.5	Long pulse for find subtle boundaries adn winter precipitation
32	5	10	Same as VCP 31	Short pulse for less pulse ambiguity (clear air mode)
12	14	4.1	0.5, 0.9, 1.3, 1.8, 2.4, 3.1, 4.0, 5.2, 6.4, 8.0, 10.0, 12.5, 15.6, 19.5	Convective storm at long range
121	9	6	Same as VCP 21	Low elevation scan with varying pulse repitition for better velocity data
211	14	5	Same as VCP 11	Reduced range ambiguity used for tropical storms (hurricanes)
212	14	4.1	Same as VCP 11	
221	9	9	Same as VCP 11	

List of volume coverage patterns (VCP) for the WSR-88D.

Given the well known and stable scan strategies established for use by NEXRAD radars, the availability of non-NEXRAD radars such as TV station radars and gap-filling radars like CASA X-band radar network (McLaughlin et al. 2005) can further assist in helping to cover areas unreachable by the NEXRAD radar coverage. The existences of these radars are based upon their particular designed usage and user interest, and these scan strategies vary and are based upon the owner requirements.

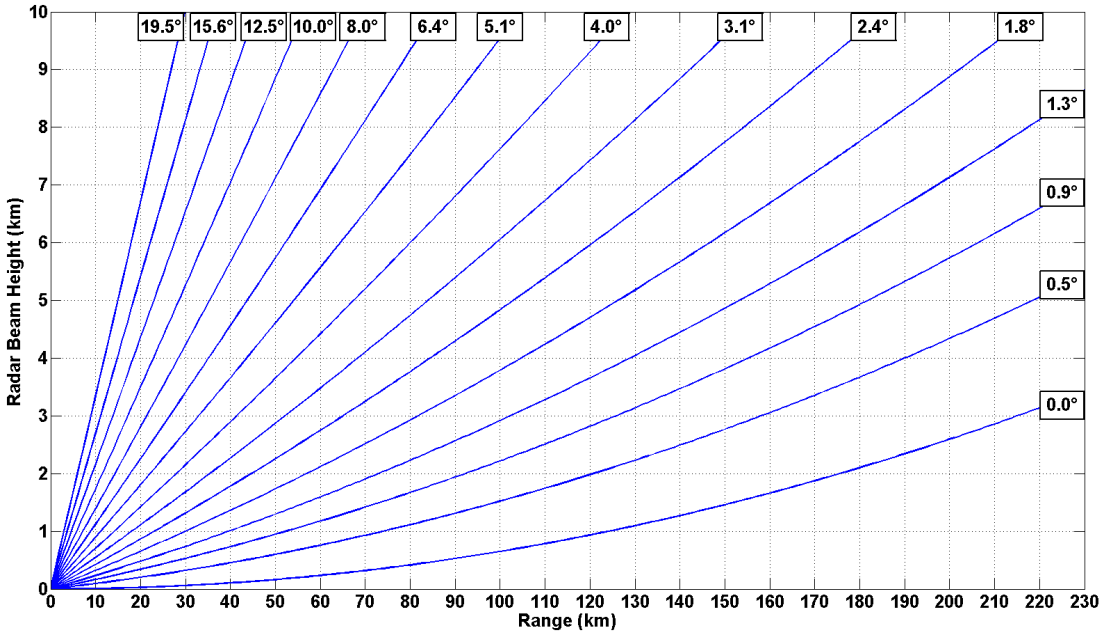

FIGURE 2.4. NEXRAD beam heights for VCP 12 indicating the height of beam center for ranges up to 230 km.

2.3. Hybrid Scan Combination and Mosaicking of Radar Data

In a scenario with overlapping radar coverage, the mosaicking of the radar data can be useful especially in regions that have severe blockage, such that a particular radar may be able to scan over an area in which other radars are obstructed. The NSSL MRMS system has incorporated this mosaicking ability into its processing (Zhang et al. 2011). One of the goals in this effort is to produce a complete coverage map of the continental U.S. (CONUS) using the current NEXRAD WSR-88D network. The mosaicking of radar measurements is a challenge especially if there are large distances between radars, however if it can be done effectively can provide illustrative rainfall maps. In MRMS, there are two mosaicking schemes, one is a 3 dimensional (3-D) merge of NEXRAD radar measurements which done using exponential distance weighting (Zhang et al. 2005), but is computationally intensive as opposed to the combination of only low level scans. The other merging is to combine

2 dimensional (2-D) single radar hybrid scan reflectivity (HSR) fields. The HSR fields are the combination of the lowest tilts along with higher tilts if the lowest tilt is blocked, so as to address beam blockage (O'Bannon 1997; Fulton et al. 1998). The combined HSR 2-D field consists of single radar HSR fields mosaicked into fields with distance weighting method where the single radar HSR field ends at the equidistance points between the radars. In the case of complex terrain, the problem of radar blockage will result in the HSR coverage from overlapping radars to vary depending upon which one is able to scan over the area of interest.

2.4. Gauge Data

Gauge data provides ground truth in measurement of rainfall, but in contrast to radar measurements provides information that is reliable within a localized radius around the gauge site. The gauge measurements in mountainous areas are advantageous due to the amount of radar blockage and maybe the only way to determine rainfall. In this type of terrain, the rainfall amounts can be vastly different depending upon the location of gauges in regards to storm movement and to the position relative to the mountains. Orographic effects can cause gauges on the windward side of the mountain to measure much more rain as opposed to the leeward side or those at lower elevations such as in in the valleys. While gauges can be effective at measuring rainfall, the dependability of measurements are deterred by errors that can occur at gauges such as stuck gauges or maybe gauges that have fallen over. Gauges also vary in the precision of measurement and in the manner that the data is recorded, and they do so in various time spans (e.g. minute, hour, day) where the timestamps can be either local time with or without daylight savings or in the preferred coordinated universal time (UTC). To obtain gauge data, the most widely available compilation of this information in

the US is provided by the NOAA Hydrometeorological Automated Data System (HADS), but gauge data can also come from other regional networks, but as stated the specifics of the data needs to be understood to correctly apply this to the application.

Good reliable gauge data can be very useful in conjunction with radar scanning data in the sense that it can be used to correct the rainfall amounts measured by radar. If there are sufficient number of gauges covering a region, the QPE can be produced using gauge-only, however this can be economically challenging considering the cost, repair and maintenance of the gauge network. However a compromise can be made in the number of gauges if combined with radar measurements. MRMS QPE has products that accomplish this where the techniques applied can be seen in Zhang et al. (2011).

2.5. Bright Band and Vertical Profile of Reflectivity Correction

Storm systems can be described as either convective or stratiform. Convective types of storms are characterized by a deep moist structure that extends into the troposphere and can reach heights above 40,000 feet with intense internal up and down drafts occurs. These types of storms build and decay within hours and can produce intense hail, flash floods, tornadoes, and powerful winds. In contrast, stratiform storms transpire at lower altitudes in the atmosphere and are slower to develop and diminish and can happen over several days and produce rain that is lighter and consistent. Stratiform storm also appear on the tail end of convective storms as can be shown in Figure 2.5.

The category of precipitating storms that occur within the radar's scanning range is identifiable based upon environment conditions and radar measurements. In cases of rainfall events, the temperature gradient from high altitudes to the surface varies from subzero to above freezing temperatures. One of the characteristics of stratiform type rain is the

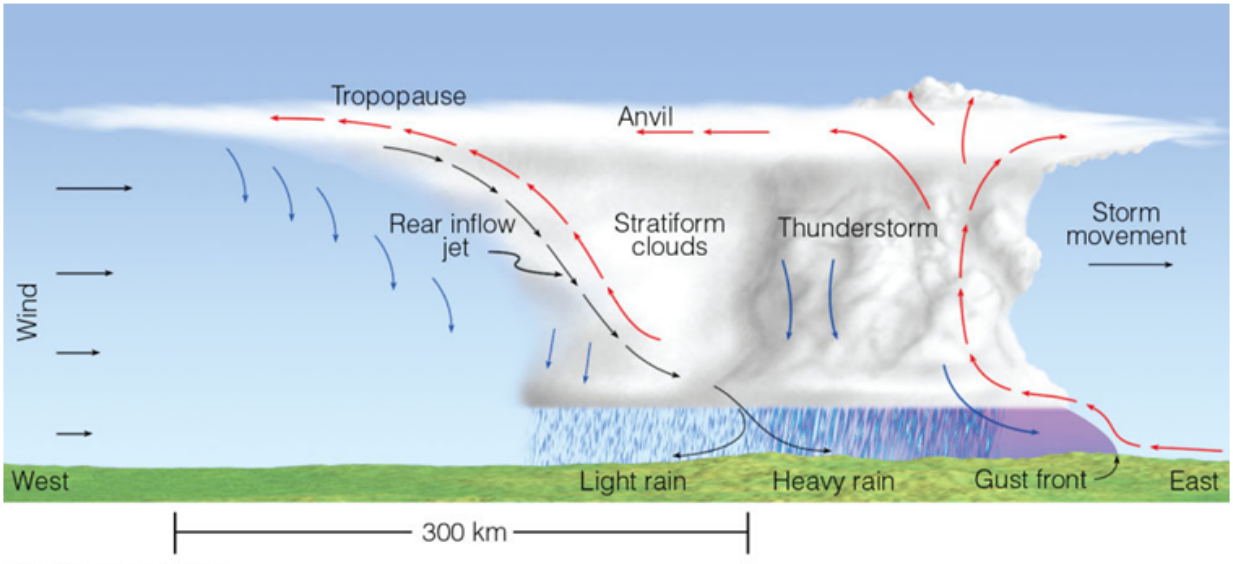

FIGURE 2.5. Structure of a storm with both convective and stratiform components with an approximate width of at least 300 km (Source: Thompson Higher Education 2007).

existence of an enhanced level of reflectivity that appears below the freezing level height. At this zero degree altitude, the hydrometeor type changes from ice to raindrops where the enhancement in reflectivity occurs over a region that contains a mixture of partially melted ice particles. This layer within the stratiform storm structure is referred to as the bright band and is typically 500 meters in width. Radar measurements at far range or taken at higher radar scan elevation will encounter this bright band region and an adjustment is needed to correct for this. Since there is an increase in reflectivity, correction is performed by decreasing the measurement in the bright band by an amount so that water content in the rainfall below and in the ice region above are consistent. This technique is referred to as a Vertical Profile of Reflectivity (VPR) correction and is significant in producing more accurate QPE. Without a correction technique the rainfall would be over estimated due to the enhanced reflectivity measurement seen in the melting layer. The development and application of VPRs to mitigate precipitation errors has been studied considerably. Some

of the advantages and disadvantages can be reviewed in Joss and Lee (1995), Vignal et al. (2000), and Vignal and Krajewski (2001).

CHAPTER 3

Multi-Sensor QPE Operational System

3.1. MRMS-NMQ

In order to achieve an appreciation of the complexities associated in developing QPE systems through the processing and merging of radar data along with other observational data. A discussion into the procedure and methodology of a current state of the art QPE system in operation would be valuable. The National Severe Storms Laboratory (NSSL) of the National Oceanic and Atmospheric Administration (NOAA) has established a software product capable of merging radar and other observational sensors for the purposes of quantitative precipitation estimation. This QPE system was initially proposed as the National Mosaic and Multi-Sensor (NMQ) QPE system (Zhang et al. 2011), and due to advancements and integration with the Warning Decision Support System Integrated Information (WDSS-II) by Lakshmanan et al. (2007), this effort has resulted in the creation of the Multi-Radar Multi-Sensor (MRMS) system. Recently, it has been transitioned into real-time operation at the National Weather Service (NWS) operations under the National Center for Environmental Predictions (NCEP) in 2014. This system ingests 3-D volume scan data from all the 146 WRS-88Ds network and approximately 17,000 rain gauges. The output provides users with high spatial resolution of 1 km with a temporal resolution of 2 min with several severe weather and QPE products. MRMS has a distributive computation architecture with four major components. The sections of the system are: 1) single radar processing, 2) two and three dimensional radar mosaics, 3) next-generation QPE (Vasiloff et al. 2007), and 4) Evaluation. Data sources comprise of level-2 radar data from the NWS WSR-88D network,

Rapid Refresh (RAP) model environmental data, model, lighting data, both HADS gauge network, and other regional rain gauge networks.

MRMS is designed for the purpose of providing rainfall estimates over the contiguous United States, which in locations with good WSR-88D radar coverage and sufficient gauge networks can perform extremely well, such as in the study performed by Kitzmiller et al. (2011) over the Tar-Pamlico River basin of eastern North Carolina which produced very good QPE results. In locales with poor radar coverage and sparse gauge networks, the ability of MRMS to give reliable QPE diminishes, such as was seen in areas surrounding the Russian River basin in Northern California near San Francisco Willie et al. (2014). This region is QPE challenged, since it is situated between coastal mountain ranges where NEXRAD radar coverage is poor. There are several gauge networks in this area, but the orographic rain effects can produce large difference in gauge readings adding to the difficulty of creating reliable QPE.

MRMS QPE derived from radar using rainfall estimates have been based upon reflectivity measurements and this requires intelligent pre-processing to assure accurate readings. However the development and integration of dual polarization for weather radar has created an added dimension in the measurement of rainfall, such that all NWS WSR-88D radars have undergone hardware upgrade to add this capability, and this implementation has been completed as of 2014 (Saxion and Ice 2012). With these added capacities, MRMS is currently in process of developing QPE algorithms that incorporate these advancements in weather radar detection.

Originally this QPE system began operating in real-time in June 2006 under the designation NMQ. It has the flexibility to be configured to run retrospectively so as to apply to case studies.

3.2. MRMS Reflectivity Quality Control QC Module

Raw weather radar measurements require the removal of non-precipitating echoes from NEXRAD reflectivity fields, which is of major concern especially in regards to determining accurate QPE. These unwanted echoes can result in erroneous QPE, and since rainfall is calculated through the accumulation of instantaneous rate measurements, these errors do accumulate and will become larger over longer timeframes. Some of the non-precipitation comes from biological targets such as insects, birds, which can infiltrate reflectivity and distort the hydrometeor returns. Ground clutter due to the side lobes of the radar beam is another issue that can contaminate the radar scans especially at the lowest elevation scan angle and at ranges closer to the radar. Contamination is also possible in the beam path due to refraction within the atmosphere and is referred to as anomalous propagation (AP). This phenomenon occurs when the radar beam path curves toward the earth surface due to unusual atmospheric refractive index.

Therefore to remove such contaminates, the procedure of quality controlling the raw radar reflectivity begins with pre-processing of the reflectivity fields by applying thresholds and other parameters to remove returns that are suspect. After this, the reflectivity fields are then subjected to removing the bloom echoes, which materialize due to the biological scatters near the radar. For this, a neural network is used to identify the bloom echoes. The identified bloom pixels are then subjected into a second stage neural network that applies constraints and parameters to further identify clutter and other non-precipitation echoes.

The process of quality controlling the raw radar reflectivity begins with pre-processing of the reflectivity fields and then subjecting this to a bloom echo neural network to identify biological echoes. The identified bloom pixels are then added into another neural network that implements 22 other features to remove clutter and other non-precipitation echoes

3.2.1. Pre-Processing Removal of Non-Precipitation Echoes

The raw reflectivity field is taken and pre-processed to remove non-precipitation echoes using simple characteristics. The neural network input features are calculated in a local neighborhood surrounding an individual gate. A check is done around this region surrounding an individual gate, which is to evaluate an echo-size parameter. This gives an indication of the amount of fill surrounding this gate. Values greater than 0.9 are considered precipitation. Echo sizes less than 0.5 are removed. Sizes in between take on the value of the majority of the neighboring bins.

Next, all the gates that fall below 12 km in height and have a reflectivity greater than or equal to zero are keep an used to indicate possible rain. At this point, the lowest range gates that are beam blocked according to the method of O'Bannon (1997) are set to be missing values.

Another undesirable feature that frequently enters into radar measurements are sun strobes. These are instances when the radar dish is pointed towards the sun. Here a heuristic approach is taken in which the radials are examined to find if 90% or more of it is filled with reflectivity values greater than 0 dBZ and whose values show linear relationship with a correlation coefficient greater than 0.8. If so, then the entire radial is removed and the values are interpolated using the neighboring radials.

Once the previous procedures are done, the echo-top parameter is considered for each gate (Steiner and Smith 2002). Echo top parameter indicates the highest elevation scan that contains reflectivity greater than a minimum threshold directly above the corresponding pixel from the first lowest scan or its surrounding eight neighbors. If this value is greater then 3km, then it is further proof that precipitation exists and the algorithm completes the steps taken to determine which gates to present to the neural networks.

3.2.2. Neural Network Precipitation Identification

With pre-processing concluded, the radar data is subjected to a succession of neural networks, which are a bloom neural network, and a second stage neural network Lakshmanan et al. (2009). The bloom neural network is applied first in order to identify biological scatters, within a calculated range around the radar, such that the probability associated with each pixel indicates if there might be biological contamination. Once the pixels that are determined be biological scatter by the bloom neural network, the probability of pixels within the bloom that are marked as biological scatters is input into the second stage neural network. This second stage neural network has 23 features in which two are derived from the biological identification scheme mentioned previously. Once the probabilities from the second stage neural network are calculated, the pixels are subjected to a clustering technique, where each cluster is determined using the max reflectivity and the bloom probability values. Clusters are removed based upon a threshold criterion. When this is complete, a final mask is applied to get the quality controlled reflectivity fields (Figure 3.1).

3.2.3. Bloom Radius

Prior to submitting reflectivity pixels into the bloom neural network, the extent to which the bloom radius extends needs to be determined. The bloom radius is the distance from the radar in which biological scatters could exist. The radius is determined by the maximum height in which birds could possibly fly. A characteristic of the reflectivity values along each radial within this bloom is that there is a steady increase in value with range up to a point where a maximum occurs and then tapers off. This attribute is associated with the limit in height that birds and insects can attain as well as the expanse in the beam width with distance.

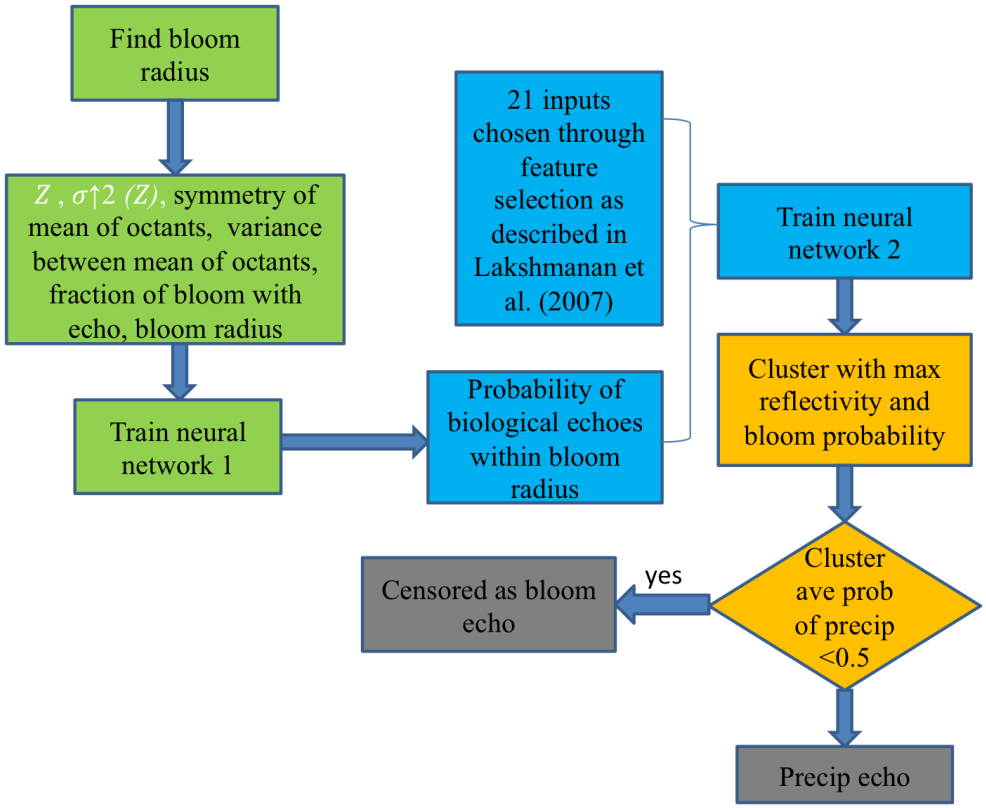

FIGURE 3.1. Flowchart depicting the first stage neural network (bloom) and second stage neural network to quality control reflectivity

The approach established to identify the bloom radius surrounding the radar has several steps, which are:

(1) Consider range gates lower than 4 km in height above ground level, which is the altitude that birds tend to fly below and is high enough that insects do not appear in much concentration above this height.

(2) At constant range, find the average reflectivity values using the "hybrid scan"

(3) Plot the averaged reflectivity values versus range and fit this curve into line segments.

(4) The longest line segment that has a negative slope in which the line segment has a Pearson correlation coefficient of 0.9 or better is the possible bloom radius.

If the resulting line segment is greater than 10 km, the radius of the bloom is the ending point of that line segment, on the other hand, if the longest segment is less than 10 km, then no bloom is presumed in the radar image.

3.2.4. Bloom Probability

Given an existing bloom with a valid line length greater than 10 km, a statistical analysis is made on echoes within the bloom radius, and the variables of interest are the mean reflectivity, variance of reflectivity, symmetry of the mean of the octants, fraction of bloom filled with echo, and bloom radius. These calculated values are then used as the feature inputs into the bloom neural network, and the output of this neural network is the probability of whether each echo is a bloom contaminant or not.

3.2.5. Identify Bloom Pixels

Although the bloom radius and the bloom probability have been calculated, there is a possibility that a storm may be embedded within the bloom. In this circumstance, the pixels will need to be separated into either storm echo or bloom echo. To identify storm echoes, a 3 km neighborhood around each gate within a radial is examined, such that a storm echo is identified when all the pixels within the neighborhood are above 35 dBZ. In the other case, a bloom echo is established if the neighborhoods of pixels have values above the 10 dBZ threshold. In each radial, the extent of the bloom is the point where a storm echo occurs or the reflectivity drops below the 10 dBZ threshold. Applying this methodology in the presence of light precipitation below 35 dBZ, these pixels will be identified as bloom, resulting in rainfall estimation of zero precipitation.

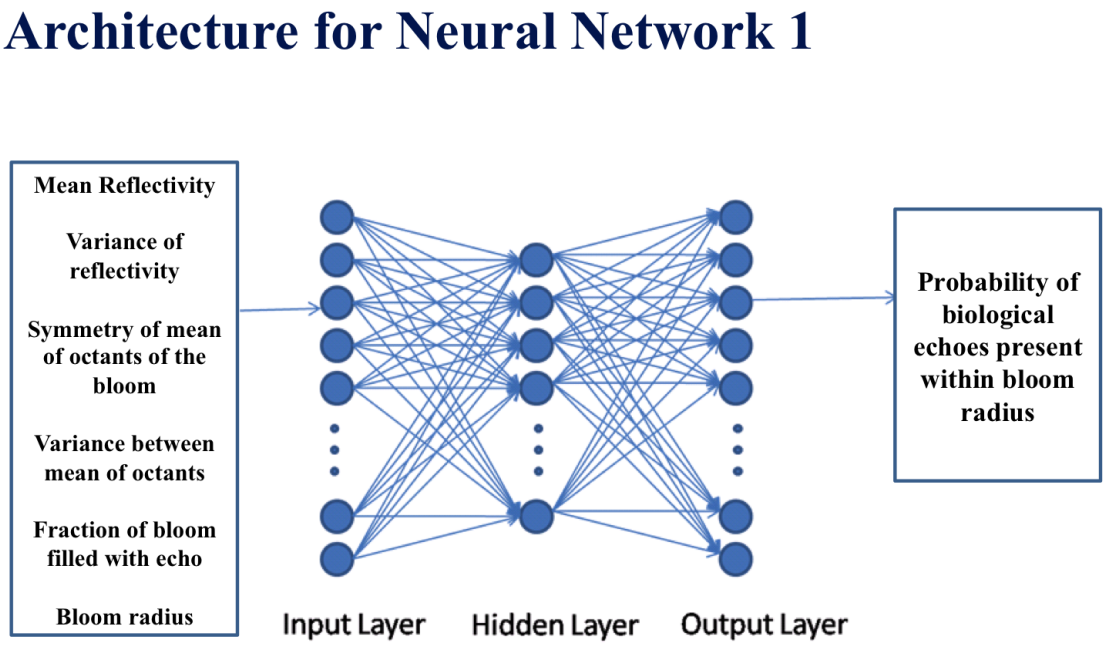

FIGURE 3.2. Flowchart showing the first stage neural network to remove the bloom echo in the quality control of reflectivity

3.2.6. SECOND STAGE NEURAL NETWORK

Now that the bloom radius and bloom probability have been determined, a second stage neural network is implemented that has 23 inputs, such that 2 of these inputs come from the bloom probability and the fraction of the bloom radius that is filled with storm or bloom echo. This second stage neural network is a scaled down version of the network established by (Lakshmanan et al. 2007), which is a resilient back-propagation neural network (RPROP) as explained in Riedmiller and Braun (1993) with one hidden layer. In this network every input node is connected to every hidden node and every hidden node is connected to every output node, and there is a direct connection from the input nodes to the output node to account for any linear relationships. Some of the input features applied in this second stage neural network stem from previous quality control efforts done by Grecu and Krajewski (2000); Steiner and Smith (2002), which is referred to as the anomalous propagation or ground

clutter (AP or GC) algorithm. The other features have been established from the Next Generation Weather Radar (NEXRAD) radar echo classification (REC) algorithm (Kessinger et al. 2003), and the quality control pre-processing in NEXRAD precipitation products (Fulton et al. 1998). Part of feature inputs are derived from the lowest elevation scan, and they are: 1) Doppler velocity, 2) Mean of Doppler velocity, 3) Standard deviation of Doppler velocity, 4) Minimum standard deviation of Doppler velocity in neighborhood, 5) Spectrum width, 6) Reflectivity, 7) Neighborhood mean of reflectivity, 8) Standard deviation of reflectivity, 9) Minimum standard deviation of reflectivity in neighborhood, 10) Spatial reflectivity of the reflectivity field or "spin" (Steiner and Smith 2002), 11) Inflections along radial (Kessinger et al. 2003). The other set of features are taken from the second lowest elevation scan, which are: 12) Reflectivity at second tilt, 13) Mean reflectivity at second tilt, 14) Difference between reflectivity value and mean, 15) Minimum standard deviation, 16) Maximum value in the vertical, 17) Vertically integrated liquid (Greene and Clark 1972), 18) Difference between the two lowest tilts, 19) Echo top of 0 dBZ, 20) Echo top of 20 dBZ, and 21) Height of maximum. The last two are from the bloom processing which are: 22) Fraction of neighborhood filled, and 23) Probability that this pixel is part of a biological echo. This results in a total of 23 feature inputs into the second stage neural network.

3.2.7. Clustering

After the output from the second stage neural network is complete, this is followed by a pixel clustering technique, which is a K-Means clustering methodology from Lakshmanan (2001); Lakshmanan et al. (2003). The pixels are clustered using the maximum reflectivity and the bloom probability values where the output from the second stage neural network is averaged within these clusters. If the cluster average is below 0.5, the entire cluster

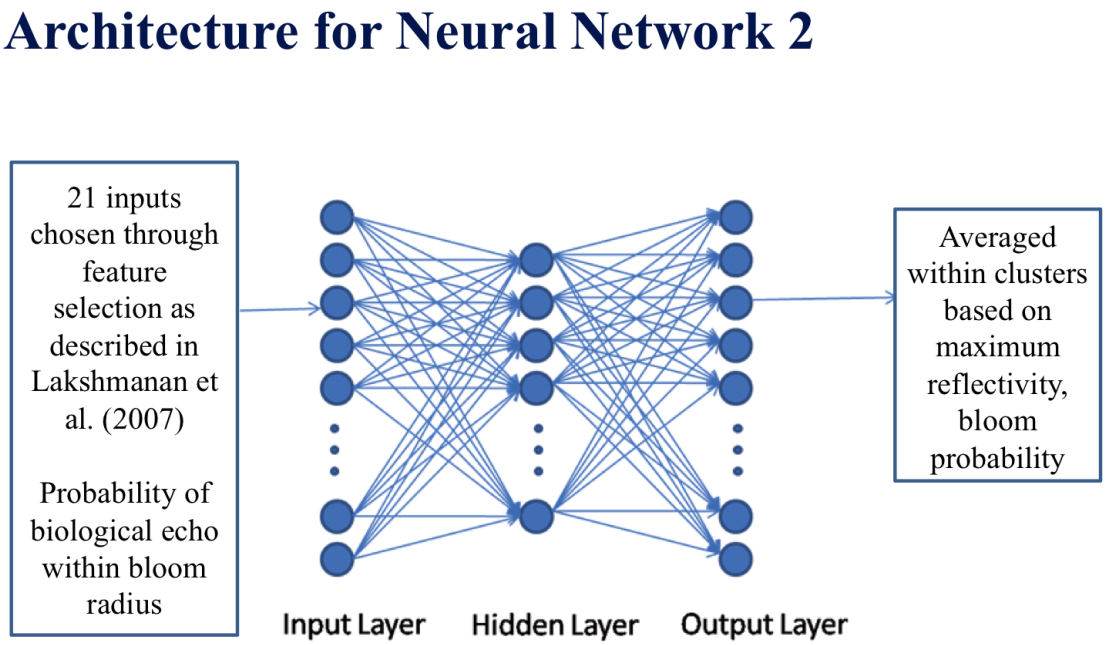

FIGURE 3.3. Flowchart showing the second stage neural network to identify the contaminated reflectivity pixel for quality control

is censored. After this is done, the final mask is done and applied to obtain the quality controlled reflectivity fields.

3.3. Single Radar Cartesian Grid

Weather radar measurements are natively recorded using spherical coordinates, which creates difficulty in users attempting to process the data in a Cartesian coordinate system. Therefore techniques are needed to re-map from the radar coordinate system to Cartesian is required. The most common methods of doing this are nearest neighbor (Jorgensen et al. 1983), linear interpolation (Fulton et al. 1998), Cressman weighting scheme (Weygandt et al. 2002), and the Barnes or exponential weighting schemes (Shapiro et al. 2003). In the effort of re-gridding, it is imperative to retain the integrity of the original data by both minimizing the amount of smoothing and keeping the introduction of artifacts low, while insuring the amount of computation required is reasonable in order to be able to operate in real-time.

Considering the various schemes, a combination of nearest neighbor and linear interpolation provided gridding that meets the aforementioned criteria for efficient re-mapping (Zhang et al. 2005). The nearest neighbor scheme is performed in the azimuthal and range directions, and a linear interpolation is done in the vertical. The radar volume bins are assumed to be 1 km x 1 degree x 1 degree in radar spherical coordinates, and the Cartesian grid has a horizontal resolution of 0.01 degree in longitude x 0.01 degree in latitude (approximately 1 km x 1 km) and 31 vertical layers ranging from 500 m to 18 km above the mean sea level. In the azimuthal plane, the grid cell simply takes on the value of the nearest radar bin, where the distance is taken from the center of the radar bin to the Cartesian grid cell. In elevation the interpolation is done by finding the two observations above and below the grid cell and interpolate between the two values (Zhang et al. 2005).

(1) Get the azimuth, elevation, and range of the center of grid cell i.

(2) Get f_1° and f_2° which are the two grid cells above and below the grid cell i, respectively.

(3) Determine the analysis value f_i^a with the following equation

$$f_i^a = \frac{(w_1 f_1^\circ + w_2 f_2^\circ)}{(w_1 + w_2)} \tag{1}$$

Here w_1 and w_2 are the weights used for interpolating the reflectivity values above and below, repectively. The weights are given by

$$w_2 = \frac{(\theta_i - \theta_1)}{(\theta_2 - \theta_1)} \tag{2}$$

$$w_1 = \frac{(\theta_2 - \theta_i)}{(\theta_2 - \theta_1)} \tag{3}$$

where θ_i, θ_1, and θ_2 are the elevation angles of the grid cell, the bins below and above, respectively. This linear interpolation in elevation preserves the vertical gradients better than using the nearest neighbor method for vertical mapping.

NEXRAD WSR-88D radars typically have a range of 300 km, unless it is a coastal radar and then its range is 460 km. The resulting Cartesian grid is centered at the radar, such that the mapping is efficient for the majority of storm events, but it does have limitations for events in which a bright band is present. In this case, the lack of horizontal interpolation creates vertical gaps that result from the spacing between the higher tilts that are closer to the radar.

3.4. Vertical Profile of Reflectivity Correction

One of the complications encountered while attempting to calculate QPE, within MRMS, from radar measurements is the existence of a bright band that produces an overestimation due to the layer of enhanced reflectivity in the region of melting ice. In order to have an efficient reliable real-time application, the VPR approach chosen by Zhang and Qi (2010) to operate within MRMS combines the mean volume scan VPR (Vignal et al. 2000) with an idealized VPR model.

There are two major types of storms encountered with weather radar scanning, where these are convective and stratiform type events. In the event of a stratiform storm, a bright band can exist, but is not always the case. It was shown by White et al. (2003) that one third of stratiform precipitation near Santa Rosa, CA occured without a bright band, where this type of rain has different DSD characteristics as Martner et al. (2008) indicated. While convective storms do exhibit a bright band feature, it is on a smaller scale and tends to trail the storm core. In some cases, the storm may be only stratiform or only just convective. This

assortment of possibilities creates a necessity to identify the type of storm that is occurring. If the stratiform storm is present, then there is a transition of hydrometeor type in altitude, such that above the 0 degree freezing level ice particles exist, and right below the freezing level is an ice-water mixture, and then finally below the melting layer hydrometeors fall as water droplets. In the presence of a bright band, it is essential to account for these changes, since as the hydrometeor passes through the bright band; it gives an enhanced reflectivity reading. Scanning in the melting region results in high reflectivity measurements and causes an over estimation in rainfall amount which needs to be accounted for. The correction to reflectivity is performed, so that there is consistency in the water content within the bright band in comparison to the measurement of water content in the ice particles above it and the raindrops below it.

In the case of bright band precipitation, the MRMS VPR correction method begins by finding the local temperature either through sounding information or with local model temperature profile. If the 0 degree height is at or below the ground level then correction is not required. Otherwise a bright band is assumed. Given the two types of storms, it is necessary to identify which storm is occurring. This is done using the method of vertically integrated liquid water (VIL) by Greene and Clark (1972). The VIL is computed for a single radar volume scan reflectivity data where the spatial resolution is approximately 1 degree x 1 km, and the temporal resolution is about 5 min.

$$VIL = \sum_{k} VILpar_k \tag{4}$$

$VILpar_k$ is the VIL within a specific (k_{th}) tilt at a particular range gate.

$$VILpar_k = LW \times DB \tag{5}$$

LW and DB are calculated from Equation (6) and Equation (7), respectively.

$$LW = 3.44 \times 10^3 ZE^{4/7} \tag{6}$$

LW is the liquid water content within a resolution bin (kg km^{-3}).

$$DB = \begin{cases} BH[\theta_{k_{top}} + 0.5BW] - BH[0.5(\theta_{k_{top}} + \theta_{k_{top}-1})] & k = k_{top} \\ BH[0.5(\theta_{k+1} + \theta_k)] - BH[0.5(\theta_k + \theta_{k-1})] & 1 < k < k_{top} \\ BH[0.5(\theta_2 + \theta_1] & k = 1 \end{cases} \tag{7}$$

The convective-stratiform delineation utilizes the VIL, such that if the VIL is greater than the threshold of 6.5 kg km^{-2}, then the gate is categorized as convective, if not then it is stratiform. Within stratiform identified storms, the region must next be determined to see if it is a bright band affected area (BBA) or not. A bright band affected area is discovered when the composite reflectivities are greater than the threshold of 30 dBZ. This threshold is based upon studies that considered different regions within the continental United States (Zhang and Qi 2010). If there is BBA, the first guess at the bright band top (BB top) is the 0 degree height + D_1, where the 0 degree level is acquired from the model sounding information or the temperature profile at the radar. The initial guess at the bright band bottom (BB bottom) is assumed to be 5 km below the BB top. D_1 is the difference between the center of the beam from the lowest tilt and the bottom of the beam at the point where the center of the beam intersects the 0 degree height (Figure 3.4).

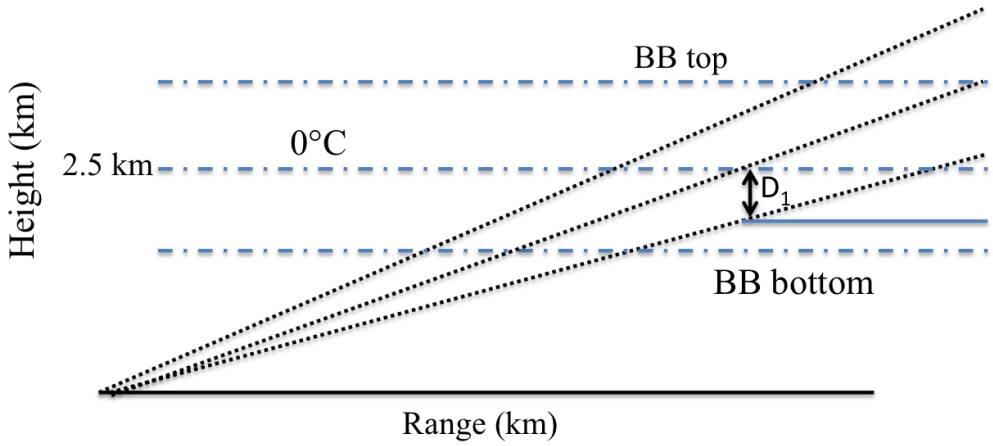

FIGURE 3.4. Initial guess at bright band top and bright band bottom. D_1 is the distance between center of beam crossing the freezing level to bottom of the beam at that range.

For every elevation scan, an apparent VPR (AVPR) is computed by taking the average of reflectivities at constant range within the BBA. The resulting mean reflectivity is achieved only when there are a sufficient number of pixels. The minimum number of pixels used for averaging decreases with increasing range, since the size of pixel increases as beam widens. Along with this, a 15-point average in the vertical is performed, such that any points that stray more than twice the mean absolute deviation are thrown out. If more then 40% are discarded then the AVPR is invalid.

AVPR is characterized by five parameters (Figure 3.5): 1) Height of the apparent BB top (h_t) (ABT), 2) Height of the apparent BB bottom (h_b) (ABB), 3) Height of the apparent BB peak (ABP) (h_p), 4) Slope above the apparent BB peak (α), 5) Slope below the apparent BB peak (β). The apparent BB peak (h_p) is the height of the maximum reflectivity below the apparent BB top. The slope α of the line between the apparent BB top and the apparent

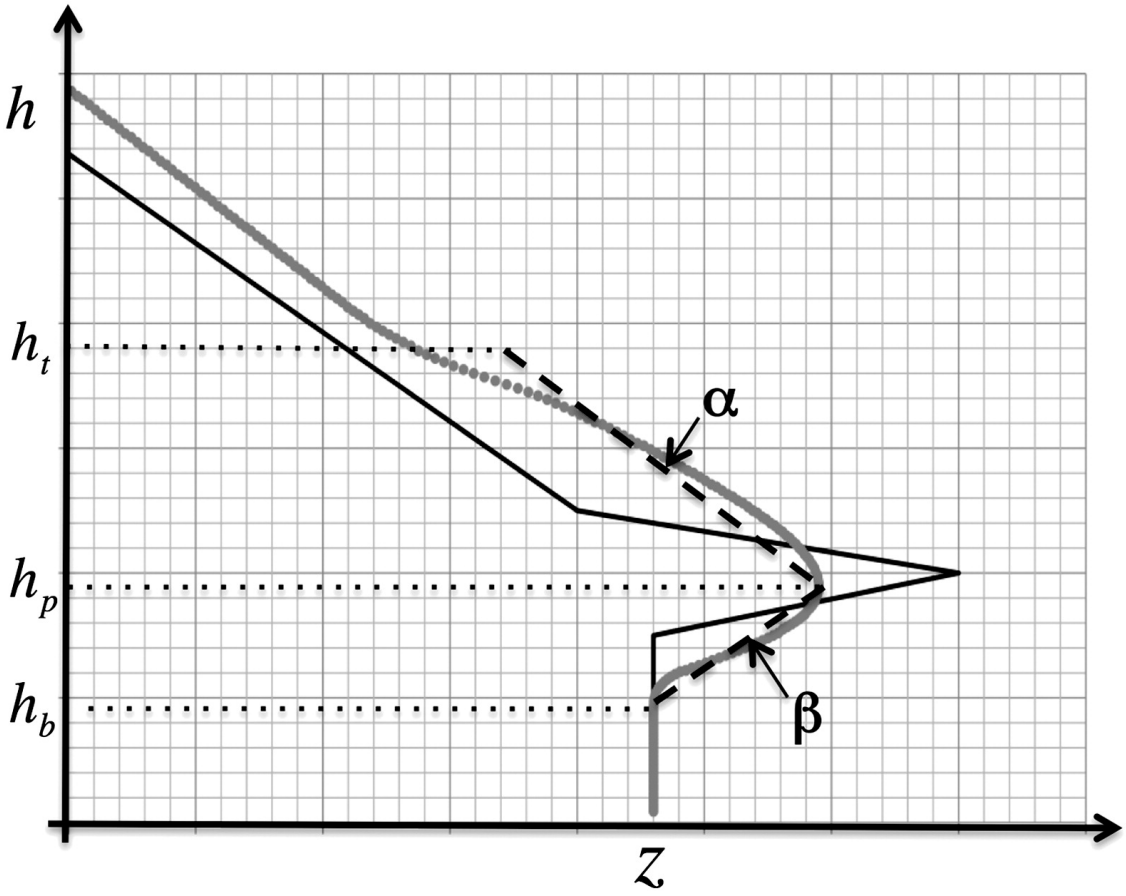

FIGURE 3.5. Illustration of a true (black solid line) and an apparent (gray line) VPR. The apparent VPR is computed on 0.5° tilt assuming the WSR-88D radar beam characteristics. The black dashed line shows an idealized linear model fitted to the AVPR in the brightband-affected area (from Zhang and Qi 2010).

BB peak is found using a least square fit to the AVPR, and the apparent BB bottom is found by searching the AVPR where the a minimum reflectivity below the apparent BB peak where the minimum threshold is 28 dBZ. Once the height (h_b) of the apparent BB bottom is known, the slope β of the line between the apparent BB bottom and apparent BB peak is determined from the AVPR also using least square fitting.

In Figure 3.6, the blue dots are the mean reflectivity at constant range, where the red line approximates an apparent VPR.

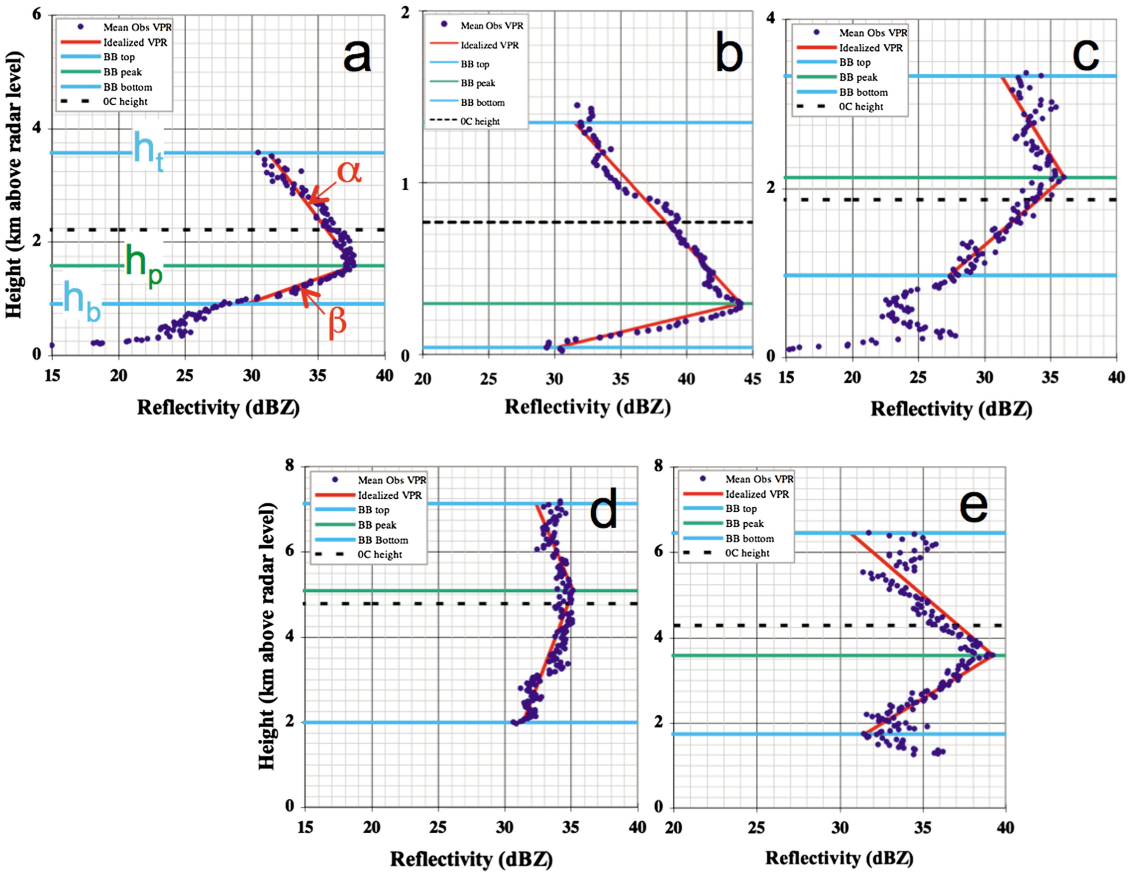

FIGURE 3.6. Apparent VPRs (blue dots) and associated linear parameters for (a) KCLE at 1000 UTC Nov 15, 2008, (b) KUDX at 0500 UTC May 27, 2008, (c) KATX at 2004 UTC Jan 7, 2009, (d) KLZK at 1300 UTC Sep 3, 2008, and (e) KFWS at 1800 UTC May 27, 2008 (from Zhang and Qi 2010).

When the AVPR is determined, the correction is applied using the model VPR fit. The log scale reflectivity correction factor $dBz_a(h)$ is computed as the following.

$$dBz_a(h) = \begin{cases} \alpha[h(r) - h_p] + \beta[h_p - h_b] & h(r) > h_p \\ \beta[h(r) - h_b] & h(r) \le h_p \end{cases} \tag{8}$$

$$dBZ_c(\phi, 0) = dBZ_o(\phi, h) - dBz_a(h); \qquad (\phi, h) \in BBA \tag{9}$$

Here h, r, and ϕ are the height of the beam, range, and azimuth of the gate. $\mathrm{dBZ}_o(\phi, h)$ represents the observed reflectivity (in log scale) also at the gate, and $dBZ_c(\phi, 0)$ (in log scale) is the corrected reflectivity.

3.5. Hybrid Scan Reflectivity

Once the quality control and VPR correction is applied, the hybrid scan reflectivity (HSR) can be created, which is essentially a 2 dimensional reflectivity field that is constructed using the lowest unobstructed elevation scans. The intention is to take this 2-D reflectivity field and calculate rainfall amounts. The HSR is developed in a manner similar to the sectorized reflectivity hybrid scan from O'Bannon (1997) and Fulton et al. (1998).

The reflectivity fields used for this are the corrected reflectivity values from the computed AVPR. Starting with the lowest tilt, each of the radials must not have terrain blockage of 50% or more. If radial(s) are blocked, then the next higher tilt is used. The rise in elevation continues until there are no more blockages. Each WSR-88D has a unique hybrid scan "look-up" table, which is derived from the U.S. Geological Survey three arc-second digital terrain map where the blockages are pre-determined. In Figure 3.7d, the correction to reflectivty has been applied.

The hybrid scan looks to provide the lowest elevation scans for rainfall estimation using the VPR corrected reflectivities. However beyond a range of 100 km, it becomes increasing difficult to obtain effective VPR correction, since the validity of reflectivity from the lowest elevation at these far ranges continue to increase in height. Also within mountainous terrain, the effectiveness of this method is less reliable due to VPR uncertainty and lowest elevation blockage.

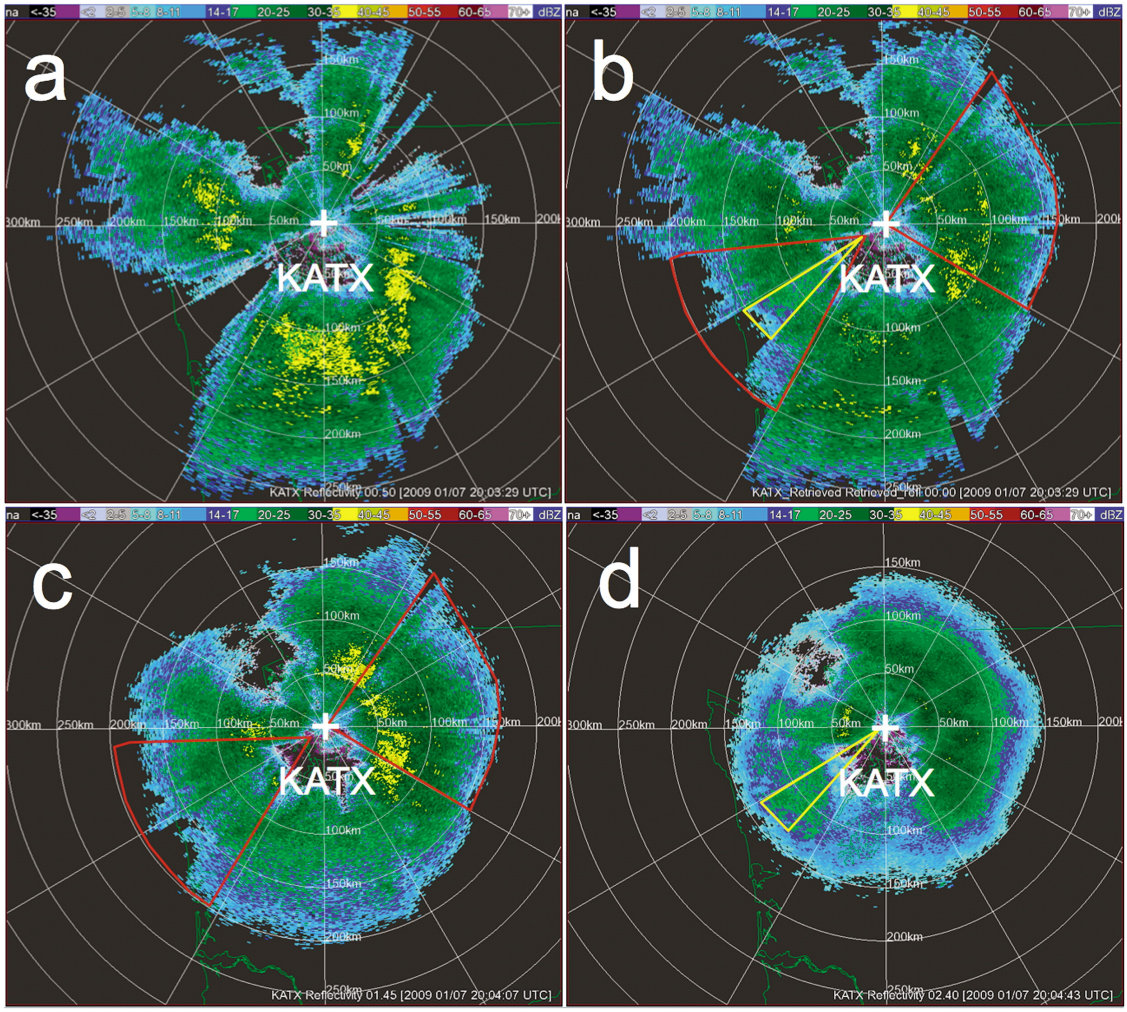

FIGURE 3.7. Base-level reflectivities on the (a) 0.58, (c) 1.458, and (d) 2.48 tilts and (b) the hybrid scan reflectivity from KATX at 2004 UTC 7 Jan 2009. The red and yellow outlined areas were the corrected reflectivities from 1.458 and 2.48 tilts, respectively (from Zhang and Qi 2010).

3.6. Mosaicking of Radar Data

The mosaicked hybrid scan reflectivity combines the single radar HSR fields using a distance weighting approach where the underlying idea is to create a multi-radar reflectivity field in which to derive QPE. This mosaic scheme and the weighting function are computed as such (Zhang et al. 2011):

$$HSR = \frac{\sum_i w_L^i \times w_H^i \times SHSR^i}{\sum_i w_L^i \times w_H^i} \tag{10}$$

$$w_L = \exp\left(\frac{d^2}{L^2}\right) \tag{11}$$

$$w_H = \exp\left(\frac{h^2}{H^2}\right) \tag{12}$$

HSR represents the mosaicked hybrid scan reflectivity, i is the index of the radar, and SHSR is the single hybrid scan reflectivity field. w_L and w_H are the horizontal and vertical weighting functions, respectively. The distance between the analysis point and the radar is given by d, and the height above mean sea level is indicated by h of a single radar HSR bin. L and H are the scale factors associated with the two weighting functions.

This mosaic scheme shows better horizontal continuity than does a nearest neighbor methodology, where the nearest neighbor can create discontinuities between radars.

3.7. Hydrometeor Identification

In determining QPE from radar measurements, it is important to classify the type of hydrometeors in order to give accurate precipitation estimations, since the choice of which rainfall rate from reflectivity relation varies according the physical state of the particles. Furthermore, the other circumstances that influence the application of the Z-R relation are environmental conditions, type of storm, and regional climate. Usually within a single radar coverage domain such as the WSR-88D, a single Z-R equation is chosen and applied according to the local weather service forecast office evaluation. However, there may exist

several different types of precipitation regimes within a single radar coverage and is more likely in the mosaicked radar sense. Therefore the classification of hydrometeors and the delineation of Z-R regions are required to effectively estimate precipitation.

The MRMS hydrometeor classification scheme implements physically based heuristic rules, such that each grid point is assigned a precipitation type, which is based upon a 3 dimensional reflectivity structure (Zhang et al. 2005) as well as environmental data where the temperature soundings are taken from the hourly analyses of the RUC model (Benjamin et al. 2004). The five precipitation types are: 1) stratiform rain, 2) convective rain, 3) warm rain, 4) hail, and 5) snow. The flow diagram to determine hydrometeor type is depicted in Figure 3.8.

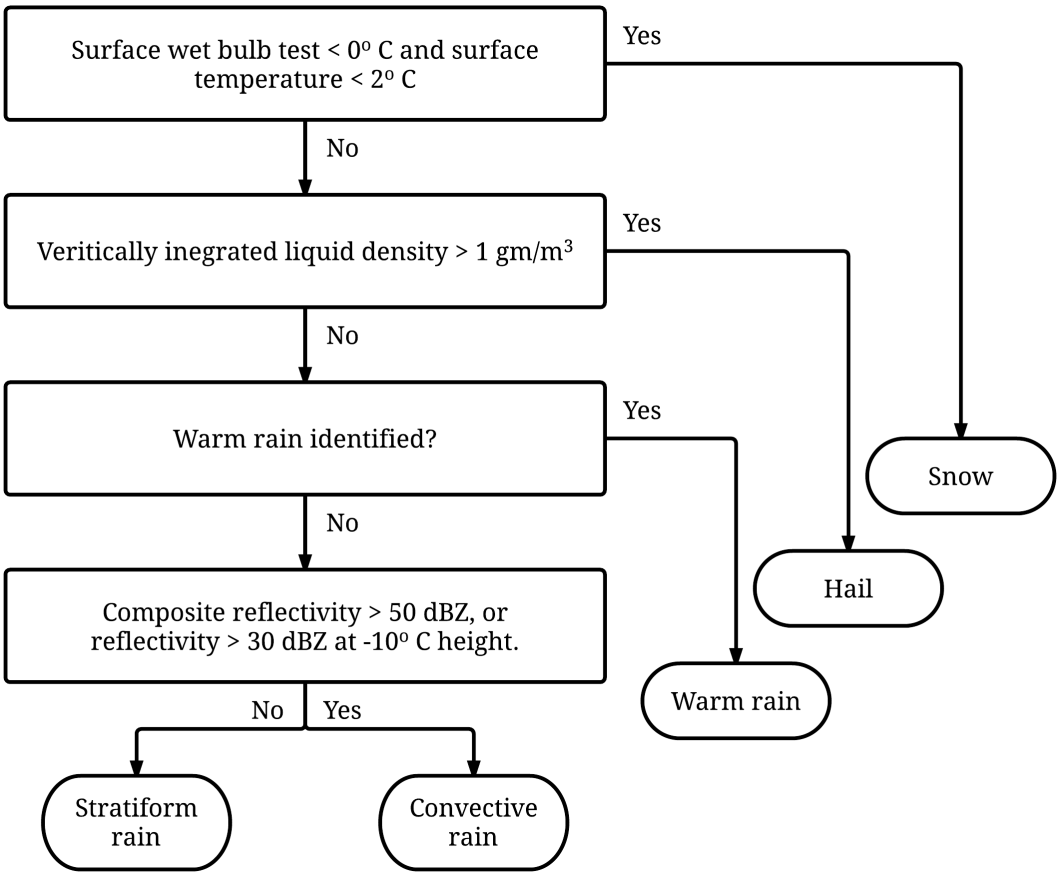

FIGURE 3.8. MRMS precipitation classification process

To begin with, all the grid cells are determined to see if precipitation exists. The threshold criteria is such that the reflectivity must be 5 dBZ or greater for a surface temperature below 2 degree Celsius and 10 dBZ otherwise. If the surface temperature is 2 degree Celsius or lower, and the surface wet bulb temperature is 0 degree Celsius, then precipitation is considered snow. If snow is not present, then the vertical integrated liquid density (VILD) is checked to look for hail, such that if the VILD is greater than 1 g m^{-3}, then it is labeled as hail. Next a check for the existence of warm rain is performed, since it is critical to distinguish this in order to apply the appropriate Z-R relationship. MRMS implements the method described in Xu et al. (2008) where the hourly mean VPR from all radars is considered. If the slope of the VPR below the freezing level is negative, then the corresponding radar is identified as "warm rain" radar. Within this particular radar region, the reflectivity must be above 35 dBZ, and the surface temperature must be above 10 degree Celsius to be identified as warm rain. If not warm rain, then the region is separated into convective and stratiform in the manner described before (Zhang et al. 2008). A convective pixel is determined if either of these conditions are present: 1) if at any height in the column above, has a reflectivity greater than 50 dBZ, 2) there is a 30 dBZ or greater echo above the -10 degree Celsius height, and 3) one or more lightning flashes occur within in the locale of the pixel. Anything not meeting any of the mentioned criteria is classified as stratiform rain.

3.8. MRMS QPE Products

Once the radar data has completed the quality control process, it is gridded into latitude and longitude coordinates and then mosaicked. Precipitation type is identified, and the quantitative precipitation estimation is calculated using the appropriate Z-R relation. The mosaicked field has a spatial resolution of approximately 1 km and an update time of 2.5

minutes. Depending upon the availability of input data, MRMS generates several rainfall products. The QPE fields of interest are radar-only, radar-only with VPR correction, radar with VPR and gauge correction, and gauge-only products.

3.8.1. Radar-Only With and Without VPR Correction

The radar-only QPE product calculates the rainfall rate directly from the measured reflectivity after the quality control processing, and the radar-only with VPR correction product is computed by applying the bright band correction techniques to the radar reflectivity. Contingent upon the precipitation type, the following four Z-R relationships are applied where Z is the radar reflectivity ($mm^6\ m^{-3}$) and R is the rain rate ($mm\ h^{-1}$).

$$Z = 300R^{1.4} \quad (convective) \tag{13}$$

$$Z = 200R^{1.6} \quad (stratiform) \tag{14}$$

$$Z = 230R^{1.25} \quad (warm\ rain) \tag{15}$$

$$Z = 75R^{2.6} \quad (snow\ at\ surface) \tag{16}$$

Z is the radar reflectivity ($mm^6\ m^{-3}$), and R is the rain rate in Equations (13,14,15) or snow water equivalent in Equation (16) where units of R are in ($mm\ h^{-1}$).

In calculating rainfall amount, the 1 hour and 3 hour accumulations are derived by summing the QPE every 5 minutes where the 6, 12, 24, 48, and 72 hour accumulations are aggregated from the 1 hour accumulations. In the case of convective pixels, the appropriate Z-R equation is applied, and the reflectivity measurements must fall below the maximum value of 55 dBZ. If hail is detected, the convective relation is applied, where the reflectivity

values have a maximum limiting value of 45 dBZ. When warm rain is identified, the Z-R for this situation is used, and the reflectivity values have a maximum of 50 dBZ (Equation 16).

3.8.2. Radar With VPR and Local Gauge Bias Correction

The current version of MRMS relies upon two gauge bias correction techniques. The first is a local gauge correction and is constructed upon the inverse distance weighting (IDW) technique of Ware (2005), which was included in the early version of MRMS. The other is the Parameter elevation Regressions on Independent Slopes Model (PRISM; Schaake et al. 2004), which draws upon rainfall climatology in a procedure called Mountain Mapper. This is included in the later versions of MRMS and provides better gauge correction in mountaineous terrain. There are a number of other ways that gauge interpolation can be accomplished (Seo et al. 1999, 2014), where this is a subject of continuous research.

The local gauge correction is constructed upon the inverse distance weighting (IDW) technique of Ware (2005). which in this study was evaluated against a Multi-quadric Interpolation (MQ) and Ordinary Kriging. The use of IDW performed better than Kriging and similarly to MQ interpolation in 30 storm events. Since performance of IDW is comparable to MQ and its computation is straightforward and efficient, this approach is the most practical for MRMS gauge correction. This methodology begins by finding the error between the gauge rainfall amount and the radar QPE amount at the gauge pixel location. These error values are then interpolated in distance from the gauge over the QPE domain of interest.

$$e_i = r_i - g_i \tag{17}$$

Here, e_i is the error at the ith rain gauge, r_i is the radar estimated rainfall amount, and g_i is the gauge measured rainfall amount at the ith rain gauge.

$$R_e = \frac{\sum_{i=1}^{n} e_i w_i}{\sum_{i=1}^{n} w_i} \tag{18}$$

R_e gives the estimated radar error at the pixel being interpolated, w_i is the weight given to the ith rain gauge, and n is the total number of corresponding gauge and radar pixel pairs. The method here is a modified inverse distance-weighting (IDW) scheme of (Simanton and Osborn 1980), where the weights are given by:

$$w_i = \begin{cases} \frac{1}{d_i^b}; & d_i \leq D \\ 0; & d_i > D \end{cases} \tag{19}$$

where, d_i is the distance between a radar pixel and the ith rain gauge, b is an exponent, and n is the total number of gauges within a radius D of a radar pixel.

The density of the gauge network is of concern in the application of this interpolation technique, due to the fact that the error associated with a gauge is applied as a constant value from the gauge location out to a distance defined by the radius of influence. In the case of a sparse network, the radius of influence will be larger, such that the gauge value will have greater influence over large areas. If there is a dense network, the extent of the influence is less, since the resulting radius of influence applied is smaller. To mitigate the extrapolation of a constant value around the gauge, MRMS weights the gauge value with a normal distribution, so that the error estimate tapers off with increasing distance from the gauge up to the radius of influence. For or every radar pixel this value is calculated as:

$$\alpha = \sum_{i=1}^{n} \exp\left(\frac{-d_i^2}{(D/2)^2}\right) \tag{20}$$

where, D is the radius of influence and n is the number of gauges within the radius of D of a radar pixel. When α is greater than 1, there are a sufficient number of gauges used to interpolate that pixel. If α less than 1, the radar estimate at that particular pixel is given the remaining weight. The following equation is the weighting function with α:

$$w_i = \begin{cases} \alpha \times \dfrac{1}{d_i^b}; & d_i \leq D \\ 0; & d_i > D \end{cases} \tag{21}$$

with all the values the same as in Equation (19). Figure (3.9) shows how α decreases with increasing distance.

The values of b and the radius of influence D are found by minimizing the mean squared error (MSE) using a cross validation scheme. Steps for this are:

(1) Initial values of b and D are selected.

(2) Cross validation is done by removing a gauge and interpolating its value using all the remaining radar-gauge errors.

(3) Difference between the interpolated value and the observed value is determined.

(4) After cross validating all gauges, the total cross-validated MSE is calculated.

The values of D can range from 10 km to 500 km in increments of 10 km, and b can vary from 0.5 to 3.0 inch increments of 0.5, resulting in 300 possible combinations. The chosen

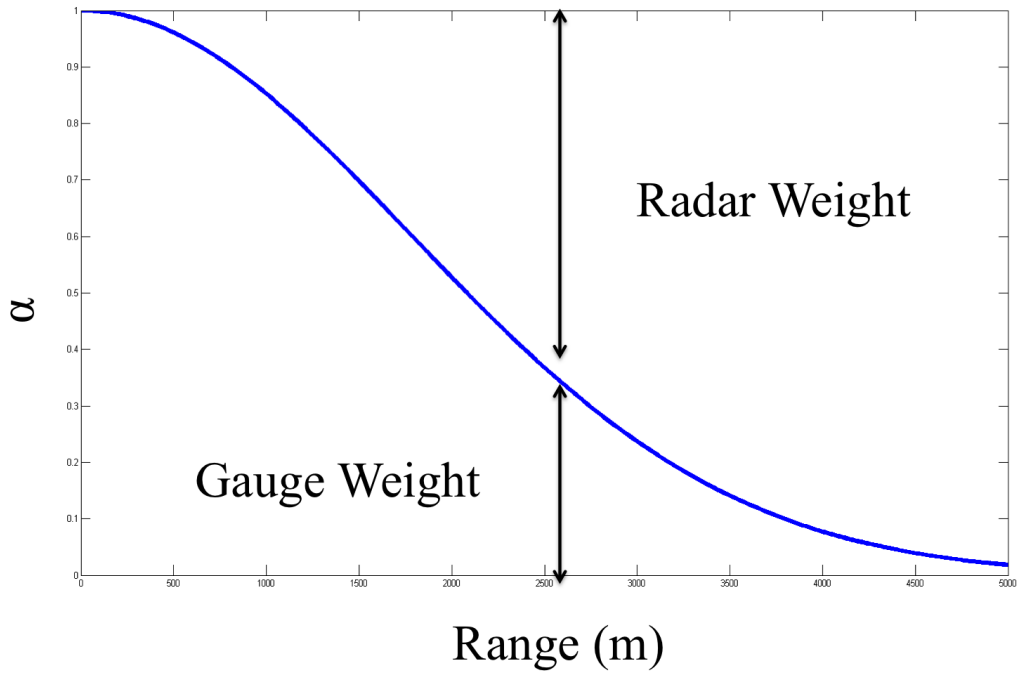

FIGURE 3.9. Normal distribution weighting as a function of distance from the gauge, where the radar QPE is given the remaining weight.

pair of values is determined by the minimization of the MSE. This cross validation scheme is performed every hour and the resulting exponent and radius of influence will differ.

The occurrence of discrepancies in gauge reading due to physical errors produces the necessity for quality control of the gauges, so as to remove faulty reporting, such as unusually high or low gauge readings. If they are found, then these gauges should be flagged and removed. These steps to accomplish are as follows:

(1) For each rain gauge site, find error differences associated with all the surrounding gauges within a 10 km radius.

(2) If 75% or more of the error differences are greater than 5 mm

(3) Remove gauge, else keep.

(4) Cross-validate to find new b and D values.

(5) Repeat step 1, by applying smaller differences of 4 mm, 3 mm and 2 mm.

(6) Terminate if more than 10% of gauges are removed.

3.8.3. Gauge-Only

The gauge-only QPE product follows from the same procedure explained previously section with the exception that there is no adjustment made with the weight of the radar QPE. It is purely based on application of inverse distance weighting on the gauge data and the gauge quality control mechanism.

CHAPTER 4

Evaluation of Multi-Sensor Quantitative Precipitation Estimation in the Russian River Basin

In this section, the challenge of using radar and rain gauges to provide accurate estimates of rainfall in complex terrain is studied. The area of interest is the Russian River basin north of San Francisco, CA, which lies within the National Oceanic and Atmospheric Administration (NOAA) Hydrometeorology Testbed (HMT). Radar reflectivity-rainfall rate (Z-R) relations are traditionally used for quantitative precipitation estimation (QPE). In this complex mountainous terrain, the challenge of obtaining reliable QPE's is hindered by beam blockage and overshooting, as well as orographic enhancement. The effectiveness of several local radars, which include four National Weather Service (NWS) S-band radars and a gap filling C-band TV station radar (i.e., KPIX), are considered for deriving QPE over this region. The precipitation estimation methodologies utilized the Multi-Radar Multi-Sensor (MRMS), also known as National Mosaic & Multi-Sensor QPE (NMQ), algorithms and an independent KPIX only (Z-R) based QPE algorithm. Considering that the radar samples a volume above the ground, the radar-gauge difference can be significantly impacted by beam height, and therefore, a time series analysis of the radar-gauge rainfall measurements is presented to illustrate this variability. The sampling relative to precipitation vertical structure is also considered in regards to the depth of the precipitation and the height of the bright band. The quantitative evaluation of different QPE products is presented.

The estimation of rainfall rate and accumulation is one of the important applications of weather sensing radars (Bringi and Chandrasekar 2001; Cifelli and Chandrasekar 2013). In complex terrain like the Russian River basin (Figure 4.1), even if a perfect empirical Z-R

relation can be applied, the accuracy of rain rate estimates is dependent upon factors such as radar calibration, ground clutter, vertical profile of reflectivity (VPR), signal attenuation, beam blockages, bright bands and anomalous propagation, etc. (Zhang et al. 2011; Kitzmiller et al. 2011; Fulton et al. 1998; Kitchen et al. 1994). The Russian River basin is situated between the Mayacamas mountain range to the east and Coastal mountains to the west where low-level elevation radar coverage from National Weather Service (NWS) Next Generation Weather Radar (NEXRAD) over this area is not possible (Maddox et al. 2002). A gap filling non-NEXRAD radar (hereafter referred to as KPIX) that provides improved coverage over the basin is also considered for the purposes of quantitative precipitation estimation (QPE). KPIX is a C-band, single polarization radar owned and operated by a commercial broadcast station and, although KPIX is not part of the NEXRAD network, the broadcast station has made KPIX data freely available to NOAA.

This study has two goals. The first is to determine the best QPE in this region using the suite of products generated by the Multi-Radar Multi-Sensor (MRMS), also known as National Mosaic & Multi-Sensor QPE (NMQ) algorithm package, which is developed by the National Severe Storms Laboratory (NSSL; Zhang et al. 2011), in a coastal region with poor radar coverage. Secondly, evaluate the KPIX contributions to QPE in this region. Kitzmiller et al. (2011) evaluated MRMS QPE over the Tar-Pamlico River basin of North Carolina eastern coastal region using only NEXRAD input for hydrological forecasting where it was shown to give good performance in regards to reference gauges. The current study looks to evaluate MRMS QPE products over the Russian River basin using NEXRAD radar input with and without KPIX and then with KPIX only. The use of these radar input combination is chosen to establish the relative impact of NEXRAD and gap-filling radars on QPE in this region. Resulting QPE performance is evaluated with 9 independent validation

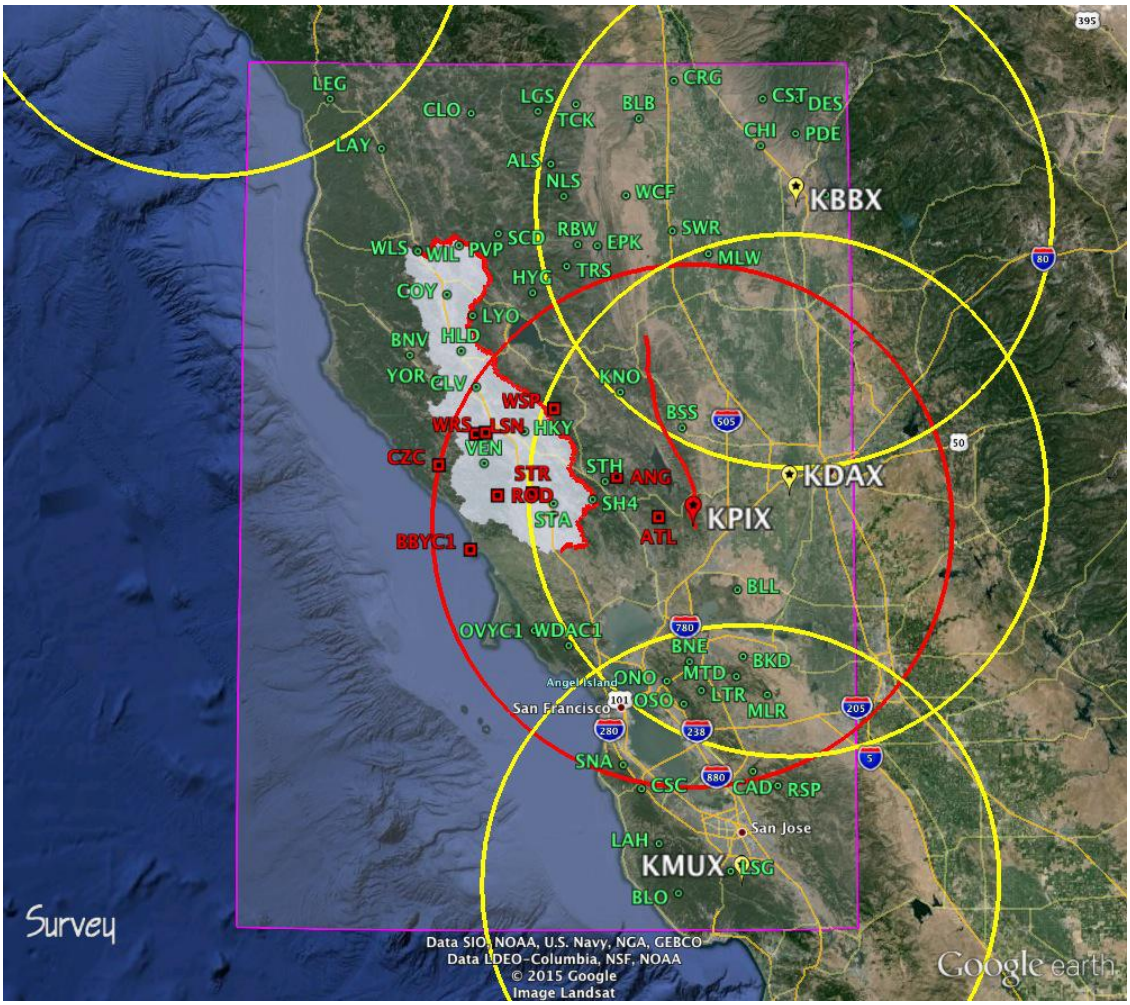

FIGURE 4.1. Area of analysis is indicated by rectangular area, and the Russian River basin is shaded in white. The four local NEXRAD radars (yellow) and C-band radar KPIX (red) are shown with 100km range rings. The analysis and validation gauge locations are designated by green circles and red squares respectively.

gauges, such that validation gauges are also referred to as independent gauges in this paper. Rainfall in this analysis consists of cool season mostly stratiform events occurring over 27 days in 2013 and 2014. The accumulation periods of significance are the 1 hour in regards to flash flooding impacts and the 6 hour to allow for comparison with River Forecast Centers (RFC) QPE products.

Currently the NWS California Nevada River Forecast Center (CNRFC) does not utilize radar information to produce the Mean Areal Precipitation used to drive the NWS River

Forecast System (NWSRFS) for the Russian River. It uses only rain gauge data and rainfall climatology in a procedure called Mountain Mapper, which is equivalently know as the Parameter elevation Regressions on Independent Slopes Model (PRISM; Schaake et al. 2004). This paper attempts to evaluate the benefits of a combined radar-gauge system to produce 6 hour QPEs that could be input to NWSRFS. It should also be noted that most of the NWS RFCs east of the Rockies utilize radar information via the MPE (Multi-Sensor Precipitation Estimator) software to provide the "Best Estimate" of hourly QPE for ingest by the RFC's client NWS Weather Forecast Offices to improve the Flash Flood Monitoring and Prediction (FFMP) software used for flash flood forecasting via high resolution (1 km by 1 degree by 5 min) gridded QPE (Kitzmiller et al. 2011). Thus being able to improve both the 6 hour QPEs and 1 hour QPEs over current gauge-only methods in the western US and would have direct impact on main-stem river flood forecasts and local flash flood forecasts.

4.1. Quantitative Precipitation Estimation Packages and Products

Off-line versions of both MRMS and Multi-sensor Precipitation Estimator (MPE) were setup at the NOAA Earth System Research Laboratory (ESRL) for retrospective QPE analyses. Both systems have been described previously in the literature (for MRMS, see Zhang et al. 2011; for MPE, see Lawrence et al. 2003; Seo et al. 2013). MPE data was only available for a subset of the rain events described; therefore, the main focus of this study is on evaluating the performance of MRMS with and without the impact of a local gap filling radar in this region. When available, MPE was used as a proxy for Mountain Mapper since the ESRL version of MRMS does not include Mountain Mapper and the MPE gauge-only QPE (i.e., Gmosaic) uses PRISM climatology in a similar fashion to the Mountain Mapper technique.

4.1.1. MRMS System Description

The MRMS system has been described extensively in the literature (e.g., Zhang et al. 2011) and only salient points with regard to the present analysis are provided herein. MRMS is a distributed computing architecture with four major processing components. These system sections consist of 1) single radar processing, 2) two and three dimensional radar mosaics, 3) next-generation QPE (Vasiloff et al. 2007), and 4) Evaluation. Data system input sources comprise of level-2 radar data from NEXRAD, Rapid Update Cycle (RUC) model hourly analyses (Benjamin et al. 2004), lightning data, and Hydrometeorological Automated Data System (HADS) and regional rain gauge networks.

4.1.2. MRMS Products of Interest: gauge-only, radar-only, radar VPR and gauge correction

Once the precipitation type has been identified and the 2-D hybrid scan reflectivity fields are mosaicked using a weighting algorithm to account for both distance and height of the radar beams from different radars, the QPE is then calculated based on the methodologies described in Zhang et al. (2011). The mosaicked field has a spatial resolution of 1 km by 1 km and an update time of 2.5 minutes. The QPE fields in MRMS include radar-only, radar-only with VPR correction, radar with VPR and gauge correction, and gauge-only QPE. MRMS produces these rainfall products based upon the availability of input data. One hour and 3 hour accumulations are calculated every 5 min, and the 6, 12, 24, 48 and 72 hour accumulations are aggregated from 1 hour accumulations. QPE results are calculated from radar reflectivity resulting from all quality control mechanisms, mosaicking technique, and the appropriate identification of precipitation type (Zhang et al. 2011). The implementation of dual polarization rainfall algorithms within MRMS is still under evaluation. Therefore the

MRMS radar-only QPE is only capable of rainfall rate from the measured reflectivity where the radar-only with the VPR correction computes the QPE from the corrected reflectivity and the default Z-R for stratiform type rainfall ($Z = 200R^{10.6}$), which in this study was replaced by the Z-R coastal mountain non-bright band rain relation given by Martner et al. (2008) and applied by Zhang et al. (2012):

$$Z = 44R^{1.91} \tag{22}$$

where Z is in $mm^6\ m^{-3}$, R is in $mm\ hr^{-1}$.

The local gauge correction is constructed based upon the technique described in Ware (2005). One of the major challenges encountered with radar rainfall estimation is attempting to derive QPE from radar reflectivity observations for areas where such observations are enhanced by melting ice particles to form the so-called bright band. In order to have an efficient real-time application for bright band correction that MRMS can depend upon, the approach taken to determine the VPR combines two methods. First is to calculate the mean volume scan VPR (Vignal et al. 2000) and second to model an idealized VPR model from the mean values (Zhang et al. 2008).

4.2. Data Set

Data in this analysis stems from a combination of operational radar and gauge observations as well as data from the NOAA Hydrometeorology Testbed (HMT) in the Russian River basin north of San Francisco, CA. Twenty-seven days of rainfall data occurring during the months of March, November and December of 2012 and February of 2014 are considered. The 27 days occurred during the following rain events: March 14-16, March 27-28,

November 17-21, November 28-30, December 1-6, December 20-23 of 2012, and February 7-9 of 2014: Dominant precipitation in this region during the cool season is a stratiform rainfall (Matrosov et al. 2014) with radar bright band heights ranging from about 1.5 km to 2.5 km above the mean sea level (MSL) as observed by the NOAA S-band profiler located at Santa Rosa, CA (STR, see Figure 4.1). Bright band heights for each day are shown in Table 4.1.

TABLE 4.1. Russian River Bright Band Heights

Date (YYYYMMDD)	BB height (m)
20120314	2000
20120315	2000
20120316	2000
20120327	1500
20120328	1500
20121116	NA
20121117	2250
20121118	2000
20121119	NA
20121120	2250
20121121	2250
20121128	2000
20121129	2000
20121130	2000
20121201	NA
20121202	2250
20121203	NA
20121204	2500
20121205	2500
20121206	NA
20121220	2000
20121221	2000
20121222	1250
20121223	1500
20140207	1500
20140208	2500
20140209	2250

Bright band (BB) heights observed by the NOAA S-band Profiler located near Santa Rosa, CA (STR) located (32.8515 degree, -122.8022 degree) at an elevation of 32 m (above MSL). NA indicates that data were not available for this date.

MRMS rain gauge input consists of 57 gauges (hereafter referred to as analysis gauges - see Table 4.2) which are a combination of California Data Exchange Center (CDEC) gauges,

NWS HADS gauges, and the NOAA HMT gauges (green dots in Figure 4.1). The set of analysis gauges serve as input into the MRMS over the NOAA HMT West Domain surrounding the Russian River basin. Validation gauges are comprised of 9 independent gauges consisting of CDEC, HADS and HMT gauges (red squares in Figure 4.1 and listed in Table 4.3). Prior to MRMS gauge processing, a QC algorithm is performed on the analysis gauges to remove uncertain gauge values (Zhang et al. 2011). For the independent gauge selection, an attempt has been made to achieve a balance of high and low elevations and a range of distances to the KPIX radar, where the gauge heights are indicated by the blue bars in Figure 4.2 relative to the beam heights and beam widths for each radar. The QC process for the validation gauges comprised of cross correlating with each other and visually identifying and removing outlying gauge values.

MRMS radar input data comprises the surrounding NEXRAD radars (KMUX, KDAX, KBHX, and KBBX) with the addition of the TV station radar, KPIX shown in Figure 4.1 with 100 km range rings. The NEXRAD radars are conducting volume scans in precipitation mode and delivering observations updated every five to six minutes, whereas the KPIX radar primarily operated in a single scan mode with an update every one minute. To gain insight into KPIX radar calibration, a common volume that occurs between the NEXRAD KDAX radar at 1.38 degree elevation and 182.8 degree azimuth and the KPIX radar at 0.5 degree elevation and 142.4 degree azimuth at a range of 56 km from both radars was selected for a 6 hour rain event occurring March 17, 2012. The mean difference in reflectivity was found to be 2.2 dBZ for measurements greater than 15 dBZ, such that KPIX is slightly underestimating compared with KDAX radar.

In addition, an analysis of beam blockage over the validation gauges is performed for the KPIX and NEXRAD radars. KDAX provides the lowest NEXRAD unobstructed scan

Table 4.2. HMT West Russian River MRMS Analysis Gauges

Station ID	Latitude	Longitude	Altitude (m)	Location from CDEC database
ADS	39.6500	-122.7250	1372	ALDER SPRINGS NEAR ELK CREEK
ANG	38.5710	-122.4340	553	ANGWIN
ATL	38.4330	-122.2500	506	ATLAS PEAK
BKD	37.9500	-121.8840	488	BLACK DIAMOND MINES
BLB	39.8080	-122.3290	130	BLACK BUTTE
BLL	38.1801	-121.9069	0	BLACKLOCK (NE1)
BLO	37.1320	-122.1700	802	BEN LOMOND (CDF)
BNE	37.9340	-122.1180	442	BRIONES
BNV	38.9870	-123.3410	256	BOONVILLE
BSS	38.7190	-122.1420	110	BROOKS
CAD	37.5531	-121.8439	347	CALAVERAS ROAD
CHI	39.7120	-121.7830	70	CHICO
CLO	38.8800	-123.0540	453	COVELO
CLV	38.8790	-123.0530	33	RUSSIAN RIVER AT CLOVERDALE
COY	39.1970	-123.1860	219	COYOTE (LAKE MENDOCINO)
CRG	39.9390	-122.1700	90	CORNING AIRPORT
CSC	37.4960	-122.3290	105	CRYSTAL SPRINGS COTTAGE
CST	39.9000	-121.7000	488	COHASSET
DES	39.8720	-121.6100	826	DE SABLA (DWR)
EPK	39.3670	-122.5170	367	EAST PARK RESERVOIR
HKY	38.7270	-122.8400	610	HAWKEYE
HYG	39.2040	-122.8050	1475	HIGH GLADE
JAR	39.7360	-121.4890	823	JARBO GAP
KNO	38.8830	-122.4170	671	KNOXVILLE CREEK
LAH	37.3200	-122.2740	130	LA HONDA
LAY	39.7020	-123.4850	560	LAYTONVILLE
LEG	39.8670	-123.7170	228	EEL RIVER AT LEGGETT
LGS	39.8330	-122.7830	1554	LOG SPRING
LSG	37.2068	-121.9428	197	LOS GATOS
LTR	37.8340	-122.0670	536	LAS TRAMPAS
LYO	39.1250	-123.0710	975	LYONS VALLEY
MLR	37.8170	-121.7790	622	MALLORY RIDGE
MLW	39.3330	-122.0170	26	SACTO R AT MOULTON WEIR (CREST 76.8)
MTD	37.8670	-121.9010	1173	MOUNT DIABLO
NLS	39.5380	-122.6670	1554	NOEL SPRING
ONO	37.8670	-122.2170	457	OAKLAND NORTH
ORO	39.5400	-121.4930	274	OROVILLE DAM
OSO	37.7830	-122.1500	305	OAKLAND SOUTH
PDE	39.7536	-121.6247	533	PARADISE
PVP	39.3670	-123.1330	311	POTTER VALLEY PH
RBW	39.3710	-122.6050	395	RAINBOW DIVERSION DAM
RSP	37.5020	-121.7360	933	ROSE PEAK
SCD	39.4080	-122.9580	551	SCOTT DAM
SH4	38.4920	-122.5330	543	ST. HELENA 4WSW
SNA	37.5790	-122.4090	141	SAN ANDREAS COTTAGE
STA	38.4790	-122.7120	171	SANTA ROSA (CDF)
SWR	39.4172	-122.1825	30	SACRAMENTO NATIONAL WILDLIFE REFUGE
TCK	39.8580	-122.6120	312	THOMES CREEK (CDF)
TRS	39.2960	-122.6540	1219	TROUGH SPRING
VEN	38.6170	-123.0170	384	VENADO
WCF	39.5410	-122.3890	122	SOUTH FORK WILLOW CREEK NEAR FRUTO
WIL	39.3500	-123.3170	587	WILLITS HOWARD RS
YOR	38.9000	-123.2330	335	YORKVILLE

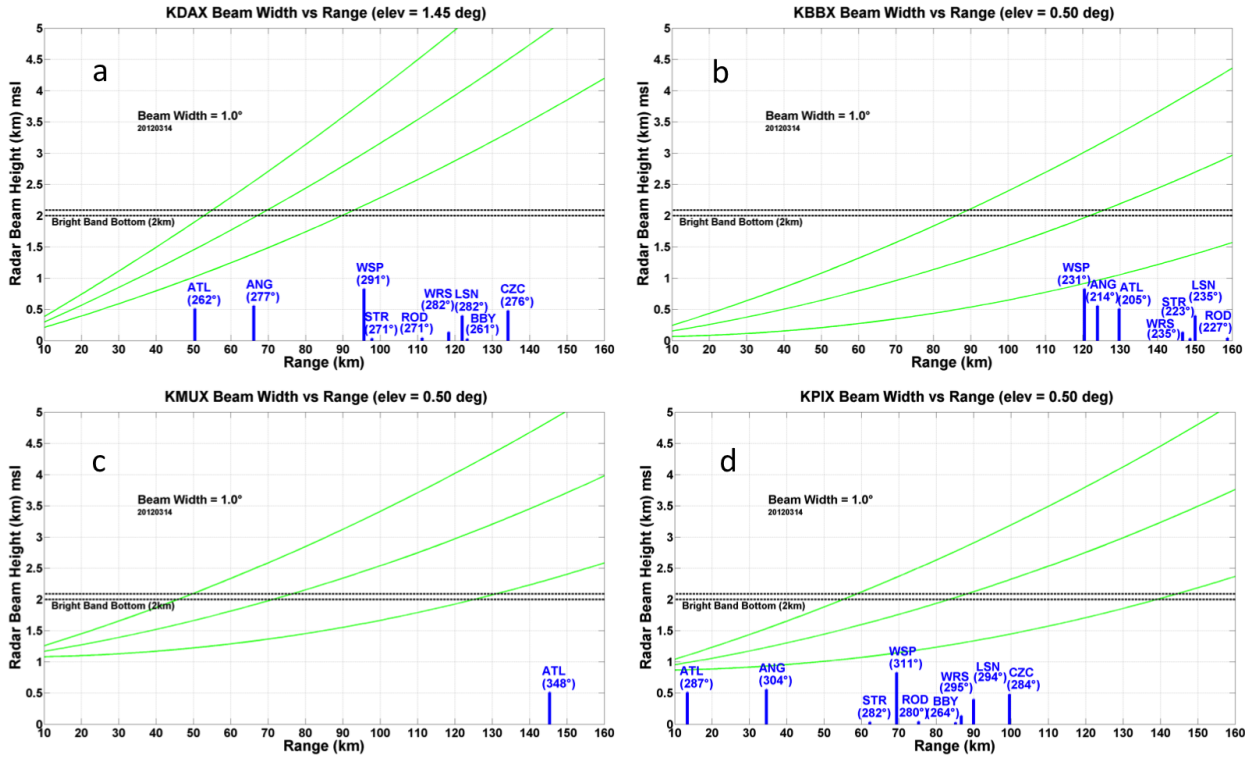

FIGURE 4.2. Lowest minimally blocked upper, center and lower edge beam heights (green lines) for 0.5 degree tilt versus ranges for the radars KMUX, KBBX and KPIX and 1.45 degree tilt for KDAX. The range and azimuth of the validation gauges are shown in blue where the top of the blue line is the height of the gauge above MSL. Bright band height for the March 14, 2014 event is approximately 2 km above MSL and is indicated by the horizontal lines.

over the Russian River valley at 1.45 degree elevation for average atmospheric propagation conditions. Figure 4.3 displays the mountain elevation profile as seen from KDAX and KPIX such that the lowest scan achievable without significant blockage over the validation gauges. The primary blockage from KDAX is due to the Blue Ridge Range as shown in Figure 4.3. The scan at 1.45 degree for KDAX is occluded by these mountain peaks as indicated by the light blue area at a range of 35 km to 55 km and azimuth between 260 and 290 degree in the direction of the Russian River basin, and the scan of the entire basin occurs between

TABLE 4.3. HMT West Russian River Validation Gauges

Station ID	Gauge Network ID	Latitude	Longitude	Altitude (m)	Gauge Type
ANG	ANG	38.5712	-122.4332	553	CDEC
ATL	ATL	38.4330	-122.2500	506	CDEC
BBYC1	BBY	38.3208	-123.0747	24	HADS
CZC	CZC	38.6107	-123.2152	478	HMT
LSNCA	LSN	38.7187	-123.0537	368	HMT
RODCA	ROD	38.5073	-122.9565	40	HMT
STR	STR	38.5154	-122.8022	34	HMT
WRSCA	WRS	38.7230	-123.0100	134	CDEC
WSPC1	WSP	38.8058	-122.7083	823	CDEC

Validation gauges are not used in MRMS processing, but are used to measure performance of various analysis methods. Station IDs ending in 'C1' are part of the National Weather Service Local Indicators (NWSLI) database.

255 and 330 degrees in azimuth. KPIX radar is situated at an elevation of 860 m and has a nearly unobstructed view of the basin and is minimally blocked by two high peaks of the Mayacamas Mountain Range (Figure 4.3) at 0.0 degree elevation scan, and is unblocked at a scanning elevation of 0.5 degree. KPIX scans over the Russian River basin between 260 and 340 degrees in azimuth. The relative validation gauge heights and direction are shown in blue.

4.3. Evaluation

Comparison of QPE's is performed on a pixel-by-pixel manner. The MRMS QPE products are output onto a gridded map in 0.01 degree latitude by 0.01 degree longitude lengths which is approximately 1.11 km N-S and 0.87 km E-W. Accumulations from the validation gauges are interpolated to the same MRMS grid to facilitate comparisons between the gauge amounts and the MRMS derived QPE. The validation gauge QPE is derived from an inverse distance weighting (IDW) scheme and is calculated using Equations (23) and (24) (Simanton and Osborn 1980),

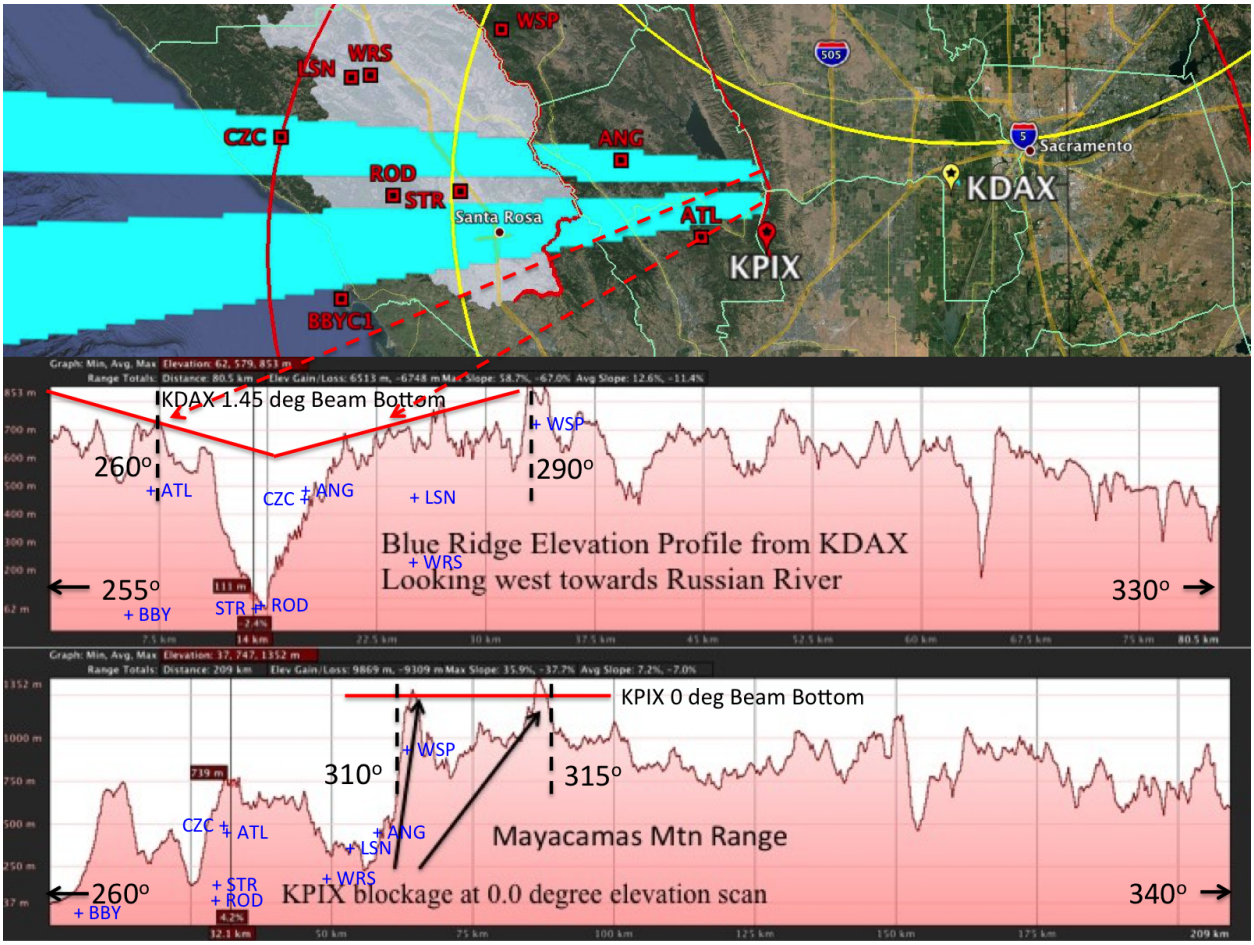

FIGURE 4.3. Mountain elevation profiles as seen from KDAX and KPIX. Light blue indicates KDAX beam blockage at 1.45 degree tilt where the red squares show validation gauge locations. KDAX beam bottom (red solid line) at 1.45 degree tilt in direction of the Russian River basin and the beam bottom for KPIX at 0.0 degree, here the blue crosses give relative direction and height of validation gauges.

$$F(x,y) = \sum_{i=1}^{n} w_i f_i \tag{23}$$

$$w_i = \frac{\frac{1}{d_i^b}}{\sum_{i=1}^{n} \frac{1}{d_i^b}} \tag{24}$$

where f_i denotes gauge value, b is a power parameter, d_i is distance from interpolation point to gauge i, and i is the gauge number. In this paper, $b = 2$ and $d = 0.5$ km radius of influence is used, such that the distance for the radius of influence extrapolates the gauge point value over the approximate area of a single radar pixel and provides a more representative comparison between QPE products and validation gauge measurements.

In addition to the MRMS QPE products, statistics are also calculated for a "Simple KPIX" QPE field. This QPE is calculated using the Martner Z-R relationship in Equation (22) that was determined best suited for non-bright band rainfall in northern California coastal regions (Martner et al. 2008) and that MRMS employs this relation for this particular region. This QPE technique determines rainfall rate from reflectivity and, because it uses only one radar and no rain gauge data, has the advantage of avoiding the complexity involved in generating QPE in the MRMS system. For Simple KPIX, the KPIX radar reflectivity measurements are gridded to a 0.01 degree lat-lon grid covering the domain of interest accounting for the earth's non-sphericity. The rainfall rates are then calculated, and the QPE hourly amounts are obtained by accumulating rainfall rates from each consecutive scan where each scan typically occurs every minute. The majority of KPIX radar scans are conducted at an elevation angle of 0.5 degree with a few at 0.0 degree, but for this non-MRMS KPIX only QPE method only 0.5 degree elevation measurements are used.

Statistics of interest for this study include the normalized mean bias (NB), normalized standard error (NSE), root mean square error (RMSE), and the correlation coefficient (CC), which are calculated by comparing the common grid points between the MRMS QPE fields and the validation gauge QPE fields. These equations are:

$$NB = \frac{\langle R_R - R_G \rangle}{\langle R_G \rangle} \tag{25}$$

$$NSE = \frac{\langle |R_R - R_G| \rangle}{\langle R_G \rangle} \tag{26}$$

$$RMSE = \sqrt{\langle (R_R - R_G)^2 \rangle} \tag{27}$$

$$CC = \frac{\sum \left[(R_R - \langle R_R \rangle)(R_G - \langle R_G \rangle) \right]}{\sqrt{\sum (R_R - \langle R_R \rangle)^2} \sqrt{\sum (R_G - \langle R_G \rangle)^2}} \tag{28}$$

where R_R is the QPE estimate, R_G is the validation gauge measurement, and the angle brackets stand for the sample average.

In order to minimize the errors introduced from miniscule rainfall amounts, a threshold criterion was used to ensure the statistics were representative of consistent rainfall accumulating events. For each hour of rainfall accumulation measurements for the 9 validation gauges, the sum of the hourly totals over a 6 hour period must exceed a threshold of 2 mm (approximately 0.08 inch). As shown in Figure 4.4, the MRMS products versus validation gauge show high normalized standard error at measurements of rainfall below 2 mm per 6 hrs. The right plots in Figure 4.4b and Figure 4.4d show the same data, but with the estimates below 2 mm removed.

4.4. Results and Discussion

The QPE evaluation consists of two components: evaluate the impact of KPIX in the lower Russian River basin and determine which QPE methodology produces the best QPE in this region. An evaluation of KPIX was conducted to quantify the impact of using this radar data for QPE since, as noted above, the nearest NEXRAD (i.e., KDAX) is severely blocked at low elevations (below 1.45 degree) over the Russian River watershed in Sonoma County

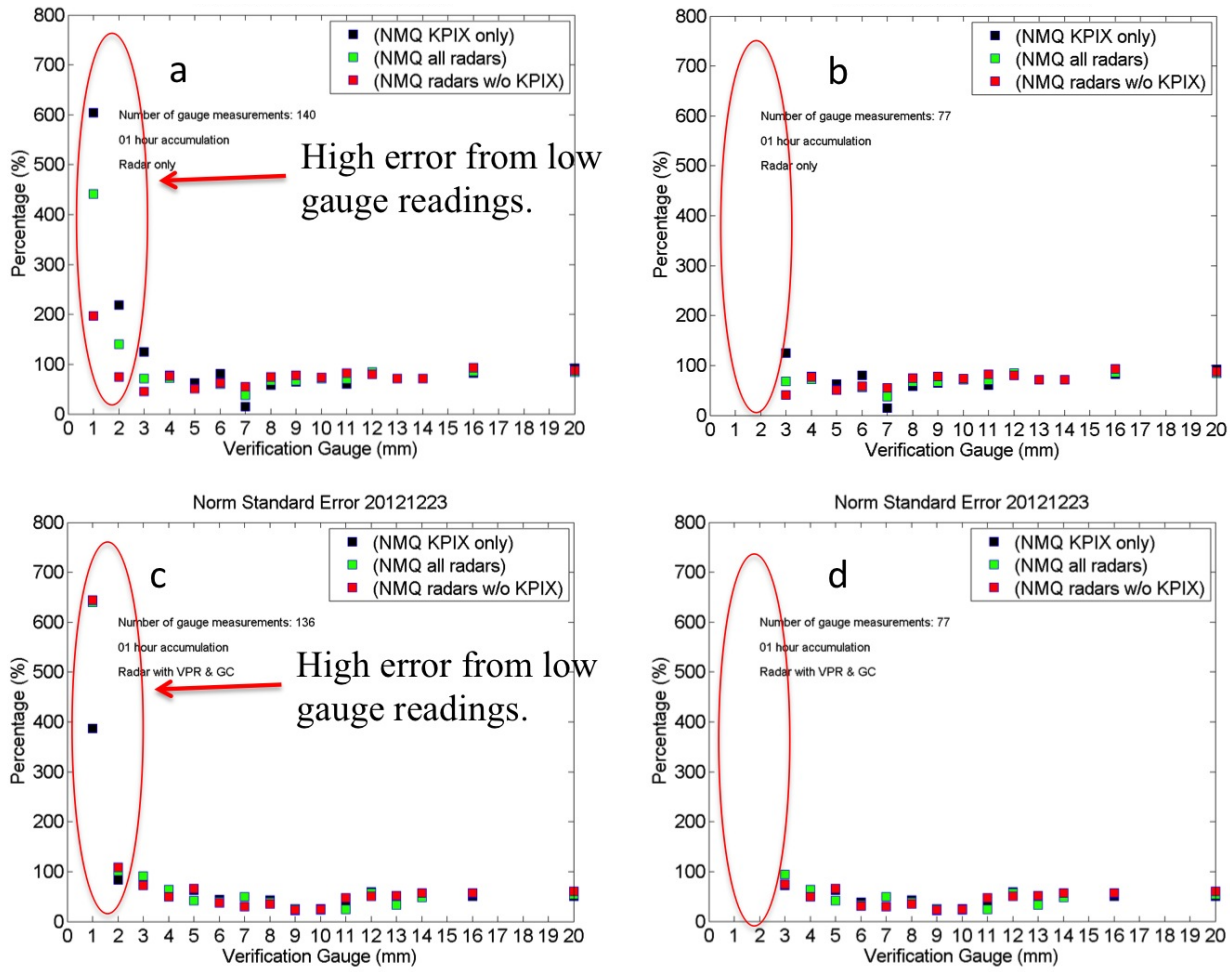

FIGURE 4.4. Normalized Standard Error (%) versus validation gauge amounts for 1 hour accumulation on December 23, 2012. (a) and (c) are errors without applying a threshold. (b) and (d) show errors after threshold. MRMS radar-only product (a) and (b). MRMS with VPR and gauge correction products is shown in (c) and (d).

and both KMUX and KBBX NEXRAD are sampling well above the bright band (see Figure 4.2). As noted above, KPIX is located on Mt. Vaca (elevation of 860 m above MSL) and has an unobstructed view of the precipitation in this area. Assuming KPIX is well calibrated and attenuation at C-band is not severe, it is anticipated that KPIX data would produce the best radar-based QPE for the validation gauges shown in Figure 4.1. Vertically pointing S-band profiler (STR) data indicates bright band height near the Russian River watershed. An example is presented in Figure 4.5, which shows a time-height section of precipitation

over the S-band profiler at Santa Rosa from 00Z on December 21, 2012 through 00Z on December 23, 2014. Figure 4.5 also shows the height of the KPIX beam at 0.0 degree and 0.5 degree in regards to the bright band observed height, and the NEXRAD radar KDAX beam height at 1.3 degree.

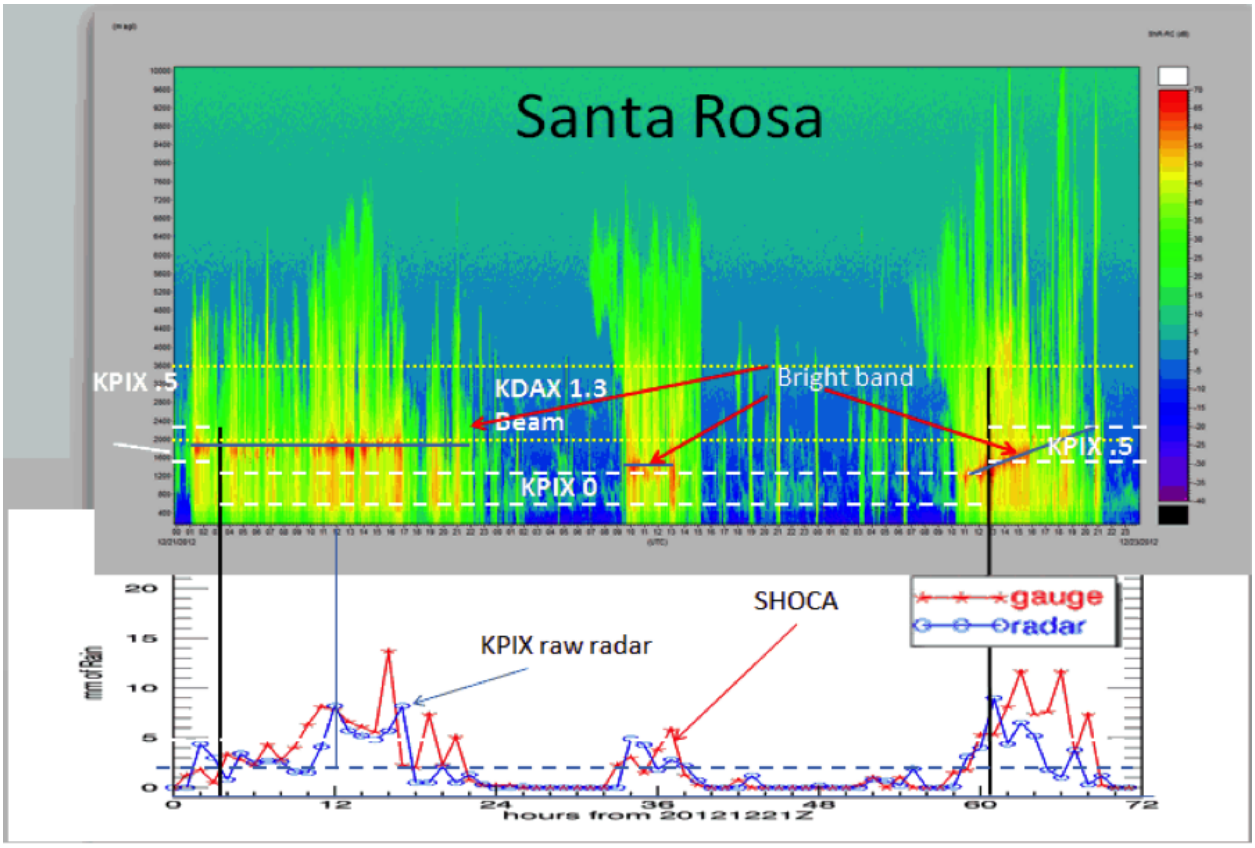

FIGURE 4.5. (top) Time series of Santa Rosa S-Prof measured reflectivity (dB) from 00Z on 21 Dec to 00Z on 23 Dec 2012. Horizontal lines (Blue) indicate height of the melt level and thus where the radar would detect the bright band if sampling at that level. Width of KDAX 1.3 degree beam (lowest unblocked beam) and the KPIX 0.5 and 0.0 degree beam are annotated (dashed white). Corresponding time series of rain accumulation from the gauge at SHOCA, which is nearest the Santa Rosa S-Prof, is plotted along with MRMS KPIX-only radar-only estimated hourly rainfall.

A visual assessment of low elevation reflectivity scans from KPIX and KDAX can be seen in Figure 4.6. This example illustrates the ability of KPIX for sensing incoming precipitation across Sonoma County as well as beam blockage suffered by KDAX.

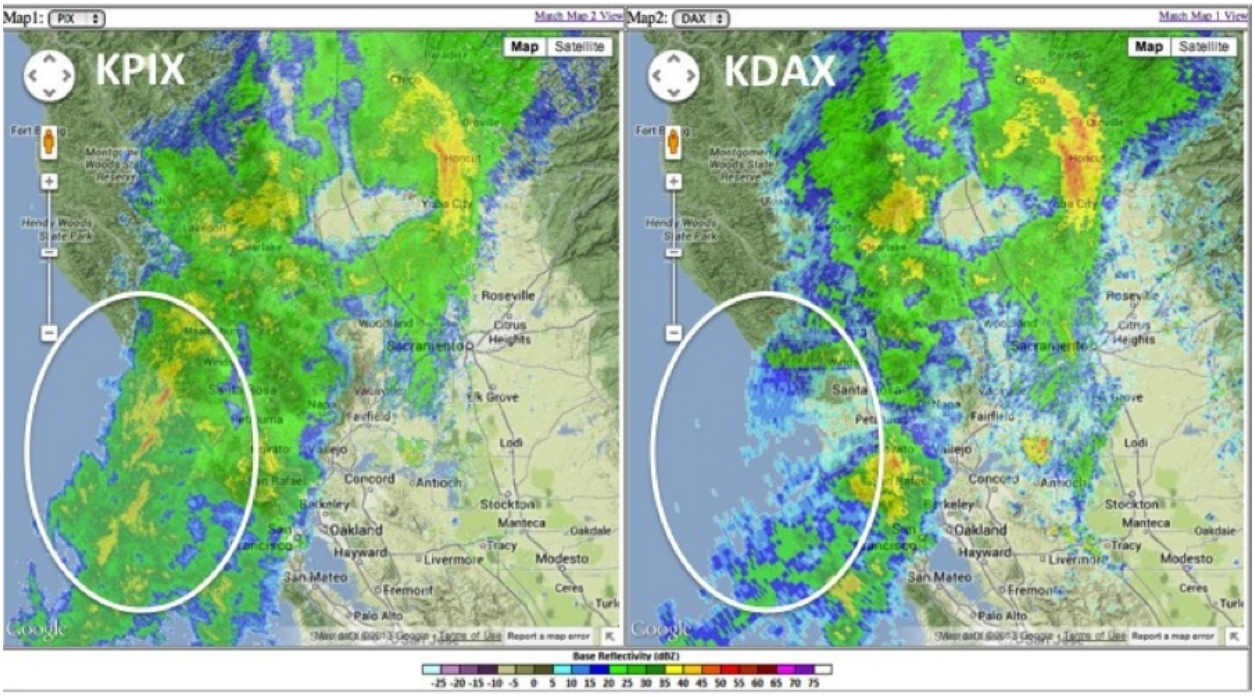

FIGURE 4.6. Image shows 14:48Z 21 Dec 2012 radar reflectivity with KPIX on the left scanning at 0.0 degrees with KDAX 0.5 degree reflectivity scan on the right. Note the significant difference in reflectivity for the heavy rainfall moving into the Sonoma Coast (region indicated by ellipse). It should be noted that higher elevation scans from KDAX would have observed this band but well up above the freezing level. However without gauges offshore and without an accurate VPR correction, KDAX would underestimate precipitation rates moving onshore.

To quantitatively evaluate the impact of KPIX and determine which method of generating QPE is best, several different QPE grids representing radar-only, gauge-only, and combination of radar and gauge correction were generated. The 1, 3, and 6 hour comparisons of QPE with the validation gauges for normalized mean bias, normalized standard error, correlation coefficient, and the root mean square error are shown in Figure 4.7. The numerical results for all four statistics are given in Table 4.4.

The MRMS QPE to the validation gauge comparisons are conditioned on the KPIX beam sampling below the bright band (BB) and the validation gauge observing more than 2 mm of precipitation in a six hour period where the choice of Z-R is appropriate for non-bright band

TABLE 4.4. MRMS Statistical Results for QPE Products

Hr Accum	MRMS Product	MRMS Radar Input	RMS Error (mm)	CC (%)	NB (%)	NSE (%)
1	gauge-only	KPIX Only	3.05	40	-32.74	63.06
1	gauge-only	NEXRAD + KPIX	3.43	42	-36.12	62.33
1	gauge-only	NEXRAD Only	3.47	40	-34.86	62.78
1	Radar only	KPIX Only	4.19	18	-6.70	72.55
1	Radar only	NEXRAD + KPIX	4.61	25	-5.57	72.71
1	Radar only	NEXRAD Only	4.96	20	2.68	78.20
1	Radar with VPR	KPIX Only	3.70	24	-23.59	68.13
1	Radar with VPR	NEXRAD + KPIX	4.33	27	-22.08	66.87
1	Radar with VPR	NEXRAD Only	4.04	31	-20.62	66.36
1	Radar with VPR & GC	KPIX Only	2.82	49	-19.52	56.36
1	Radar with VPR & GC	NEXRAD + KPIX	3.14	50	-20.27	56.51
1	Radar with VPR & GC	NEXRAD Only	3.17	49	-18.00	56.36
1	Non-MRMS Product (Simple KPIX QPE)	KPIX Only	3.22	55	-41.80	63.47
3	gauge-only	KPIX Only	6.77	58	-32.56	57.68
3	gauge-only	NEXRAD + KPIX	7.72	59	-36.70	58.09
3	gauge-only	NEXRAD Only	7.65	59	-35.01	58.65
3	Radar only	KPIX Only	8.42	38	-19.60	63.55
3	Radar only	NEXRAD + KPIX	9.42	40	-16.62	64.38
3	Radar only	NEXRAD Only	9.26	42	-11.98	66.75
3	Radar with VPR	KPIX Only	7.94	46	-34.47	61.43
3	Radar with VPR	NEXRAD + KPIX	8.91	46	-31.38	60.48
3	Radar with VPR	NEXRAD Only	8.38	52	-32.12	59.83
3	Radar with VPR & GC	KPIX Only	5.96	66	-18.72	49.47
3	Radar with VPR & GC	NEXRAD + KPIX	6.87	65	-21.08	50.52
3	Radar with VPR & GC	NEXRAD Only	6.72	66	-19.53	50.90
3	Non-MRMS Product (Simple KPIX QPE)	KPIX Only	7.59	63	-40.55	60.08
6	gauge-only	KPIX Only	10.83	64	-34.36	53.96
6	gauge-only	NEXRAD + KPIX	12.43	65	-38.70	55.77
6	gauge-only	NEXRAD Only	12.22	65	-36.78	55.76
6	Radar only	KPIX Only	12.98	44	-25.76	59.54
6	Radar only	NEXRAD + KPIX	14.85	44	-21.93	59.70
6	Radar only	NEXRAD Only	14.19	47	-19.76	61.64
6	Radar with VPR	KPIX Only	12.73	50	-39.93	58.71
6	Radar with VPR	NEXRAD + KPIX	14.43	49	-35.74	58.30
6	Radar with VPR	NEXRAD Only	13.51	57	-36.93	57.95
6	Radar with VPR & GC	KPIX Only	9.24	71	-20.16	44.59
6	Radar with VPR & GC	NEXRAD + KPIX	10.70	71	-23.05	46.64
6	Radar with VPR & GC	NEXRAD Only	10.37	71	-20.76	45.36
6	Non-MRMS Product (Simple KPIX QPE)	KPIX Only	12.52	66	-40.87	56.77

MRMS QPE products and Simple KPIX QPE for 1, 3, and 6-hour accumulation period showing the RMS error, correlation coefficient, normalized mean bias, and normalized standard error. MRMS products are gauge-only, radar-only, radar with VPR, and radar with VPR and gauge correction.

conditions. The conditioning means that comparisons between QPE products and validation gauges occur only when the top of KPIX beam is below the bright band (Figure 4.2) at the

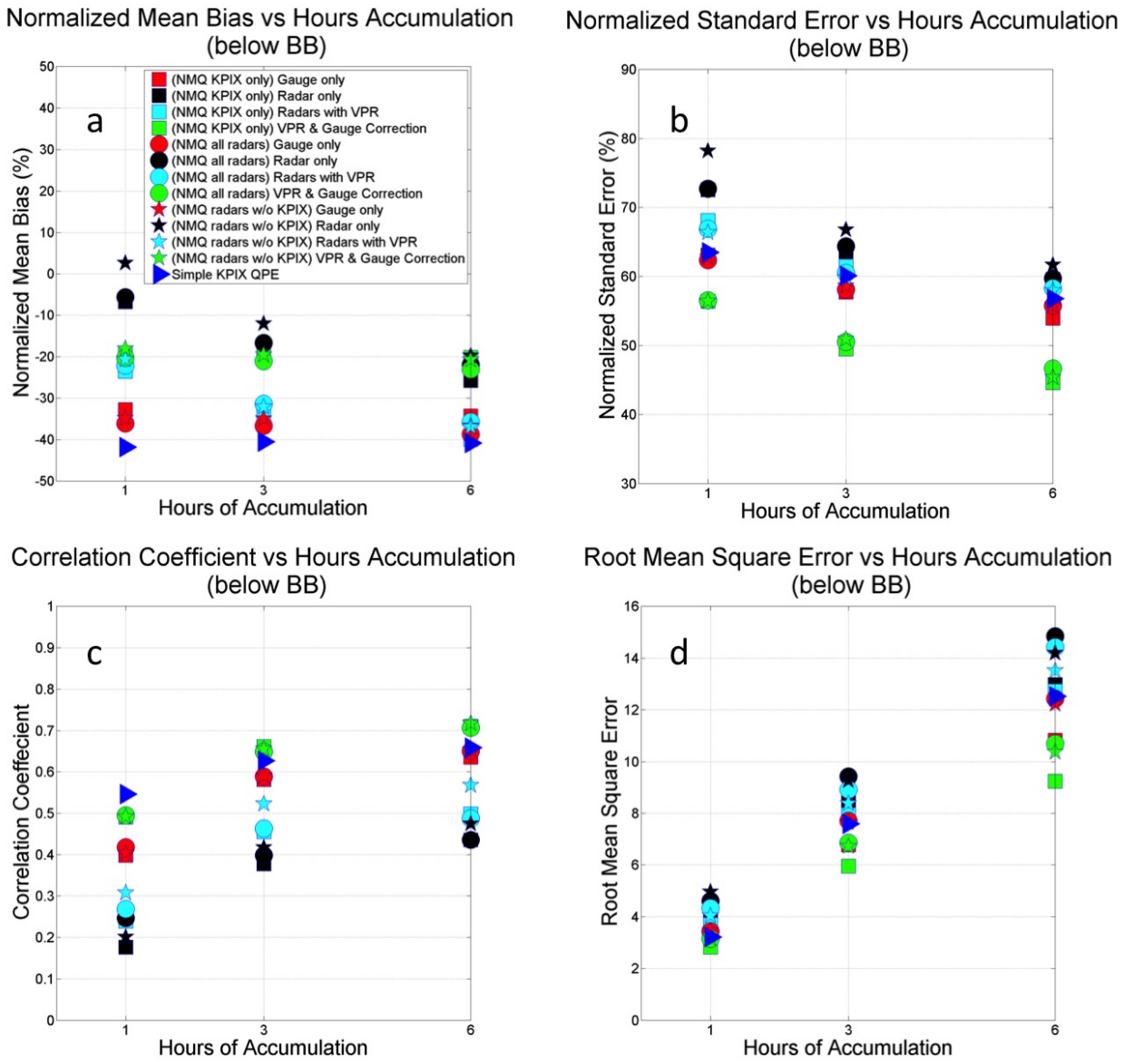

FIGURE 4.7. 1, 3, and 6 hour statistics for MRMS QPE products and Simple KPIX QPE considering below the bright band. Normalized mean bias is shown in (a), normalized standard error in (b), correlation coefficient in (c) and the root mean square error in (d). QPE products are indicated by color black is radar-only, red is gauge-only, green is radar with VPR and gauge correction, and blue is Simple KPIX. MRMS radar input is designated by shape where squares are KPIX only, circles are NEXRAD with KPIX, stars are NEXRAD only, and triangle is Simple KPIX.

location of each validation gauge. Sampling below the BB (i.e., rain region see Figure 4.2) is anticipated to show the biggest impact of KPIX for QPE performance. The primary metrics of measurement are the normalized bias and the normalized standard error. This is

done to show the percentage differences between the radar and gauge pairs. The additional metrics of correlation coefficient and root mean square error are provided and give additional information regarding the QPE performance. It should be noted that in the MRMS code used for this retrospective analysis, the observed rainfall from the analysis gauges for the hour is used for bias correcting the radar analysis for that hour. Operationally this would not be possible, as not all the gauges report on an hourly basis with rainfall computed at the top of each hour. This provides a significant advantage to the gauge bias correction scheme for MRMS. Figure 4.7 also includes the "Simple KPIX" analysis for comparison.

In general, the normalized mean bias (Figure 4.7a) shows that, for below the BB, almost all the methods underestimate QPE with respect to the validation gauges for the 1 to 6 hour accumulation periods. Figure 4.7a also indicates that for each MRMS product group (e.g., radar-only QPEs), the biases tend to be within close proximity of one another, which gives the sense that varying radar input doesn't alter the bias significantly. For one hour accumulations, the MRMS radar-only QPE shows the least amount of bias in comparison to the MRMS QPE with VPR and gauge correction and the MRMS gauge-only products, however the radar-only also show low correlation (Figure 4.7c). An example of the data scatter for 1 hour accumulation of the MRMS QPE products and the Simple KPIX QPE is seen in Figure 4.8 when driven by KPIX only radar input. The radar-only bias slightly increases (becomes more negative) as the accumulation period increases and is essentially the same as the VPR and gauge correction QPEs at the 6 hour accumulation period. For the other statistics, MRMS radar-only gives the highest error for all products (poorest performance). The Simple KPIX QPE produces the greatest negative bias and is much larger than the MRMS KPIX QPE, but at the same time shows good correlation results.

Although a VPR correction was not anticipated to impact QPE for locations below the BB, the results show that the MRMS radar with VPR correction (Figure 4.7a, Table 4.4) decreases (i.e., makes worse) the negative bias; however, the VPR correction slightly decrease (i.e., improves) the normalized standard errors (Figure 4.7b) and other statistics over radar-only. The larger bias with VPR is most likely due to the fact the MRMS software is using the Rapid Update Cycle (RUC) model analysis of freezing level instead of the S-Profiler (STR) observed freezing level, where the height used for correction maybe lower than the direct profiler observations. Additional analysis is needed to verify this hypothesis but is beyond the scope of this study.

Considering the normalized absolute error for these same products (Figure 4.7b), the best performance is seen in the MRMS with VPR and gauge correction, and there is very little difference in performance among the products with different radar input. The VPR and gauge correction QPE also performed best in terms of correlation coefficient (Figure 4.7c) and for RMS error (Figure 4.7d) over the range of accumulation periods.

MRMS gauge-only products provide the second best performance overall. However, these products have a large consistent negative bias in 1, 3, and 6 hour accumulation QPE, which is also somewhat surprising given the location of several analysis gauges in the Russian River basin (Figure 4.1). The gauge bias is explored in more detail below. The results for NSE show similar trends to the correlation coefficient and to the root mean squared error (Table 4.4).

In order to understand and interpret the large bias given by the MRMS gauge-only results in reference to the validation gauges (Figure 4.7a, 35-40% negative bias), a non-MRMS gauge bias analysis between the MRMS input gauges and validation gauges (i.e., the green and red gauges in Figure 4.1, respectively) was conducted. This approach calculates

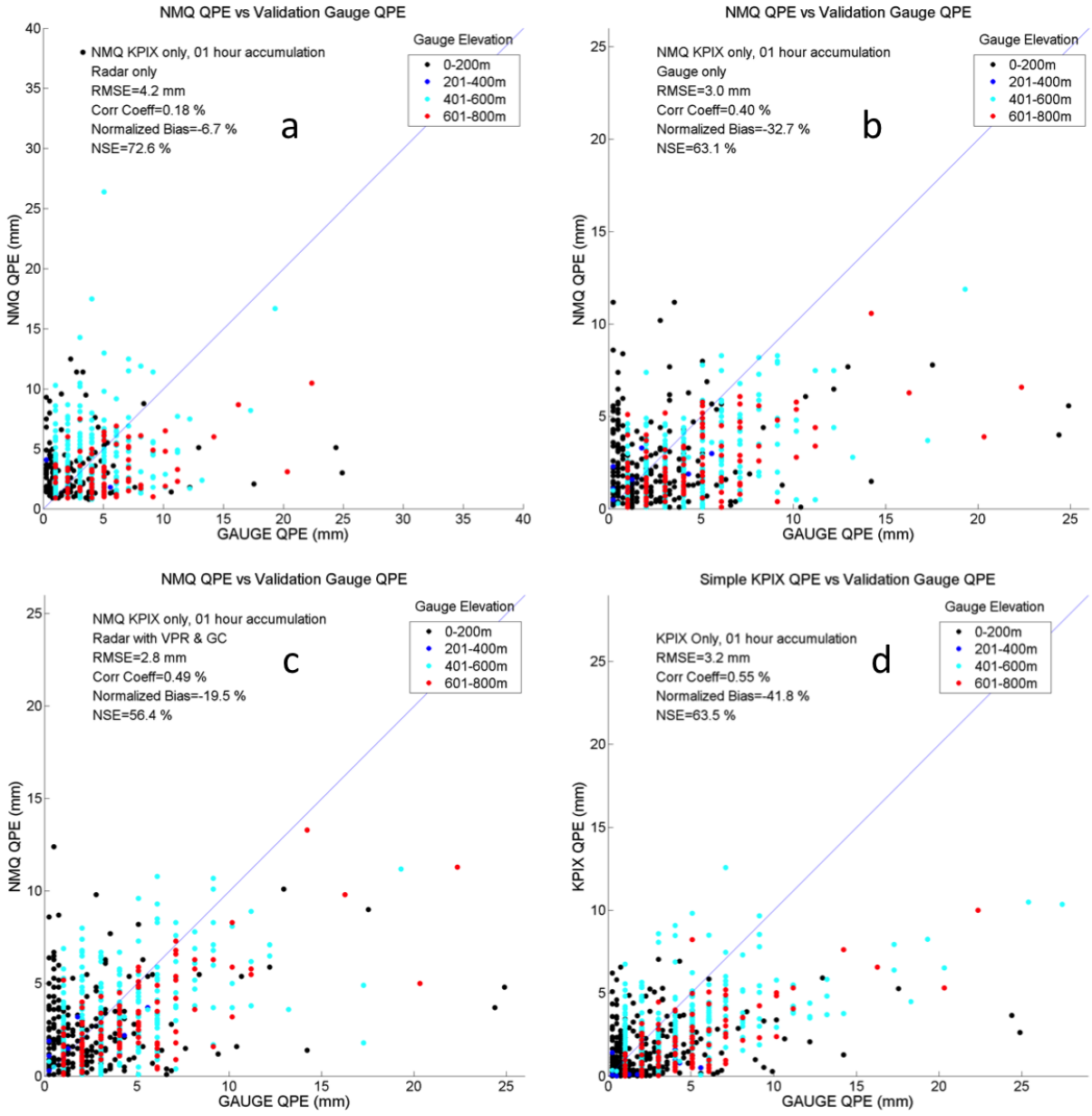

FIGURE 4.8. Scatter plots of MRMS QPE vs. validation gauge using KPIX only as input for below the bright band, where MRMS radar-only (a), MRMS gauge-only (b), MRMS radar with VPR and gauge correction (c), and non-MRMS KPIX only (d). The validation gauge elevations are color coded.

the bias between individual validation gauges and the surrounding analysis gauges within a specified radius of influence. In Figure 4.9, the normalized bias is shown for each validation gauge and corresponding analysis gauges that are within a particular radius (color coded with symbols). The radius of influence is varied from 5 km to 40 km where the overall

results show good agreement between the gauges. The cumulative bias is indicated by the red dashed line and is within 10% of zero. As mentioned previously the MRMS gauge-only product is QC'd and then corrected using radar data (Ware 2005), therefore the large biases seen between MRMS gauge-only product may stem from either the QC process or the radar correction technique.

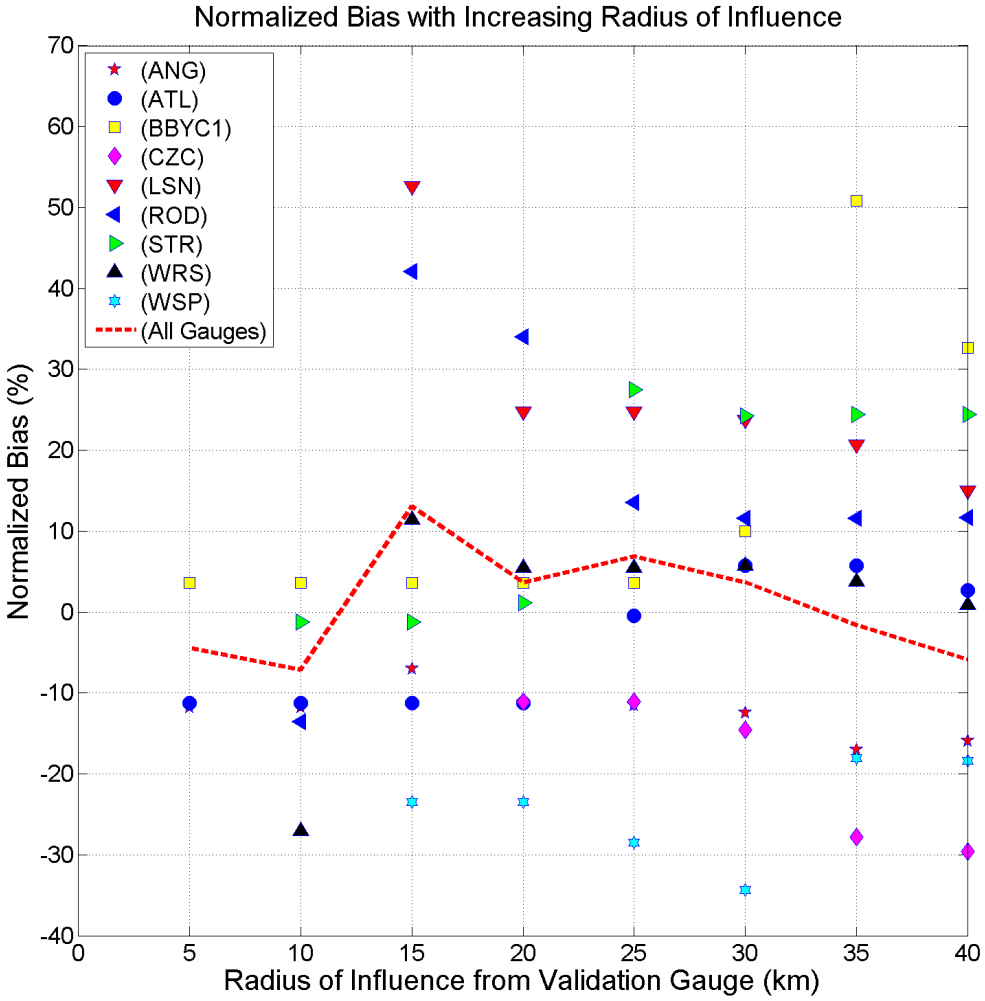

FIGURE 4.9. Normalized mean bias between each validation gauge and analysis gauges within radius of influence. Individual validation gauges are color coded with symbols. The overall normalized mean bias is shown with the red dashed line.

MPE was used to contrast the performance of the MRMS QPE on a subset of cases (10 days) where MPE data was available. MPE uses a different approach to construct gauge-only and bias adjusted radar QPEs. Specifically, the MPE gauge-only QPE (Gmosaic) uses PRISM climatology, similar to the Mountain Mapper technique utilized by the CNRFC. Similar to MRMS, the MPE results shown in Figure 4.1 indicate that the combined radar-gauge MPE product (Mmosaic) performed better than Gmosaic, further pointing to the importance of using radar data for QPE in the Russian River basin.

4.5. Conclusions and Future Works

The results from these coastal rainfall events indicate that the MRMS QPE product that implements VPR and gauge correction gives the best overall performance. Moreover except for the bias, the non-MRMS "Simple KPIX" radar-only QPE does as good as the MRMS radar-only QPE products where the large bias can be attributed to KPIX calibration and attenuation. Results from varying the MRMS radar input on the QPE products denote that there is not much difference in performance between KPIX and NEXRAD, such that the use of KPIX only radar input is equivalent to driving MRMS with NEXRAD only radar-input. Conceptually, the combination of KPIX and NEXRAD would provide the best combination of input data and would be thought to perform best overall. However the errors due to the complex terrain gradient may outweigh this advantage. QPE using KPIX can be compromised due to the manner in which the radar is calibrated, where the amount of calibration, clutter filtering, and scan strategies have not been formalized. As such, KPIX's primary purpose is to be useful to operational forecasters for improved situational awareness (i.e., a heads-up on storms moving into the area).

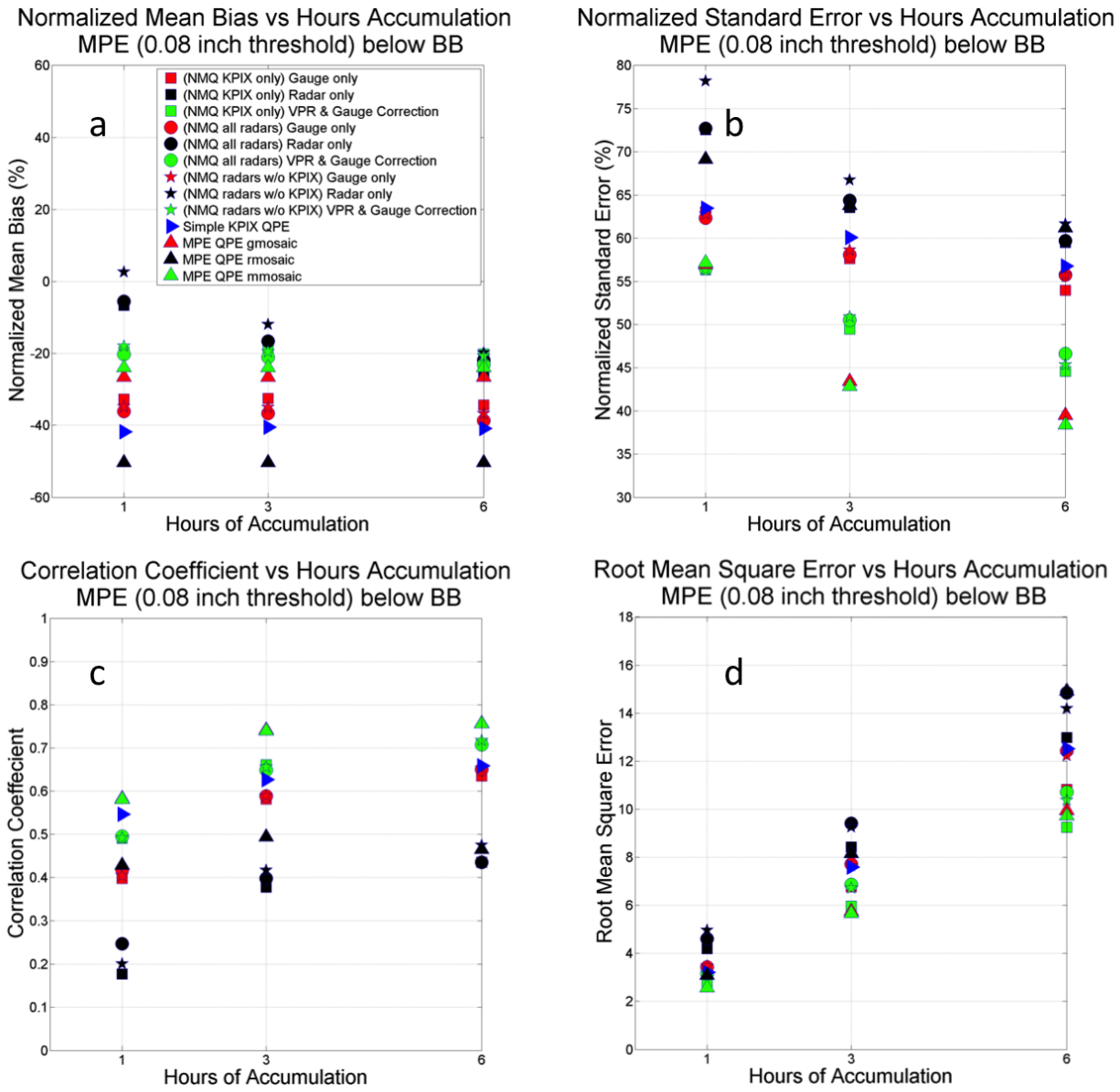

FIGURE 4.10. 1, 3, and 6 hour statistics for MRMS QPE products, Simple KPIX QPE and MPE considering below the bright band. MPE results are for 10 days of data. Normalized mean bias is shown in (a), normalized standard error in (b), correlation coefficient in (c) and the root mean square error in (d).

In real-time QPE for the purposes of flash flood monitoring and prediction, the MRMS product radar with VPR correction shows good performance without the use of gauge correction. "Simple KPIX" for this type of application does show good correlation but has large bias. Given the lack of available gauge data for real-time applications, the value of KPIX

data becomes more important for forecasters in order to better observe incoming precipitation and assess flash flood potential at short time intervals (one hour or less). The 6 hour accumulations tend to follow similar trends where the errors are reduced.

Future research tasks include evaluating a QPE approach, which uses KMUX only measurements. The KMUX radar is located farther away (see Figure 4.1) and its measurements above the basin of interest even at the lowest beam elevation of 0.5 degree generally come from ice regions above the freezing level. It was shown, however, that for deep precipitating systems, a model VPR correction applied for reflectivity only measurements produced reasonable QPE (Matrosov et al. 2014). Although these results were obtained using multi-year cool season event analyses, they were focused on one gauge comparisons (i.e., CZC in Figure 4.1). The existence of bright band in this region compels the necessity of VPR correction. It will be instructive to analyze how the model VPR corrected single NEXRAD KMUX radar-only based QPE estimates can replicate the spatial variability of rainfall in the basin. Future research will also be directed at understanding the large bias in the MRMS gauge-only QPE.

CHAPTER 5

Architecture of RAMS QPE

In forming the stages of the RAMS QPE, it is imperative to understand the approach implemented by other QPE processing methods, such as the MRMS and MPE QPE systems so as to gain perspective on the various components. There is commonality in the general steps needed to achieve the outcome, but each step differs in the technique used to handle the individual task. Currently the RAMS QPE is designed to operate in a retroactive analysis mode using archived data that is available for download. The use of this system for real-time application will require further evaluation and integration requirements to transform this into an operating environment. The flowchart illustrating the data processing steps is shown in Figure 5.1.

The radar data input into the system is required to have dual polarization measurements in order to successfully begin the processing. The ingest of radar data that has currently been performed on three radar platforms which are the NEXRAD WSR-88DP, NASA NPOL, and NOAA NOXP radar, such that the two prior operate at S-band frequencies, and the latter operates at an attenuating X-band frequency. Other dual pole radars can be ingested, as long as the incoming data format is comprehended, and that it can be converted for input. The radars are handled individually, where the single radar rain rates are calculated for the lowest tilts. In order to derive these estimations, the polarimetric variables required are the horizontal reflectivity (Zh), differential reflectivity (Zdr), specific differential phase (Kdp), linear depolarization ratio (LDR) and the correlation coefficient (Rhohv) along with an environmental variable for temperature. All of these variables are input into the Colorado State University Hydrometeor Classification System for Rainfall Estimation (HCS-R), where the

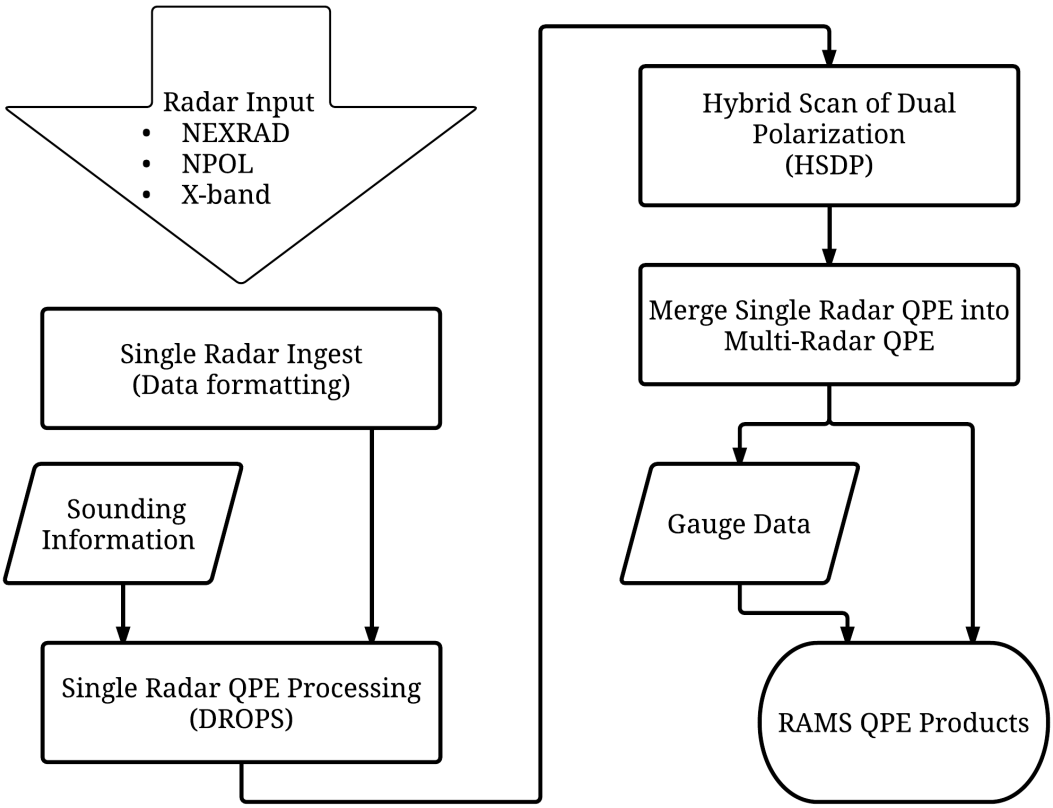

FIGURE 5.1. Flow diagram for the RAMS QPE Architecture

main objective is to distinguish the presence of ice either whether mixed with precipitation or by itself. Knowing the type of hydrometeor along with the polarimetric measurements, rain rate is then calculated based upon a set of variable thresholds and conditions. Using the single radar QPE output, the next phase is to generate the Hybrid Scan of Dual Polarization (HSDP) by joining the lowest tilts. Following this, the merging of multiple HSDP is then performed to create a mosaicked instantaneous rain rate map covering the domain of interest, which can be accumulated to generate the radar-only QPE product. The availability of gauge data allows for the production of gauge based rainfall products, which are the gauge-only QPE and the radar with gauge corrected QPE product. The RAMS QPE system is designed to operate within a domain that is constrained to a regional boundary. The spatial resolution for the initial implementation is set to 0.01 degree latitude by 0.01

degree longitude (approximately 1 km by 1 km), which is done to coincide with the MRMS system resolution, however this is an adjustable parameter. In terms of temporal resolution, RAMS QPE is arranged to generate hourly QPE amounts, at the top of the hour, such that these sums are derived from the accumulation of the instantaneous rain rates. Other QPE amounts for 3, 6, 12, and 24 hour time frames can be aggregated from the hourly result.

5.1. Ingest of Radar Data

The data format of the RAM QPE is particular in that the variables for horizontal reflectivity (Zh), differential reflectivity (Zdr), specific differential phase (Kdp), linear depolarization ratio (LDR) and the correlation coefficient (Rhohv) need to appear in the original data. If any of the variables are missing, the radar data will need further manual evaluation to determine if it can be ingested based on what is available. In the reformatting procedure, the data values remain unchanged, but the variable references are modified to match predefined names, where the radar data retains the radar polar coordinates. Information about the scanning strategies should also be comprehended to assess what scanning elevation angles are available, since the best choices are to use the lowest elevation scans. However in complex terrain, the lowest angles may have blockage, so it should be evaluated prior to see if they are applicable to the area of interest. The other metric of primary interest is the scan execution time frame, in that it is helpful to realize how long it takes to complete individual scans, as well as the total time to complete a full volume scan. This is important in terms of the final mosaic, since it will become necessary to synchronize scans from multiple radars. Since radars can have different ranges based upon the frequency of the radar, an evaluation of the location and coverage area needs to be completed, so as to determine effectiveness of adding particular radars in to the mosaic. Therefore, the lowest practical elevations scans

are selected and converted to the RAMS QPE Netwok Common Data Form (NetCDF) file format containing the necessary polarimetric variables. The flowchart displaying the ingest of radar data processing steps is shown in Figure 5.2.

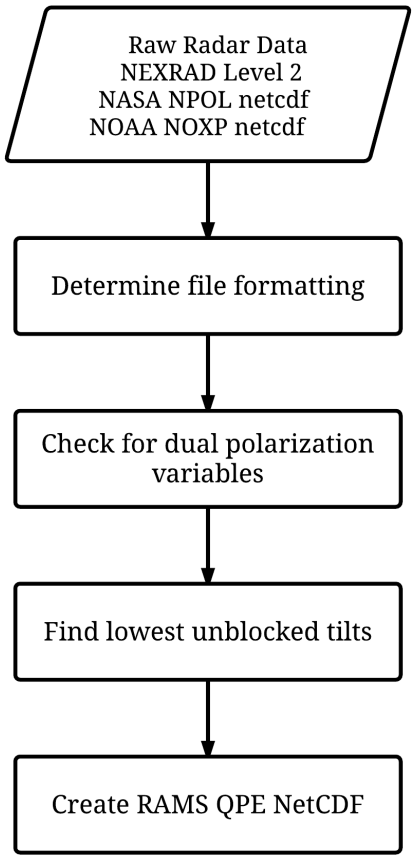

FIGURE 5.2. Flow diagram for the ingest of radar data into the RAMS QPE system.

5.2. Single Radar QPE Processing (DROPS)

Once the selected radar tilts have been identified, and the data prepared for input into Dual Polarization Product System (DROPS); the rain rate can then be calculated for each elevation sweep. For example in a typical NEXRAD radar operation, there are 360 radials within a sweep and 720 gates within a radial. The rain rate is calculated for each gate, such

that each radial is handled sequentially and the gates within each radial are individually processed. Finding the rain rate requires two steps, the first is the hydrometeor identification process (HCS-R), and from this the rainfall estimation is calculated based upon the hydrometeor type, the polarimetric variables and the environmental temperature. In or near mountainous areas, the amount of radar blockage needs to be evaluated. For most radars operating in such locale, there is typically a blockage map for the radar that can be applied to the processed rain rate fields to mask out any gates that undergo occultation. If there is no blockage information, the rain rate field is taken as is. In this case, if the hydrometeor is not identified in the case of a blocked gate, then no rainfall amount is calculated. At the conclusion of this module, the rain rate fields are generated for each of the lowest elevation scans from the radars within the domain. The flowchart for the hydrometeor identification and the rain rate process is shown in Figure 5.3.

5.3. Hybrid Scan of Dual Polarization (HSDP)

In this procedure, each set of single radar sweeps are combined to create a Single Radar Hybrid Scan of Dual Polarization (HSDP). This step requires the radar radials to be re-gridded from intrinsic radar polar coordinates into a rectangular coordinate system. As mentioned previously, the new coordinate system chosen is based upon latitude and longitude, with 0.01 degree side lengths. The first part of this process is to take each radar sweep and then grid it into the new coordinate system bounded by the domain, where a simple linear interpolation in azimuth is applied to complete the gridding. Once this is carried out, the combing of multiple sweeps can be accomplished. The method for this step is to overlay the gridded rain rate fields generated from individual volume scans. This is possible, since the gridding was completed using the established domain coordinates. To obtain the best

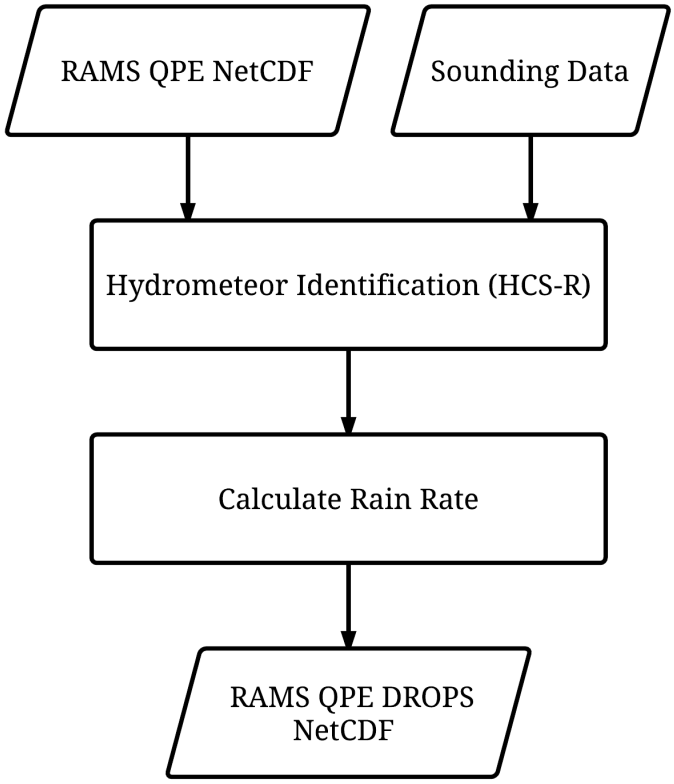

FIGURE 5.3. Flow diagram of the hydrometeor identification and rainfall rate process within the RAMS QPE system.

rainfall estimation, it is practical to retain the lowest elevation scan. Therefore to begin with, all the values contained in the lowest gridded sweep are assigned to the HSDP, and the sweep at the next highest elevation scan is joined with the HSDP. For each pixel in this union, if the individual value exists in the HSDP, then the value at the higher sweep is ignored. On the other hand, if the HSDP pixel contains no value, then it assumes the value contained within the sweep being joined. This overlaying of pixels within a coordinate map preserves the values for rain rate at the lowest elevation and seeks to fill in missing values with information from higher scans. One of the primary reasons for this stems from the awareness that radials and gates may be missing especially if partial to full beam blockage is encountered. In the termination of this process, the single radar Hybrid Scan of Dual

Polarization is generated from the lowest sweeps contained within a volume scan. This is depicted in the flowchart of the hybrid scan of dual polarization process in Figure 5.4.

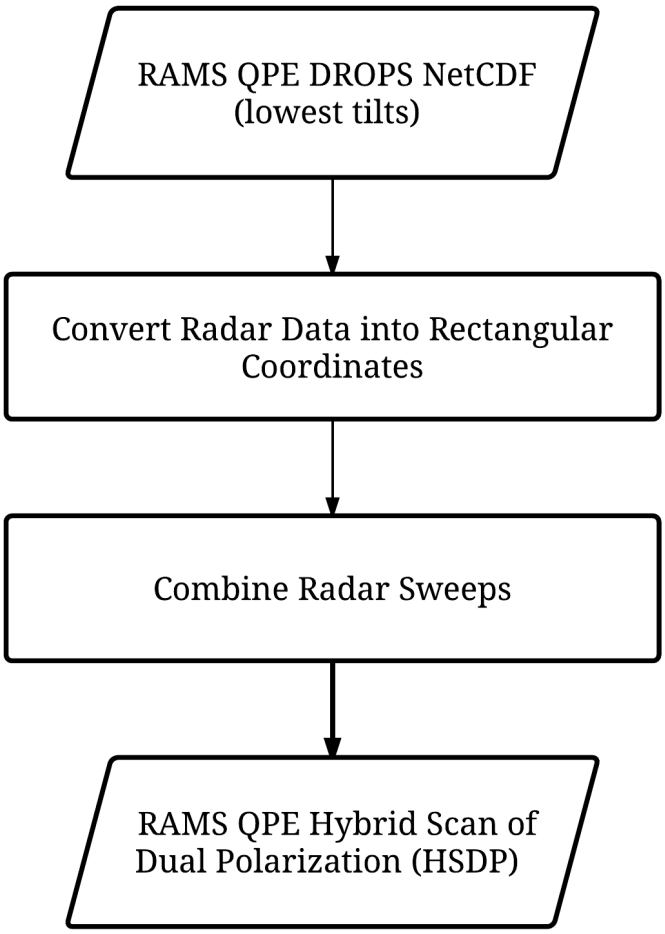

FIGURE 5.4. Flow diagram of the Hybrid Scan of Dual Polarization (HSDP) in the RAMS QPE system.

5.4. Mosaicking Multiple Radar QPE

Once the single radar HSDP is established, these individual radar hybrid rain rate maps are merged together to form a mosaicked rain rate field that is bounded by the domain boundaries. The merge of the individual radar is performed in a manner that is similar to that of the HSDP process. Again the individual radar HSDP spatial resolution retains the

precision from the gridding of the HSDP, and this allows the overlaying of the layers of these rain rate fields, which match spatially. Combining single radar into a multiple radar field is carried out as follows. In this process, each pixel in each single radar HSDP is aligned with the corresponding pixel from the other radar HSDP rain rate fields resulting in a column of pixels that correspond in latitude and longitude. The number of values that have common coordinates depends upon the number of individual radar HSDP with valid rain rate values. If more than one value occurs within a column of pixels that share the same location, then the maximum value is found and placed into the latitude-longitude coordinates of the merged radar HSDP, else the singular value is used or there is no value for that particular position. Since all radars do not coordinate scans or operate on a common timing sequence, a technique that selects a common set of singe radar HSDP fields is required, where the occurrence of each is close enough in time to allow for reliable combining of the instantaneous rain rates. The set of single radar HSDP that are chosen to be merged are selected using a binning approach, such that the single radar HSDP with timestamps that occur within a 5 minute window are considered to be merging candidates, where the length of the timing is based upon the NEXRAD volume scanning repetition time. If the single radar HSDP occurs more than once during the timing window, the first one is taken and the other is thrown out. This is done to keep with simplicity and allow for further refinement. On the other hand, if there are missing single radar HSDP fields, the merge is nevertheless completed with what is presented. In the end, the mosaic is completed every 5 minutes based upon availability of the radar scan information, and that gaps can occur. The flow diagram displaying the mosaicking of multiple hybrid scan of dual polarization process in Figure 5.5.

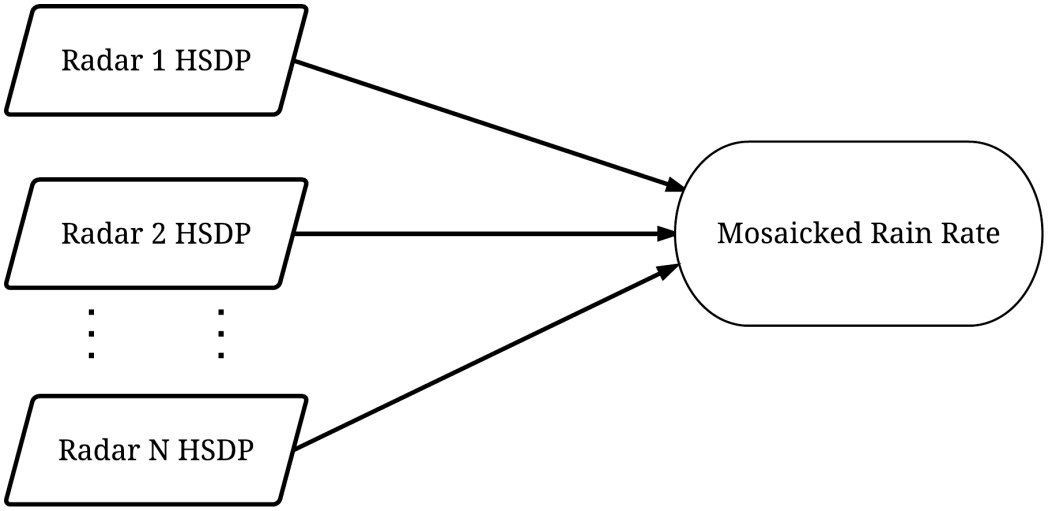

FIGURE 5.5. Flow diagram showing the mosaicking of multiple HSDP radar maps in the RAMS QPE system.

5.5. Gauge Correction Technique

It has been demonstrated that the application of gauge correction to radar-only QPE can improve the performance of these products (see Ch. 4). A simple gauge correction is performed that is a derivative of the methodology implemented by the NSSL MRMS system, which is based upon analysis performed by Ware (2005). The approach is to use point gauge values and extrapolate them over a radius surrounding the gauge to create a gauge-only rainfall estimation. Since the inverse distance weighting (IDW) relation is similar, the same manner in determining the radius of influence and the value of exponent is retained. The choice to implement this based upon the results from Ware, (2005), which compared the performance of the IDW method with the Multi-quadric Interpolation (MQ) and Ordinary Kriging methods, and it was found that IDW performed as well or better.

CHAPTER 6

RAMS QPE Single Radar QPE Processing

In this chapter, the details of the techniques applied in the processing of the RAMS QPE single radar data are presented. However, before the data can be ingested, the individual radar file format is evaluated, Once verified it can then be converted into the RAMS QPE Netwok Common Data Form (NetCDF) file variable structure. The verification of the radar data fields is such that to visually inspect the data structure and to insure the necessary dual polarization information is existent. Along with this is to ascertain the assemblies of sweep elevation angles in regards to both the individual scan time and the time to complete the full volume coverage pattern. After the radar data is confirmed for ingest, it is sent into the rainfall estimation procedures. This requires first identifying the hydrometeor type and then applying the appropriate rain rate relation. The radar data during these steps are kept in polar coordinates, so as to maintain the integrity of the data. These data steps will be demonstrated by considering the two NEXRAD radars and the NPOL radar near Asheville, NC. In this analysis, the individual radar dual polarization variables are compared and the results shown. The performance of the single radar in this HMT-SEP region is evaluated to see how well the CSU DROPS QPE algorithms generate rain rate versus surrounding rain gauge data.

6.1. Single Radar Ingesting

The ingesting of radar measurements for the RAMS QPE system is contingent upon the obtainability of dual polarization variables. In the particular domain of interest, the radars considered for QPE processing need to have this capability, such that this requirement is principally driven by the usage of the CSU dual polarization algorithm code. In the

application of this QPE code, there are several radar platforms that are known to work based upon prior usage. These being the WSR-88DP NEXRAD network, as well as NASA NPOL, CASA X-band and a few other dual polarimetric types of radars. In the initial development of this RAMS QPE structure, the domain is established in the area surrounding the Pigeon River basin near Asheville, NC. The radars that are located within the boundary of this domain are NEXRAD, NASA NPOL and NOAA NOXP. In that the two priors are known entities, and that the NOXP radar has yet to be evaluated and ingested into the RAMS QPE system. So it will require some effort in assessing the radar before it can be modified into the proper format for CSU DROPS algorithm processing. On the other hand, the NEXRAD has a well documented radar file format essentially referred to as level 2 data, which has been minimally processed to remove clutter contaminants and does provide the moment data. NASA NPOL formatting data files also are very detailed, and in this analysis the raw data was used which contains clutter contamination, and the moment data is acquired as recorded. The NPOL radar is an S-band mobile field radar with scanning capabilities similar to NEXRAD. The NOXP data is also provided with clutter contaminants, along with the necessary dual pole variables. This radar is an X-band radar and is a mobile field radar, however this data was not available for this analysis.

The dual polarization parameters required by the CSU rainfall estimation algorithm are the horizontal reflectivity (Zh), differential reflectivity (Zdr), specific differential phase (Kdp), linear depolarization ratio (LDR) and the co-polar correlation coefficient (Rhohv). Even if these measurements are provided, it is reasonable to assess the quality and check for systematic biases. Some of comparisons considered are Zdr versus Zh, Kdp versus Zh, and Kdp versus Zdr. These plots in Figures 6.1 - 6.3, give an indication of the dual polarization measurements by comparing the Zdr and Zh to see if there are any unexpected discrepancies.

These results look at the two NEXRAD radars KGSP and KMRX and the NASA NPOL radar, which are all S-band radars that occur within the vicinity of the Pigeon River basin. The elevation angle is 1.46 degree for KGSP, 1.44 degree for KMRX, and 1.50 degree for NPOL, such that this data reflects all the scans for these particular tilts that occurred for the day of May 15, 2014. There were two major storm events passing between the radars that consisted of approximately 14 hours of rainfall. In observing the Zdr vs Zh plot for all three radars (Figures 6.1 - 6.3), they all show good comparison between them, such that at light rain measurements (approx. Zh $<$ 20 dbZ), the Zdr is close to zero and steadily increases as the reflectivity increases. This is expected since as reflectivity increases, the raindrop size is also expected to increase, which results in large Zdr measurements (Beard and Chuang 1987).

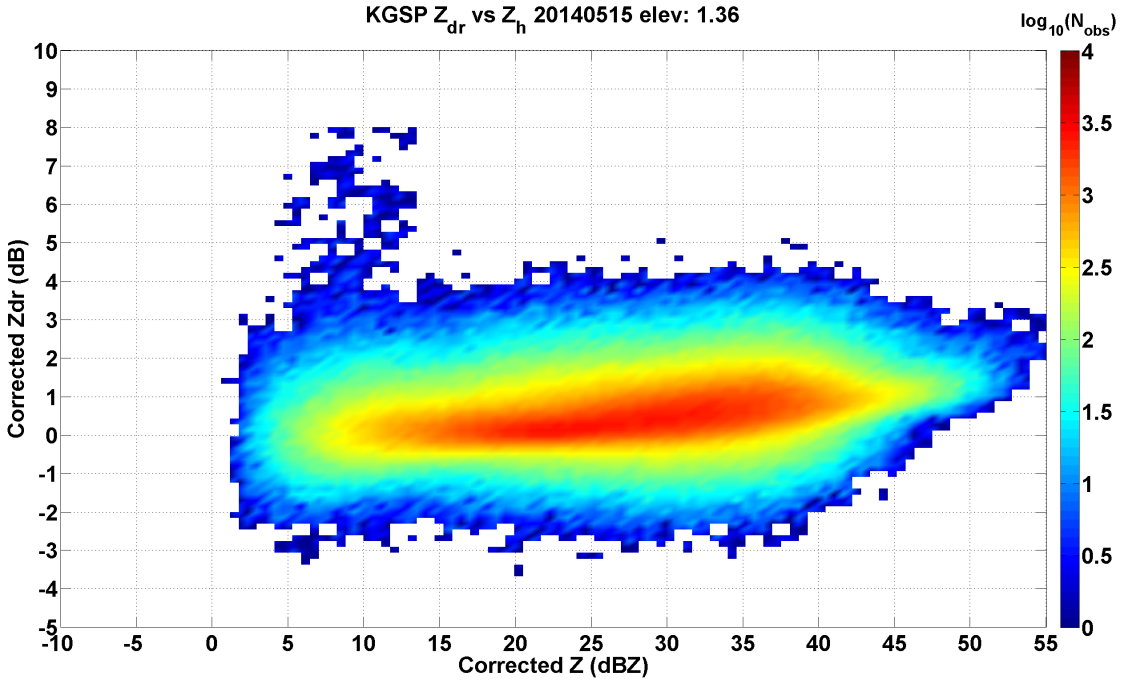

FIGURE 6.1. Differential Reflectivity versus Reflectivity for KGSP radar.

In regards to specific differential phase (Kdp) biases, a comparison is made to both reflectivity (Zh) and differential reflectivity (Zdr) to see if the radar measurements are relating

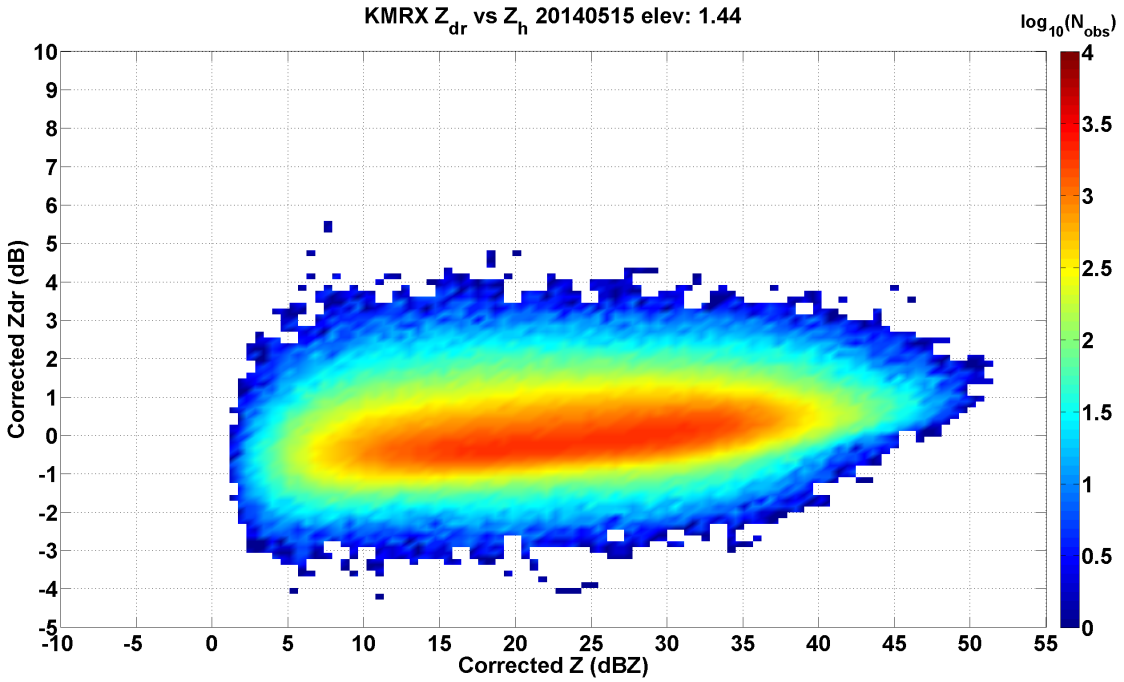

FIGURE 6.2. Differential Reflectivity versus Reflectivity for KMRX radar.

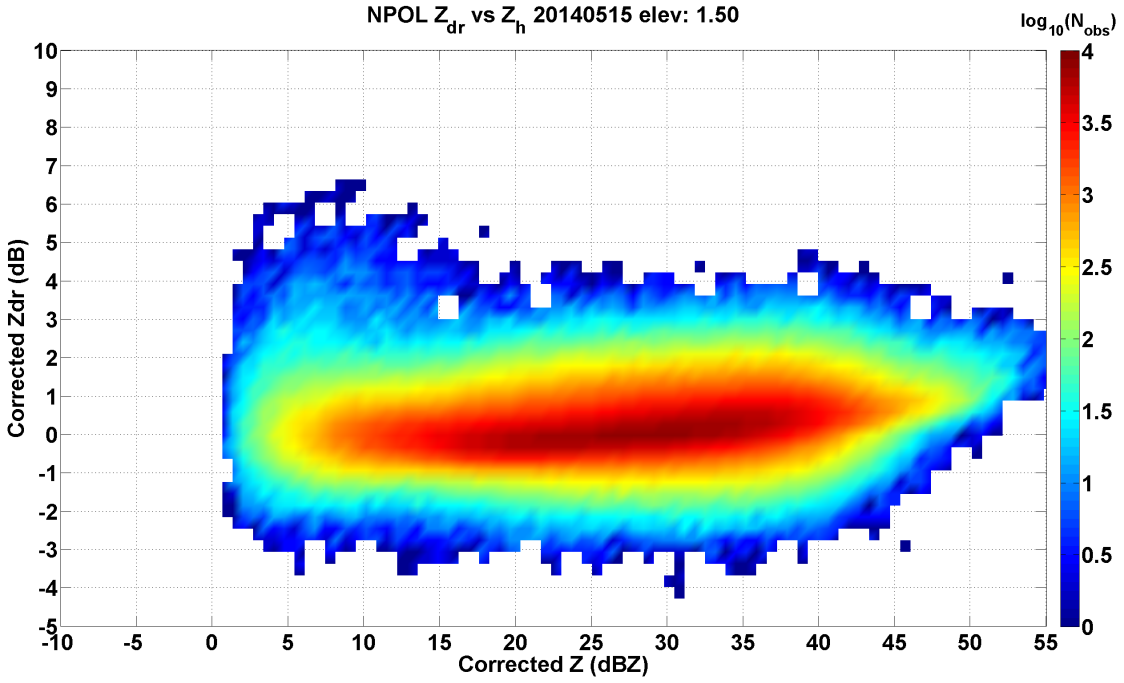

FIGURE 6.3. Differential Reflectivity versus Reflectivity for NPOL radar.

as expected. Kdp is generally close to zero for light to medium rainfall amounts (Zh less than 45 dBZ), as the rainfall increases the number of drops and the size of the drops tend

to increase as well, which results in larger positive Kdp values. Large Kdp measurements indicate that there is a large difference in the propagation of the horizontal and vertical polarized waves through oblate spheroids, such that the horizontally polarized wave is delayed more than the vertically polarized wave. The plots in Figures 6.4 - 6.6 again show the results for KGSP, KMRX and NPOL for the same scan elevation angles as before. In Figure 6.4, the plot indicates that the majority of Kdp values are small for light rainfall (Zh values below 30 dBZ), which is good, since Kdp is expected to be small for low to medium intensity rainfall measurements. In light rain the hydrometeors are essentially round and both the vertical and horizontal wave propagation are equally delayed and keeps phase difference close to zero. The other two radars roughly follow the same trends, but are slightly different due to the unique scans that are done over the passing storms of that particular day. Negative Kdp values are not physically realizable, but they due appear and are an artifact of the estimation technique applied to obtain Kdp from the differential phase measurements and are more likely to occur near storm edges and around clutter contamination.

The other dual polarization association made is between the specific differential phase and differential reflectivity. These results are displayed for the three radars in Figures 6.7 - 6.9 for KGSP, KMRX and NPOL. These plots show how Kdp is changing in with respect to the Zdr. In the presence of rainfall, as Zdr gets larger, this indicates an increase in the ensemble raindrop size, and the corresponding Kdp measurement should show an increase. This appears to be the situation for all three radars, which is what is expected. A note for NPOL results (Figure 6.9), the Kdp shows negative values which does not have any physical meaning. This is result can be associated to the manner in which Kdp was estimated from differential phase (Phidp). NEXRAD in the processing of is specific differential phase eliminates negative Kdp values.

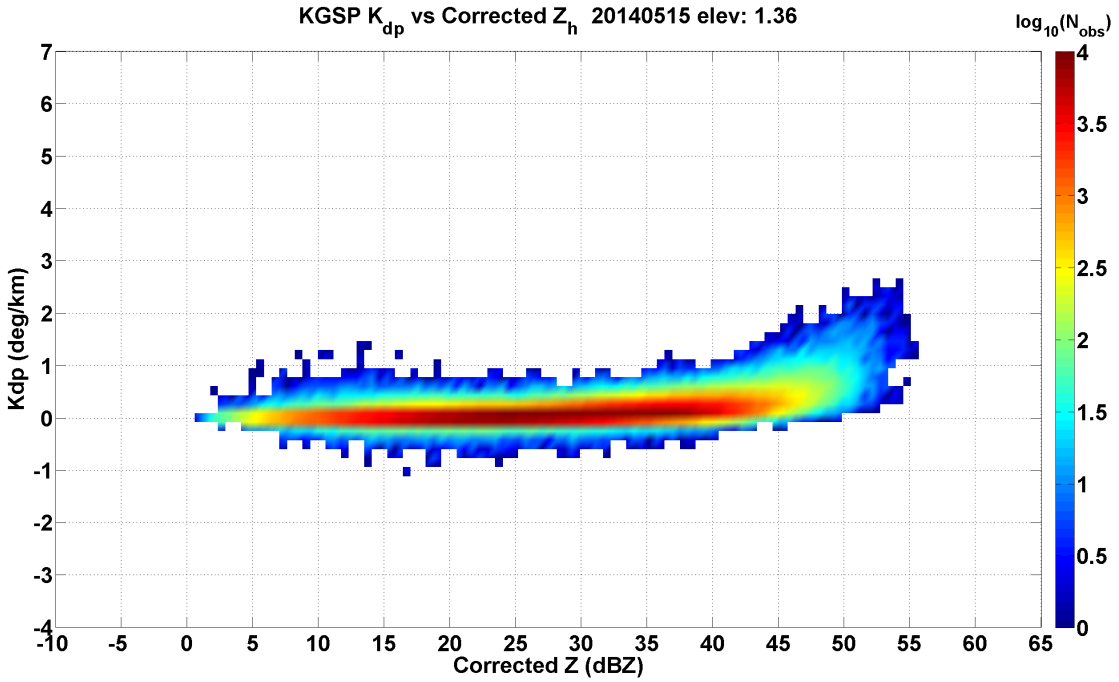

FIGURE 6.4. Specific Differential Phase versus Reflectivity for KGSP radar.

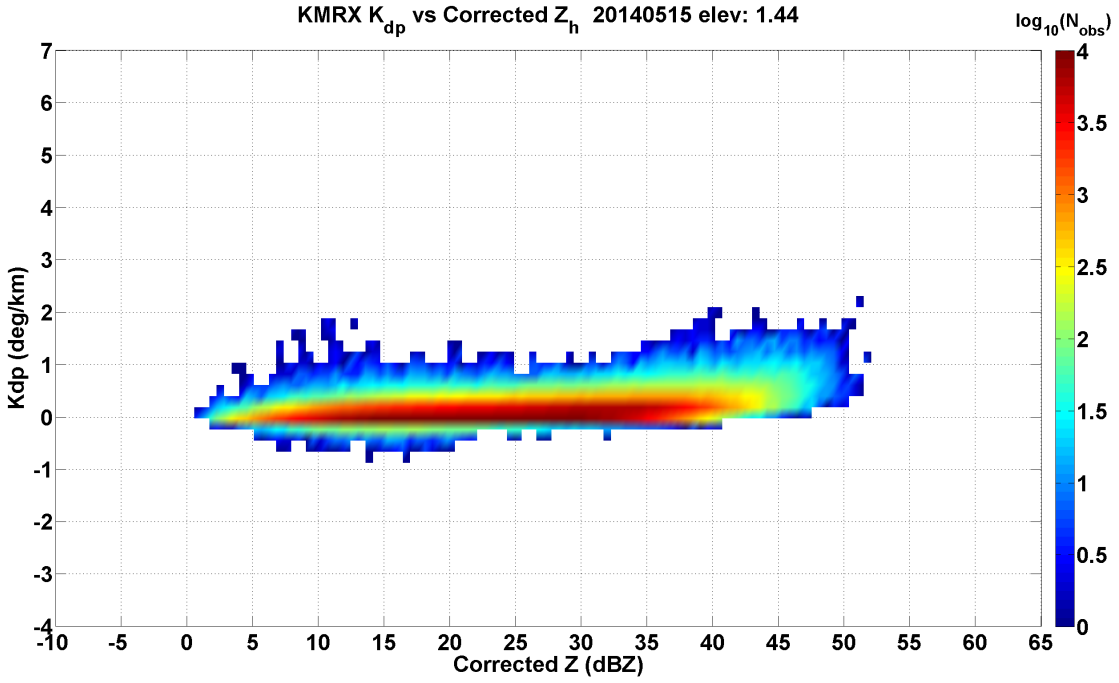

FIGURE 6.5. Specific Differential Phase versus Reflectivity for KMRX radar.

The comparisons of the dual polarization parameters for consistency in regards to these three radars all show good outcomes. The next step is take the data format from NEXRAD

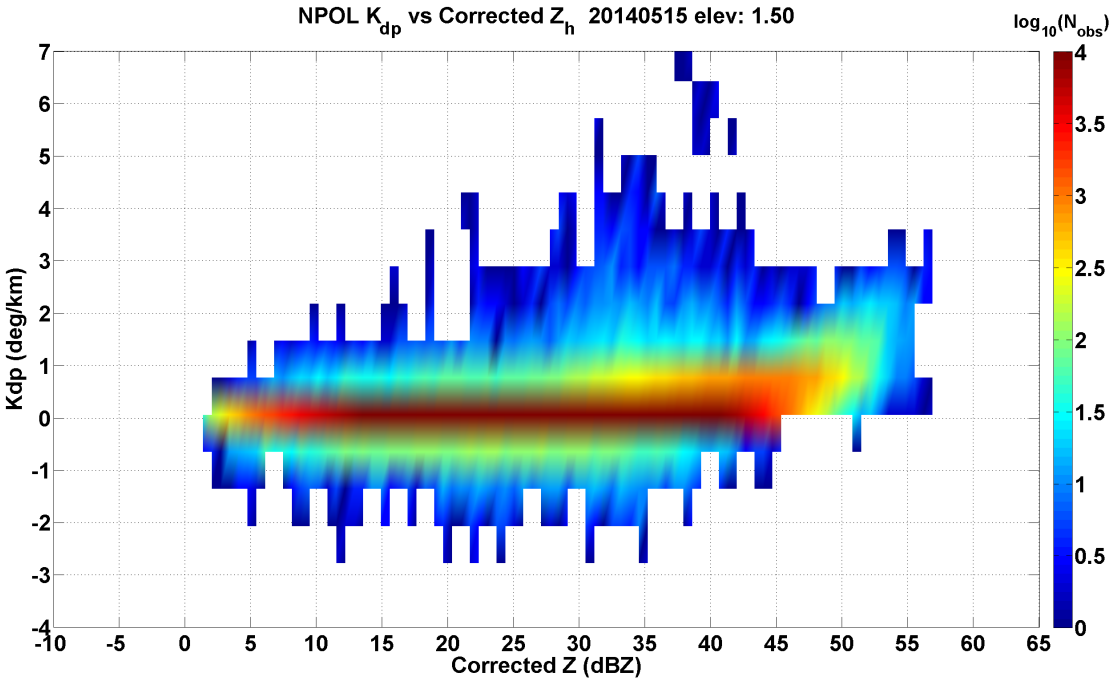

FIGURE 6.6. Specific Differential Phase versus Reflectivity for NPOL radar.

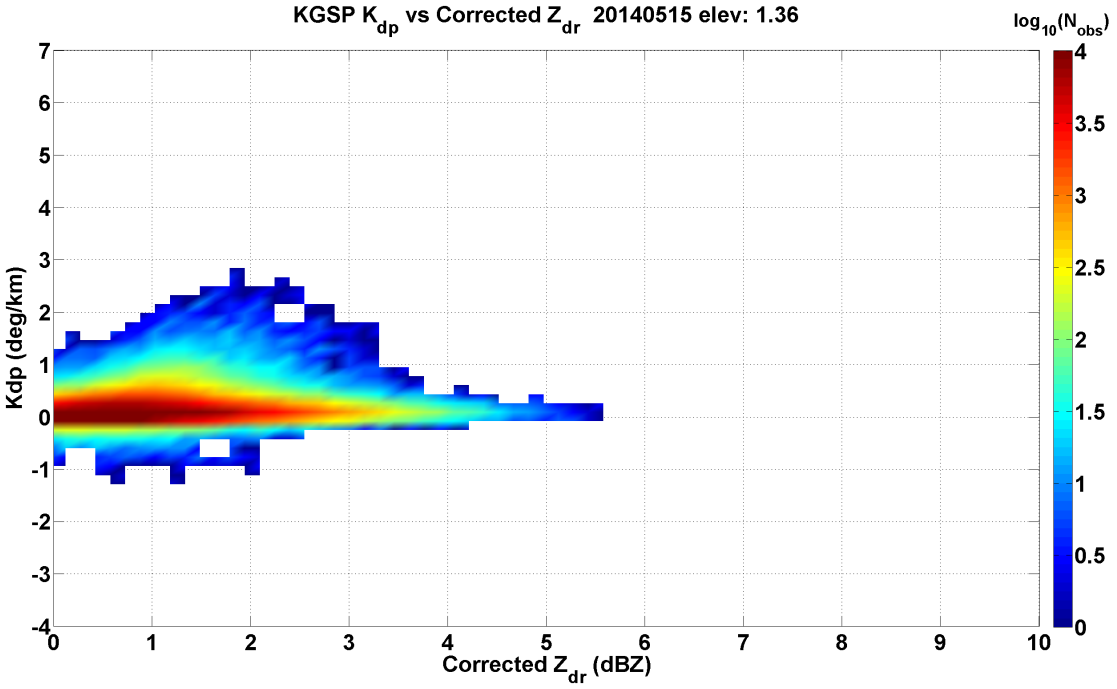

FIGURE 6.7. Specific Differential Phase versus Differential Reflectivity for KGSP radar.

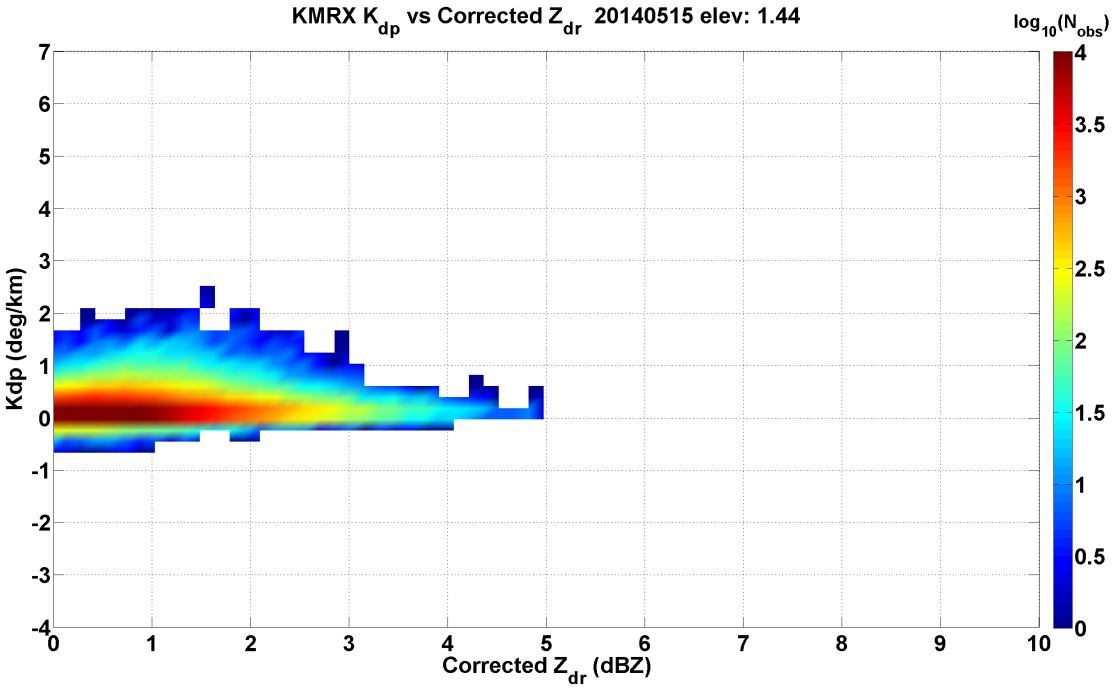

FIGURE 6.8. Specific Differential Phase versus Differential Reflectivity for KMRX radar.

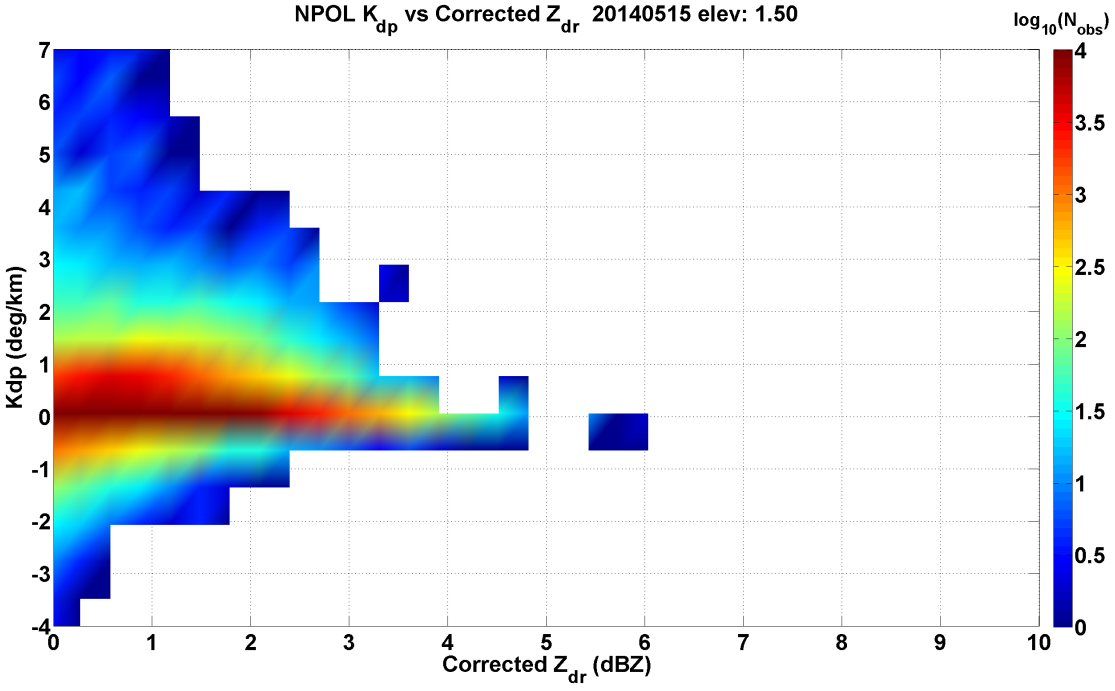

FIGURE 6.9. Specific Differential Phase versus Differential Reflectivity for NPOL radar.

and NPOL and put them into a NetCDF format. For NEXRAD, this conversion has been established, where the data is read from level 2 data and converted directly into a NetCDF format. NPOL data already comes in NetCDF format, so this processing involves renaming the variables to match the expected names. The CSU DROPS process is structured in a manner that currently can only process universal file format (UF) files, and therefore requires that the NetCDF file be converted into UF file format. UF files typically consist of a full volume scan; where this is a construct that contains all the sweeps associated with a particular volume scan. For this purpose of RAMS QPE processing, every individual scan is processed to create as a singe UF file with an elevation filename identifier as opposed to processing multiple scans within a volume scan. Once this is done it is ready for input into the remainder of the QPE steps. During this processing the data remains unchanged in radar polar coordinates, the processing is done to reorganize the data and rename the variable descriptors, while preserving the integrity of the data.

6.2. DROPS and Hydrometeor Identification and Rainfall Rate

The Hydrometeor Classification System for Rainfall Estimation (HCS-R; Cifelli et al. 2011) is implemented into DROPS, such that it is constructed using a fuzzy logic methodology that results from efforts of Lim et al. (2005); Liu and Chandrasekar (2000), where the inputs again are the five previously mentioned dual polarization measurements of horizontal reflectivity, differential reflectivity, specific differential phase, co-polar correlation coefficient, and linear depolarization ratio, along with an environmental variable that is associated with the melting layer height. The output from the classification system can be one of three hydrometeor types, which are rain, mixture, and ice. The category of rain types consists of drizzle, moderate rain, and heavy rain, and the mixture being wet snow or a rainhail

mixture. The ice classification is comprised of dry snow, graupel, and hail. The advantages of implementing fuzzy logic versus other techniques such as a decision tree, classic statistical decision theory, neural networks, and fuzzy logic is that it has the capacity to make clear decisions based on overlapping and noise contaminated data. The fuzzy process has three parts. First is the fuzzification procedure, which is an approach that takes precise input values and converts them into fuzzy sets using a corresponding membership degree. Secondly is the inference step that is a rule-based approach to attain the individual proposition strength, and lastly the defuzzification process, which is a combination of rule strength and the choice of the best characteristic. With respect to other non-fuzzy methods, obtaining the prior probability and the probability density functions can be extremely difficult. However, the fuzzy logic approach employs simple rules to describe the system as opposed to implementing a cadre of analytical equations, and thus simplifying the classification of hydrometeors. Along with reasons stated above, other benefits of fuzzy logic are the robustness and execution speed.

Numerous functional forms offer acceptable representation of membership functions (MBFs), such as triangular, trapezoidal, Gaussian shapes, S and Z curves, and beta functions. For the purpose of the classification system, a beta function is chosen for following reasons. In the problem of hydrometeor classification, the membership functions should exhibit a wide flat region with a maximum value of one. In the case of rain as the hydrometeor type, reflectivity can vary over a wide range of values depending upon the intensity. In other words, it is preferred to have a region (say, 25 dBZ $<$ Zh $<$ 60 dBZ) as opposed to a single unique value of reflectivity to indicate rain. In order to represent these characteristics with a MBF is to have a function that is constant over the region and then tapers off outside the region.

In order to achieve this kind of response, a beta function offers the most desirable characteristics, and therefore it is chosen as the shape of the membership functions. In addition, the derivative of the beta function is continuous, which allows for further flexibility for the possibility of adjustment of the parameters.

$$beta(x, m, a, b) = \frac{1}{1 + \left(\left(\frac{x - m}{a} \right)^2 \right)^b} \tag{29}$$

such that, there are three parameters that define the shape of a beta function, namely, the center of the function m, the width a, and the slope b.

The current hydrometeor classification system for rainfall estimation (HCS-R), is based upon the model proposed by Liu and Chandrasekar (2000), and then modified by Lim et al. (2005). The differences from the previous to the current classification system, includes the fact that, there are three output types as opposed to ten, as well as an adjustment in the classifier for linear depolarization ratio so as to handle low signal to noise ratio that can lead to unreliable LDR. In addition, there are three other modifications compared to the previous algorithm. The first is in the detection of the melting layer, which employs the gradient of Zdr and Zh to determine this height (Bringi and Chandrasekar 2001). Next is allowing the height membership function to coincide with the varying height of the melting layer as oppose to an area average. The other change is in the inference process in which an additive weighting method (Zrnić et al. 2001) is included along with the product method to create a hybrid approach.

This hydrometeor identification process is performed for each radial and on a gate-by-gate basis. Once the HCS-R process is completed, the hydrometeor type is determined and

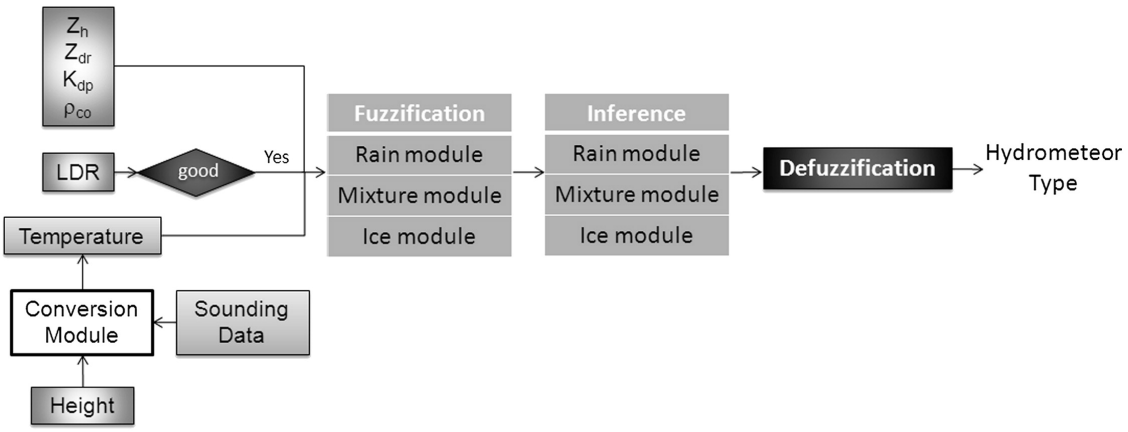

FIGURE 6.10. Flowchart describing the Hydrometeor Classification System for Rainfall Estimation (HCS-R) (from Cifelli et al. 2011).

then ready for the next phase of calculating the rainfall rate. Using the derived hydrometeor type along with the reflectivity, differential reflectivity and the specific differential phase measurements, the rain rate can be calculated. There are several rainfall estimation equations that are applied depending upon the rainfall intensity and the standard error measurements of dual polarization variables (Cifelli et al. 2011).

$$R(K_{dp}, Z_{dr}) = 90.8(K_{dp})^{0.93} 10^{(-0.169 Z_{dr})} \tag{30}$$

$$R(K_{dp}) = 40.5(K_{dp})^{0.85} \tag{31}$$

$$R(Z_h, Z_{dr}) = 6.7 \times 10^{-3} (Z_h)^{0.927} 10^{(-0.343 Z_{dr})} \tag{32}$$

$$R(Z_h) = 0.0170(Z_h)^{0.7143} \tag{33}$$

where Z_h is radar reflectivity (mm^6 m^{-3}) , R is the rainfall rate (mm h^{-1}), Z_{dr} is differential reflectivity (dB), and K_{dp} is specific differential phase (degrees km^{-1}). The three Equations (30, 31, 32) include dual polarization characteristics, such that these relationships

are derived from theoretical investigation by assuming a variety of gamma drop size distribution (DSD) parameters that are typically found in physical observations. The description of the DSD distribution and the parameters used to describe them are discussed in chapter 8 of Bringi and Chandrasekar (2001). The gamma DSD parameter ranges are $10^3 \leq N_w \leq 10^5$ mm^6 m^{-3}, $0.5 \leq D_0 \leq 2.5$ mm, and -1 $\leq \mu \leq 5$ with R ≤ 300 mm h^{-1}, where N_w is the normalized intercept parameter, D_0 is the median volume diameter, and μ is the shape parameter. In Equations (30) and (32), the differential reflectivity measurement assumes that the shape of the drop as a function of size follows from the Beard and Chuang (1987) equilibrium model.

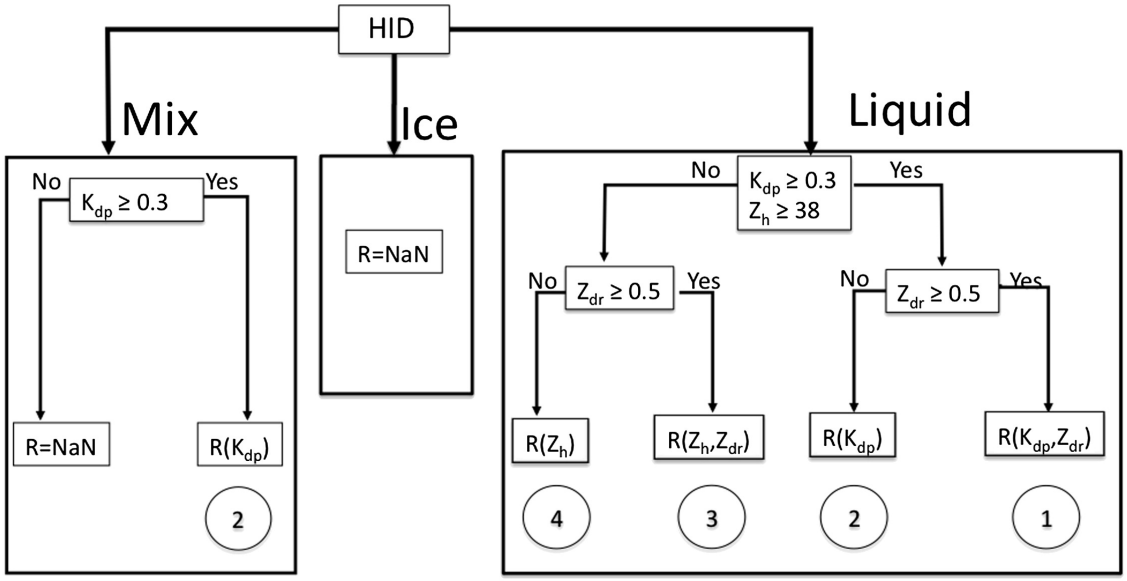

FIGURE 6.11. Flowchart describing the CSU-HIDRO algorithm logic (from Cifelli et al. 2011).

In the HCS-R process, the Colorado State University hydrometeor classification (CSU-HIDRO) of Lim et al. (2005) is used in the rain identification for this process. The thresholds values that are applied to determine which rain rate relation to employ follow from Petersen et al. (1999) and the outcomes reported in Bringi et al. (1996) where the latter study quantified the error characteristics of the polarimetric variables Zh, Zdr, and Kdp. Petersen

et al. (1999) considered the flash flood occurring in Fort Collins on July 28, 1997 where this event was used to evaluate rainfall algorithm performance against gauges. The radars employed were the CSU CHILL located near Greeley, CO and the NEXRAD KCYS located in Cheyenne, WY. In this event, application of three rain rate equations using the following threshold holds where identified. A blended rainfall product that applied the R(Kdp, Zdr) estimate in moderate to heavy rain when Z $<$ 38 dBZ, then a linearly weighted R(Kdp, Zdr)/Z-R estimate of rain rate in areas of light rain when 35 $\leq$ Z $\leq$ 38 dBZ, and lastly a pure Z-R estimate to handle conditions when Zh $<$ 35 dBZ and when the values of Kdp and Zdr fall below a threshold, where these thresholds for Kdp and Zdr were assessed by visual inspection of collocated grid points of Kdp, Zdr, and Zh values. The noise thresholds were conservatively determined to be approximately 0.3 degree km^{-1} for Kdp and approximately 0.5 dB for Zdr when reflectivities are above 38 dBZ.

The overall perspective of rainfall estimation selection in CSU-HIDRO is to identify conditions in which a particular rain rate estimator's performance is maximized. As an example, if the hydrometeor is rain, then R(Kdp, Zdr), which has the lowest error characteristics, is the preferred estimator as long as Kdp and Zdr are above their respective noise thresholds. If ice is existent, then R(Kdp) makes the best sense, since Zdr is expected to be near zero. In circumstances where Kdp and Zdr are too noisy or absent, the estimator R(Zh) is used as the final alternative.

Another significant concept in the application of dual polarization rainfall relations is the derivation of Kdp. The established manner of estimating this variable requires finding the slope of Φ_{dp} profiles (Equation 34), which is a noisy unstable computation where challenges in the estimation of the specific differential propagation phase lie in the existence of

phase wrapping and statistical fluctuations in the range profiles of the differential propagation phase. Even though practical unfolding approach exists, it requires several ad hoc adjustments. Usually this can be achieved by using a high pass filter except that the filter expects a smooth and continuous function as the input. Given a typical range profile of total differential phase Ψ_{dp}, this is comprised of both Φ_{dp} and differential backscatter phase shift δ_{hv} as well as measurement fluctuation (Equation 35).

$$K_{dp}(r) = \frac{1}{2}\frac{d\Phi_{dp}(r)}{dr} \tag{34}$$

$$\Psi_{dp}(r) = \Phi_{dp}(r) + \delta_{hv}(r). \tag{35}$$

In estimating Kdp, the variation in the estimates of Ψ_{dp} will be amplified during the differentiation, giving a large variance in the Kdp estimates. In order to mitigate these issues, a new Kdp estimator is employed (Wang and Chandrasekar 2009). Phase wrapping is in fact an artifact coming from mapping an angular variable along unit circle into the real axis. Wang and Chandrasekar (2009) showed that the estimation can be shifted to a complex-valued range profile of the differential propagation phase exponentials which results in a simpler estimation and thus it avoids the calculation for phase unfolding. Its numerical evaluation maintains better accuracy as a result of the exponential form function. To this end, a regularization framework was established, and a cubic smoothing spline was implemented to fit a better regression function. This technique was shown to have good results with rain gauges in the study done by Wang and Chandrasekar (2010), which was implemented using the National Science Foundation (NSF) Engineering Research Center for Collaborative Adaptive Sensing of the Atmosphere (CASA) X-band frequency scanning

radar network (McLaughlin et al. 2009) scanning over gauges in the Little Washita River watershed. Therefore this method is integrated into the DROPS QPE processing procedure.

6.3. Performance of Single Radar QPE Using DROPS

To evaluate the performance of the DROPS QPE methodology when applied to KGSP, KMRX and NPOL radars, a comparison of the one hour radar rainfall accumulation was performed against the surrounding NOAA Hydrometeorological Automated Data System (HADS) gauges. The HADS gauges picked for this evaluation are within the scanning range of the three radars, and the hourly accumulation are taken from the events occurring on May 15, 2014. The statistics for these comparisons are the normalized mean bias, normalized standard error, root mean square error and correlation coefficient, which are as listed previously in the four Equations (25 - 28). It should be noted that the rain gauge data is used without any quality control to remove unreliable gauges.

The normalized standard error displaying the radar QPE versus the range from the radar are shown in Figures 6.12 - 6.14 for KGSP, KMRX and NPOL radars, respectively. In these results, as the range from the radar is increased in 20 km increments, all the gauges that appear within that particular radius are included in the statistics. Figure 6.12 shows the results for KGSP for each of the three lowest elevation scans of 0.53, 0.88 and 1.3 degrees (VCP 12). In this data set, the lowest elevation scan shows the greatest amout of error as opposed to the two next higher tilts, and the errors tend to increase as the range of the radar increases, where the increased errors seen in the lowest tilt can be associated to the smaller sample size that is a result beam blockage in the direction of the storm. For the KMRX radar the trends are similar to KGSP, however the overall errors for KMRX are higher than those realized by KGSP. The three lowest elevation angles for this radar are 0.47, 1.44 and

2.40 degrees (VCP 21). The second and third tilt are higher than KGSP, which is due to the difference in scan strategies of the two radars at the beginning of this event, through the progression of storm on the day, KMRX did switch its scan strategy to VCP 12. The NPOL results can be seen in Figure 6.14, where this radar's lowest tilts are at 0.98 and 1.5 degrees, which are executed consistently during this day. In comparing all three radars, the NPOL and KGSP show similar results, while KMRX gives much higher errors. The placement of NPOL and KGSP is such that, NPOL is situated to the north of KGSP at approximately 35 km in distance and placed in the area to the southeast of the Appalachian Mountains. KMRX is located in a valley to the west of the mountains and is located to the northwest and approximately 178 km from KGSP. The individual radar location may have some effect on the results, since the gauges considered are those that are within range of each radar. KGSP and NPOL will have some gauges in common, while KMRX will not have any gauges in common with the other two radars.

An alternative approach in evaluating radar QPE to gauges was to consider the comparisons in 20 km range bins beginning with 0-20 km up to 80-100 km radar ranges. This was done again for all three radars using the lowest tilts recorded. The results in this comparison for KGSP are shown in Figure 6.15, where the errors are slightly larger overall in contrast to the cumulative ranges in Figure 6.12, but they do follow the same trends. The Figures 6.16 and 6.17 give the results for KMRX and NPOL, respectively. Overall, the errors are greater for the lowest tilt and decrease slightly on the next higher one. In further evaluation, these results from DROPS QPE compared with HADS gauges are contrasted with the study conducted by Ryzhkov et al. (2005), which used the polarimetric KOUN WSR-88DP radar validated against the Agricultural Research Service (ARS) Micronet consisting of 42 rain gauges. The locations of these particular gauges are approximately 70-80 km from the

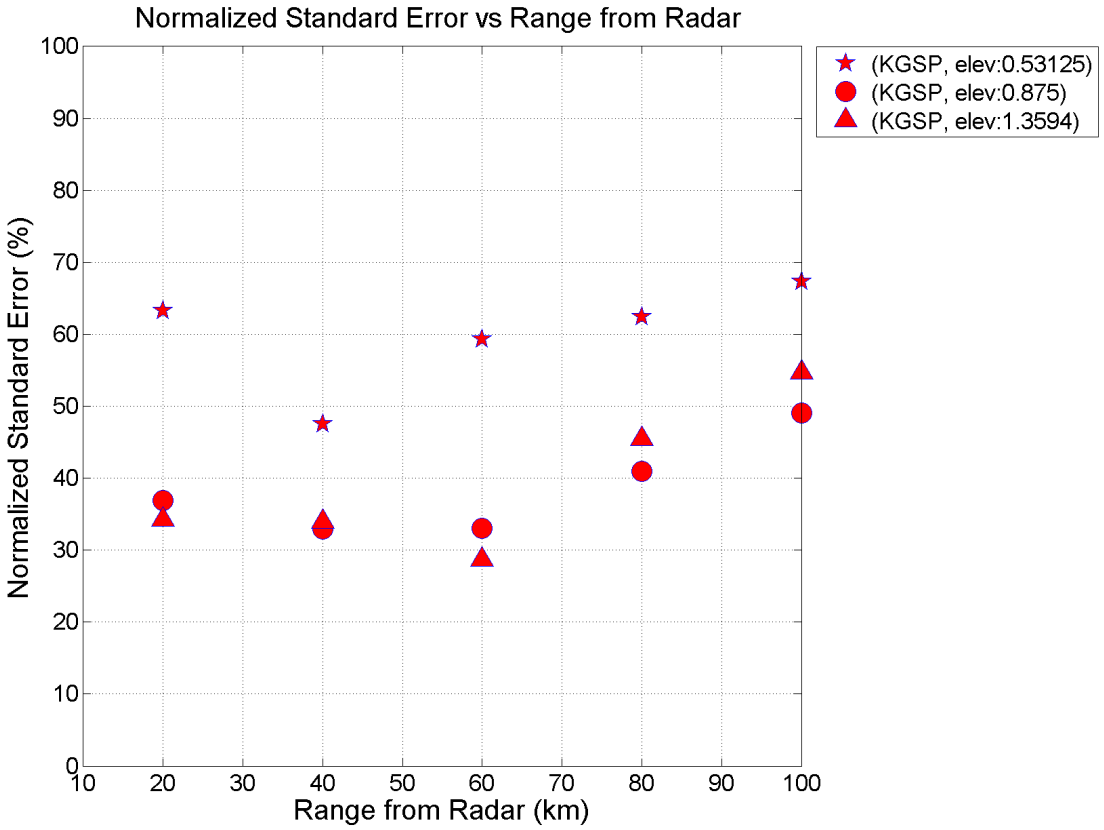

FIGURE 6.12. Normalized Standard Error for KGSP radar vs. range, where the range includes only those gauges less than that particular distance.

KOUN radar. To match the range with the KGSP and NPOL, the 60 km and 80 km range bin results are considered. For these ranges, the statistics are slightly higher, but still show good comparison. Ryzhkov et al. (2005) calculated the fractional rms error as such,

$$FRMSE = \frac{\sqrt{\langle (T_R - T_G)^2 \rangle}}{\langle T_G \rangle} \tag{36}$$

where T_R and T_G are radar and gauge hourly totals. Their results for rainfall amounts that occur between 5 mm and 30 mm results in errors that fall between 36% and 46% using their dual polarimetric rainfall algorithms for approximately 1813 radar-gauge pairs. The calculated error using Equation (36) for KGSP and NPOL in the range bins of 60 km and

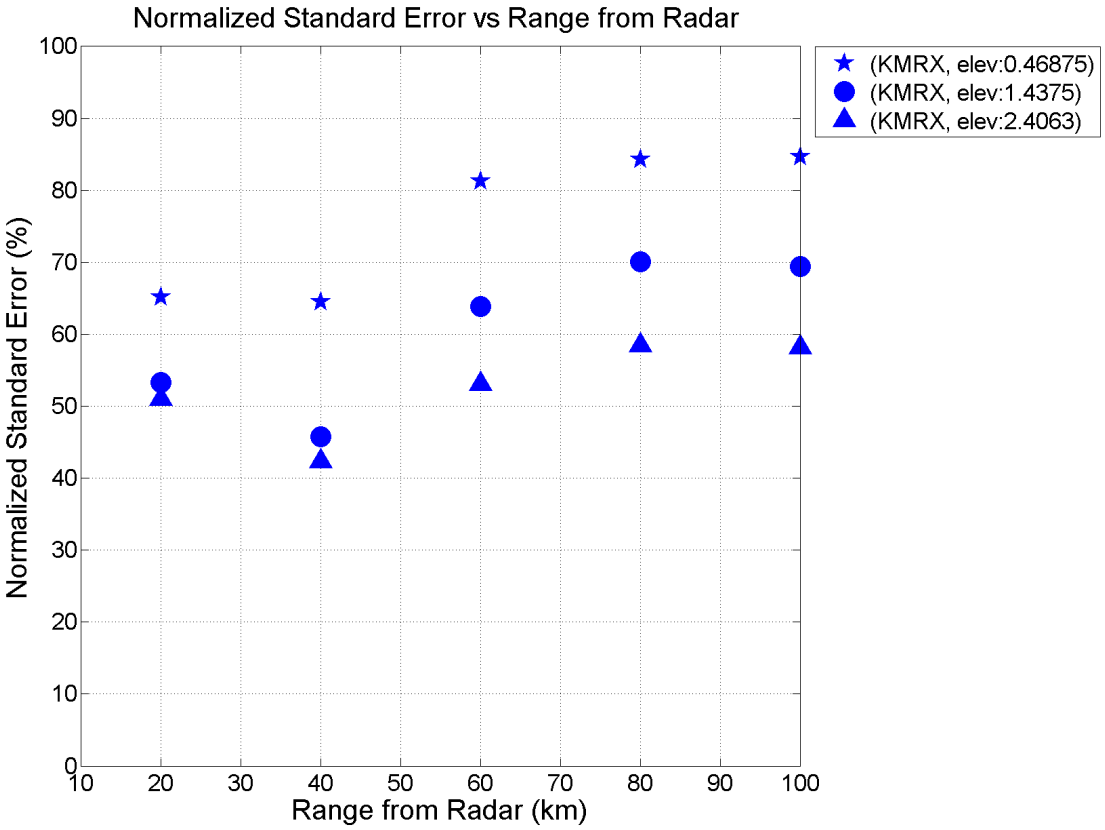

FIGURE 6.13. Normalized Standard Error for KMRX radar vs. range, where the range includes only those gauges less than that particular distance.

80 km occur within 40% and 70%. However the number of radar-gauge pairs is considerably less at 86, where additional data is needed to strengthen the statistics as well as performing quality control on the gauge set.

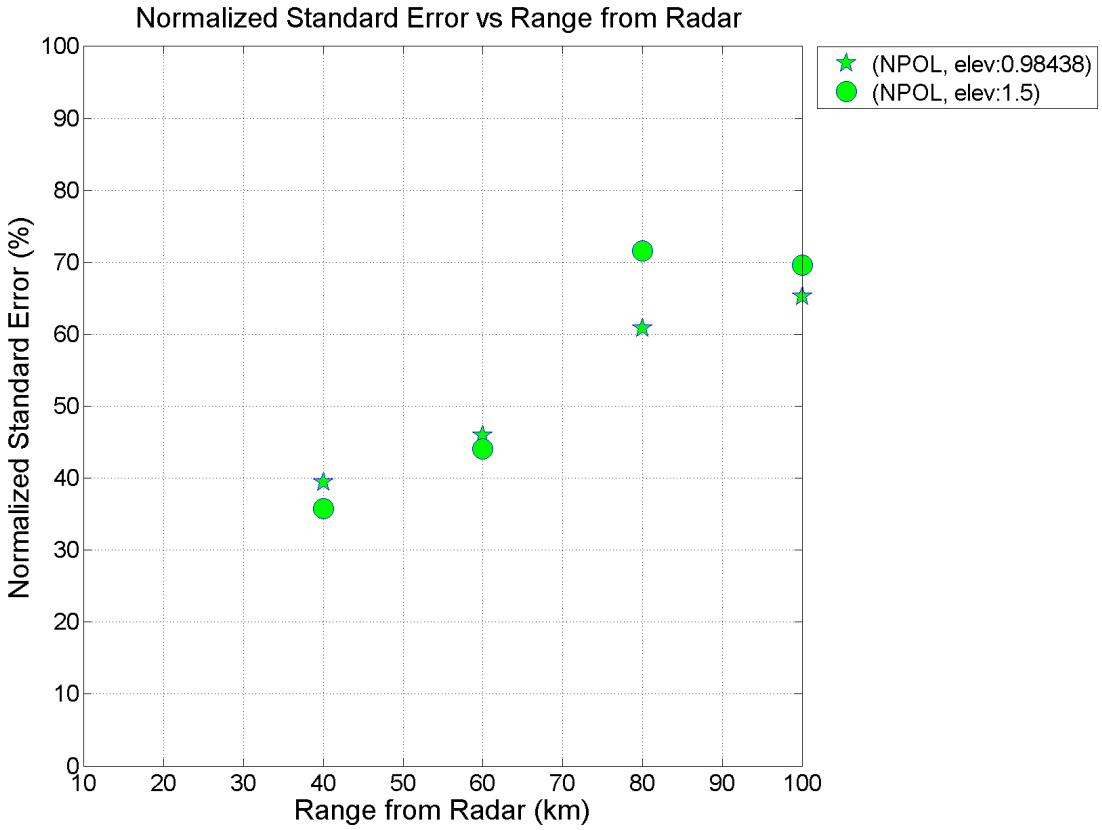

FIGURE 6.14. Normalized Standard Error for NPOL radar vs. range, where the range includes only those gauges less than that particular distance.

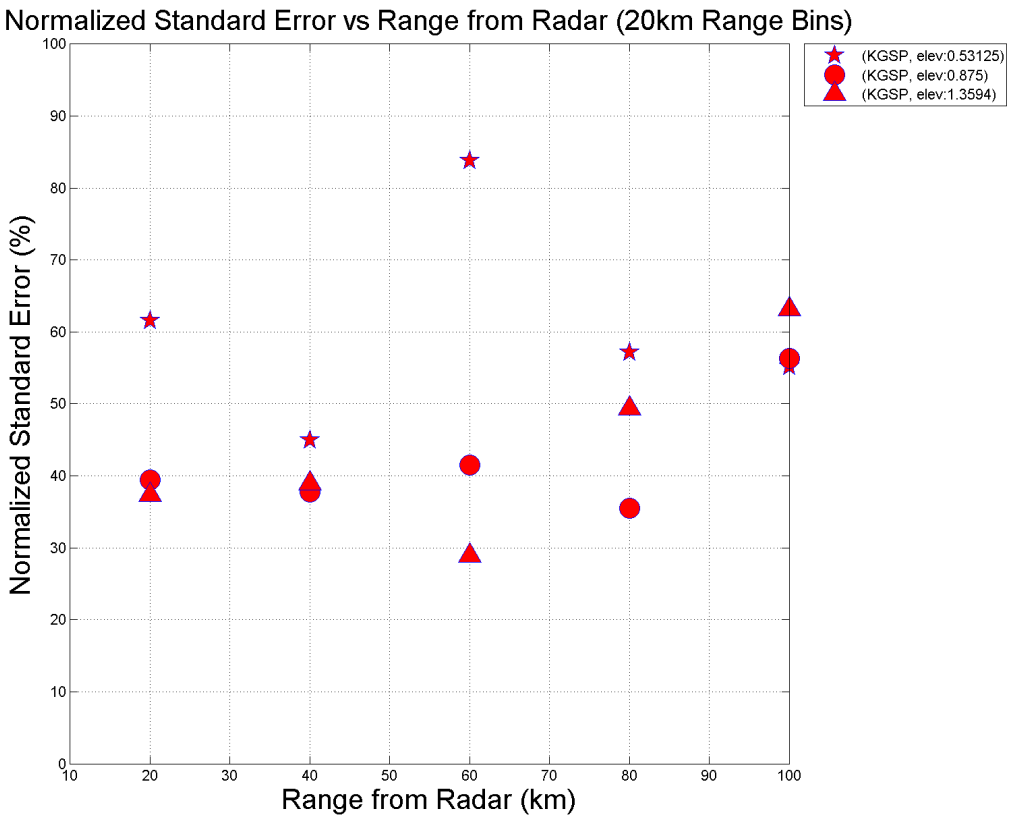

FIGURE 6.15. Normalized Standard Error for KGSP radar vs. rangebins, where the rangebins include only those gauges that are within a 20 km wide range bin.

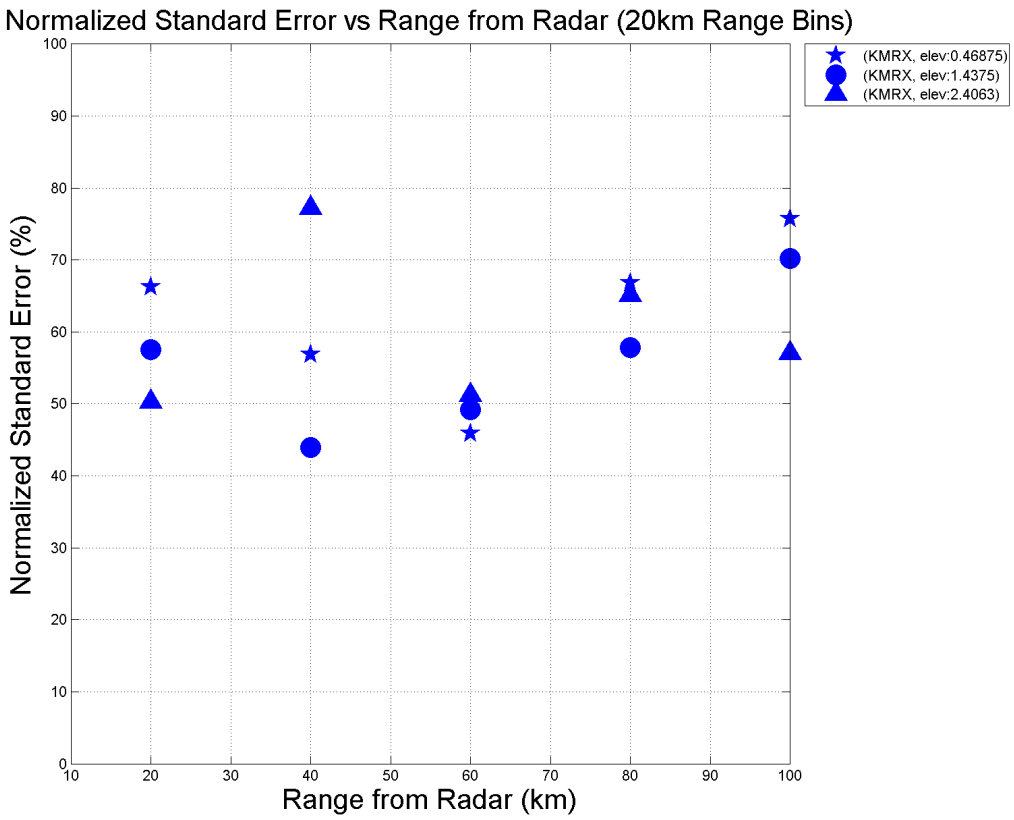

FIGURE 6.16. Normalized Standard Error for KMRX radar vs. rangebins, where the rangebins include only those gauges that are within a 20 km wide range bin.

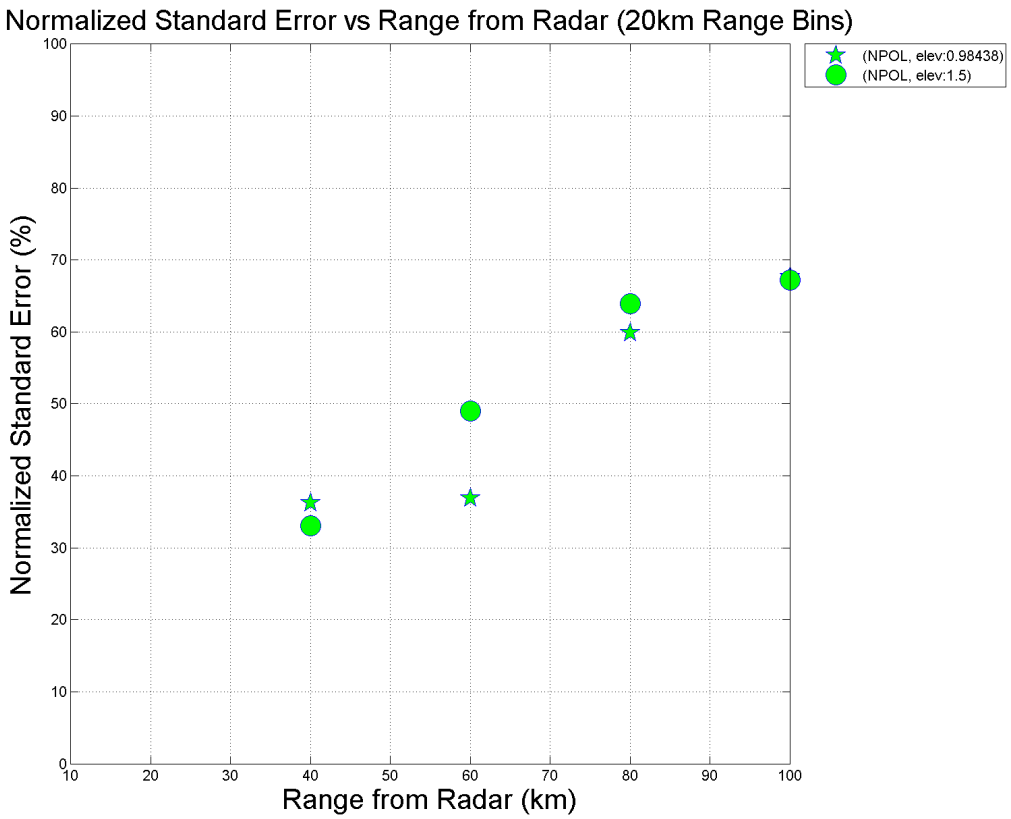

FIGURE 6.17. Normalized Standard Error for NPOL radar vs. rangebins, where the rangebins include only those gauges that are within a 20 km wide range bin.

CHAPTER 7

RAMS QPE Gridding

7.1. Gridding of QPE to Domain Coordinates

The pulsed electromagnetic energy from radar follows a conical beam pattern as it propagates from the dish of the antenna into the atmosphere. The radar antenna scans azimuthally beginning at 0 degrees and completing a full circle to 360 degrees, where 0 degrees is aligned with north. In addition the elevation angles range from 0 degree to 90 degrees, such that 0 degree is parallel to the ground. The radar operates by scanning complete sweeps using pre-determined elevation angle steps. The volume scans that result from a set number of complete sweeps are recorded in spherical coordinates (r, ϕ, θ), where r is the distance from radar, ϕ is the azimuth angle and θ is the elevation angle off the horizon. The propagation of the radar beam is assumed to follow a path that can be described using a 4/3 earth model (Doviak and Zrnic 1993). This can be related with the following equations:

$$h = [r^2 + (k_e a)^2 + 2 r k_e a \sin\theta]^{1/2} - k_e a \tag{37}$$

$$s = k_e a \sin^{-1} \frac{r \cos\theta}{k_e a + h} \tag{38}$$

where a represents the earth's radius, k_e represents the 4/3-effective earth radius, h is the height of the center of the radar beam, and s is the distance between the radar and the projection of the bin along the earth surface. The bearing and distance between two locations on the earth's surface is done using a spherical trigonometric approach referred to as the great circle distance, where these calculations are performed in latitude and longitude

coordinates. On the other hand, using a position's latitude and longitude, the location of another point which is some great circle distance away (e.g., s) can be found with the initial bearing (e.g., Θ) on the path of the great circle. Using this principle, along with the radar ray path equation, every radar bin with its native coordinates (r, Θ, Ψ) can be mapped to the earth's latitude and longitude coordinates (lat, lon, h) after the radar's location is known. Using the same approach as Liu et al. (2007), which was applied to an X-band network of radars (McLaughlin et al. 2009). These equations are:

$$lat_2 = \sin^{-1}(\sin(lat_1)\cos(\frac{s}{a}) + \cos(lat_1)\sin(\frac{s}{a})\cos(\Phi)) \tag{39}$$

$$lon_2 = lon_1 + \arctan(\sin(\Phi)\sin(\frac{s}{a})\cos(lat_1)\cos(\frac{s}{a}) - \sin(lat_1)\sin(lat_2)) \tag{40}$$

In the RAMS QPE processing, the lowest radar elevation angle scans are converted from the radar spherical coordinates into a rectangular system using the above equations where the dimensions of the coordinates are set to 0.01 degree by 0.01 degree in latitude and longitude (Liu et al. 2007). This is done to coincide with the MRMS choice of coordinates.

7.2. Radar Blockage

Radars operating near mountains have the possibility of blockage over certain scanning azimuth angles. In a complex terrain, it is desirable to know the blockage angles seen by a radar for the various elevation scans and especially for the lower tilts. In terms of all the NEXRAD radars, blockage maps have been determined and are made available, but for radars that are mobile such as NPOL and NOXP in the case of the NOAA Hydrometeorology Testbed Southeast Pilot Study (HMT SEP) domain, the blockage is not known immediately. If the digital elevation maps are known and the radar site latitude, longitude, and elevation

are stated, then the blockages can be determined in manner shown by Kucera et al. (2004), which is to relate the position and height of the beam to the ground location determined by the digital elevation map. The scanning heights of the radars considered for the RAMS QPE can be seen in Figures 7.1 - 7.4. These plots show the beam width and height in regards to NASA rain gauges located within the mountainous areas. The blue height bars show the relative distance and height in comparison to the beam width. This is shown only for the lowest elevation scan with a clear path over the majority of the gauges. Scans below this elevation will be partially to fully blocked at particular azimuth angles.

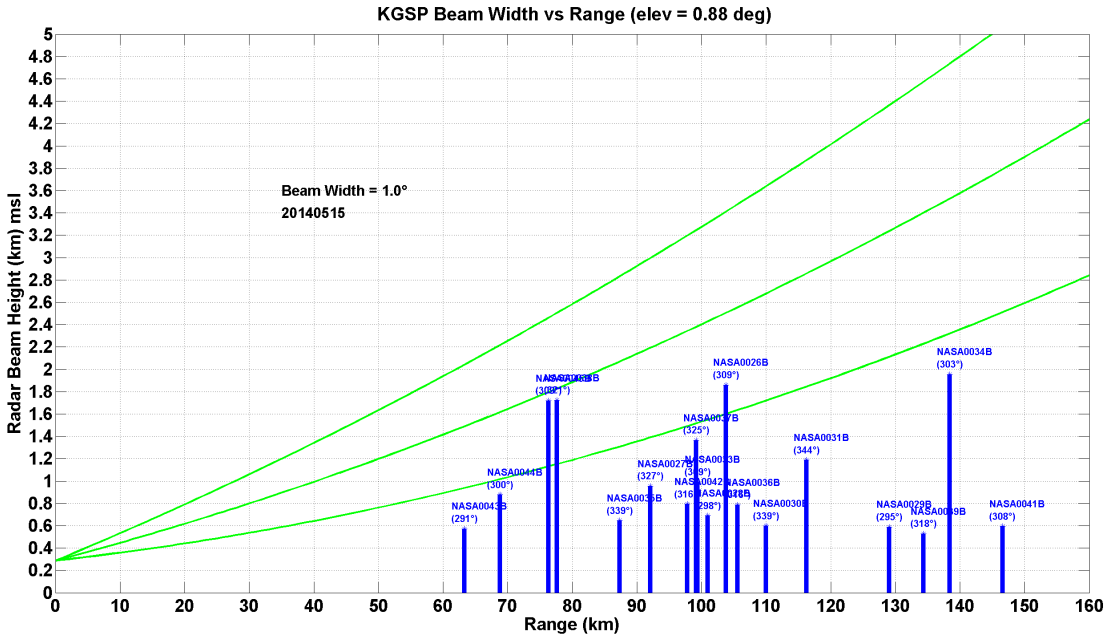

FIGURE 7.1. KGSP beam height over gauges within and around the Pigeon River basin, where the relative distance and height are indicated by the blue bar.

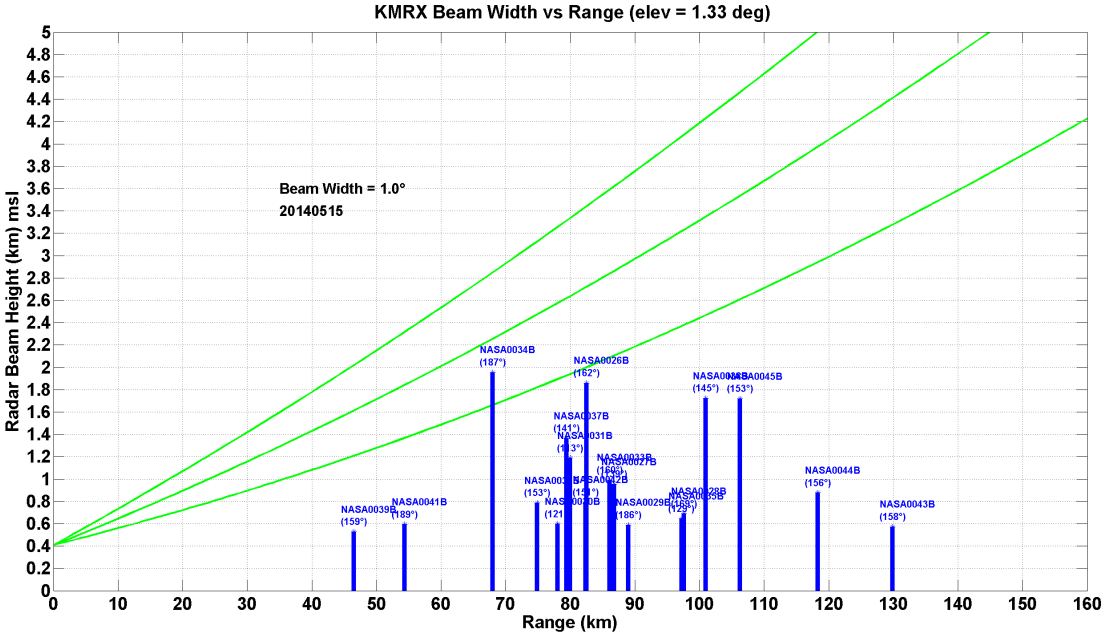

FIGURE 7.2. KMRX beam height over gauges within and around the Pigeon River basin, where the relative distance and height are indicated by the blue bar.

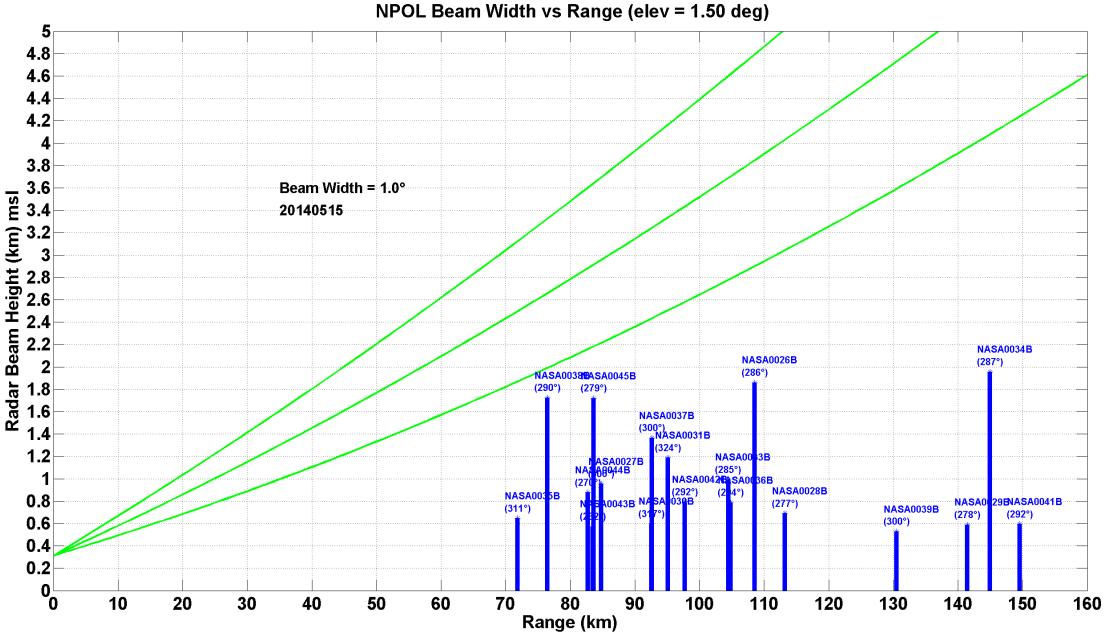

FIGURE 7.3. NPOL beam height over gauges within and around the Pigeon River basin, where the relative distance and height are indicated by the blue bar.

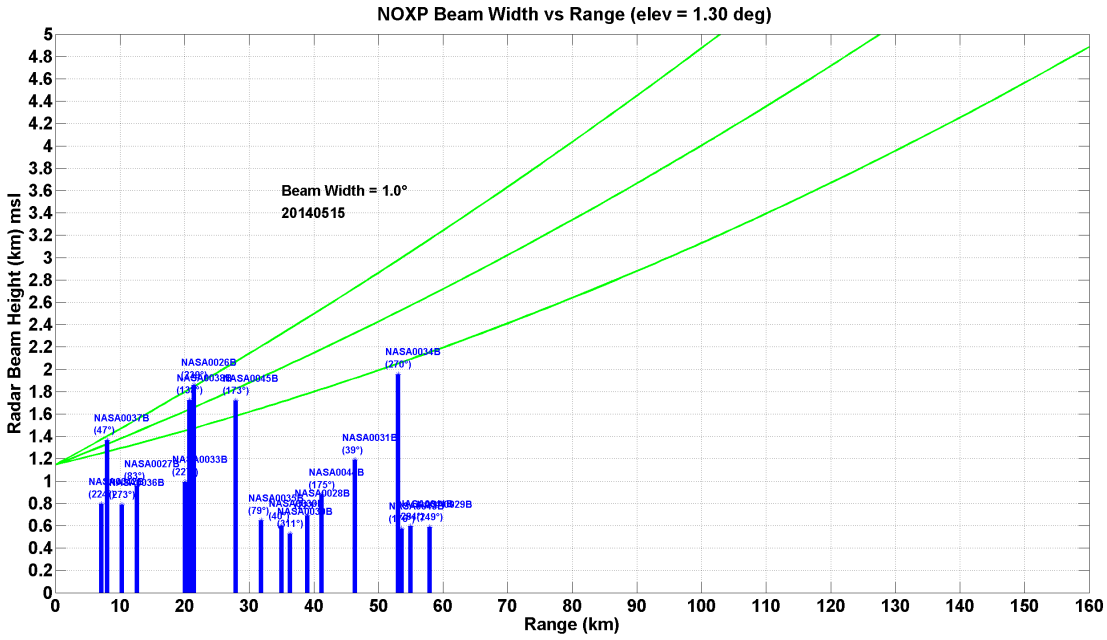

FIGURE 7.4. NOXP beam height over gauges within and around the Pigeon River basin, where the relative distance and height are indicated by the blue bar.

7.3. Combining Single Radar QPE Scans into a Hybrid Scan of Dual Polarization

The gridding of the radar spherical coordinates and then the combining of the single radar multiple tilts in the RAMS QPE is completed using a simple approach that joins the lowest elevation scans into a Hybrid Scan of Dual Polarization (HSDP). First of all, each of the lowest sweeps associated with a particular radar are placed into a rectangular lat-lon coordinate system by applying the great circle mapping techniques shown in the four Equations (37 - 40). The boundaries of the domain are set prior to the conversion, where the coordinate spatial resolution is set to 0.01 degree latitude by 0.01 degree longitude. As an example considering only one radar, the first step is gridding each of the three lowest tilts of the radar sweeps into the specified coordinate boundary to create three levels of gridded data with heights associated to the elevation scan angle. Since the objective is to derive

rainfall estimates, it is ideal to retain the measurements that are closest to the ground, so that all the data from the first tilt is kept to create the initial HSDP. However in complex terrain, there are many instances where certain radials from the lowest tilt in the radar data are compromised due to beam blockage, and missing pixels are expected. The next step is to apply the next highest gridded elevation scan to the HSDP. If there are missing pixels in the HSDP derived from the lowest tilt and those matching pixels exist in the next highest elevation scan, then higher tilt existing pixels are added into the HSDP. The HSDP at this point results in a mixture of the two scans, where the lowest elevation data is retained and the second tilt fills in the missing pixels. This procedure continues by combining the third tilt and so forth. An example in Figure 7.5 shows the rain rate fields from the KGSP radar at 0.53, 0.92 and 1.32 degree elevation scans and the HSDP resulting from combining scans in the mentioned steps. This method was applied to the reflectivity fields for the same data, where this is shown in Figure 7.6.

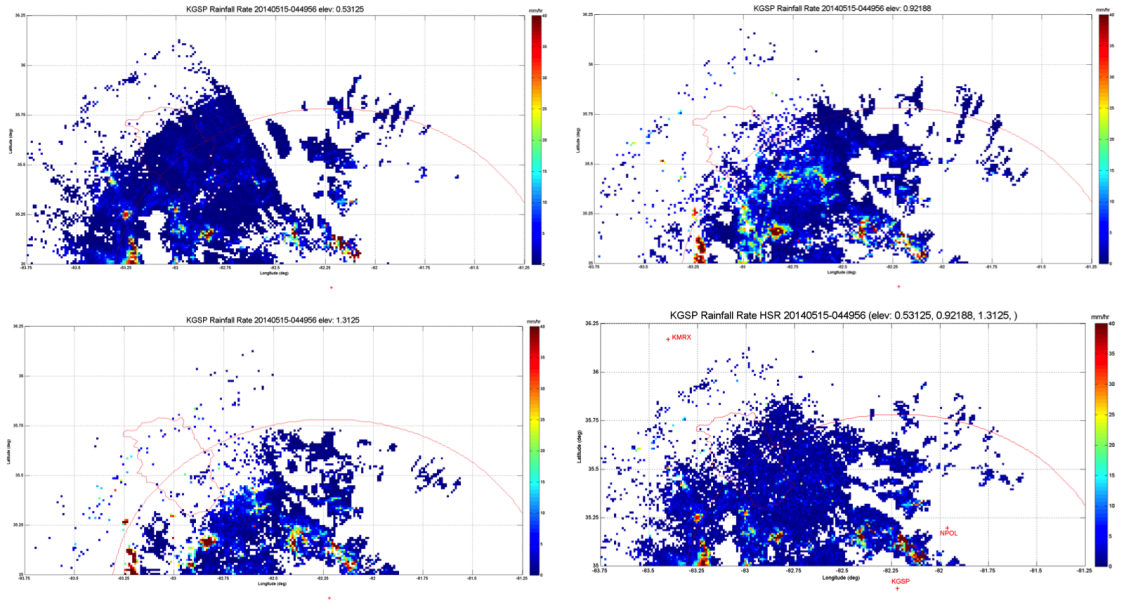

FIGURE 7.5. HSDP for KGSP radar by combinine the three lowest tilts to create the hybrid scan of dual polarization for the rain rate fields.

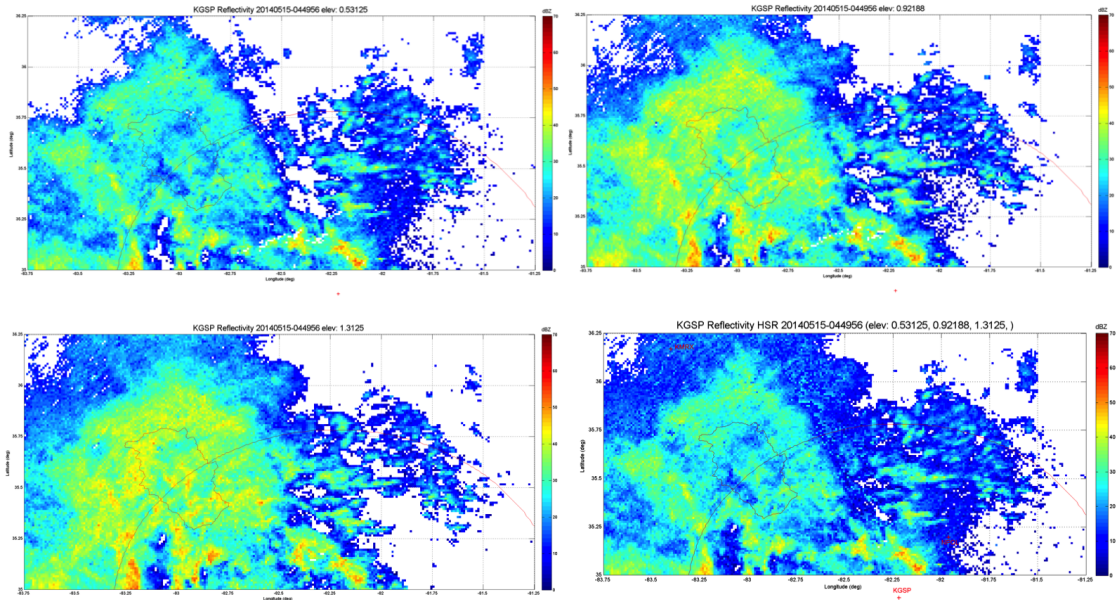

FIGURE 7.6. HSDP for KGSP radar by combinine the three lowest tilts to create the hybrid scan of dual polarization for the reflectivity fields.

7.4. Mosaicking Multiple Radar QPE

7.4.1. METHODOLOGY

The mosaicking of the radar images can be carried out once the individual radar hybrid scans of dual polarization (HSDP) are available. Since the domain coordinates are equivalent in each of the single radar HSDP, the merging consists of essentially overlaying each of the HSDP data pixel fields. Depending upon the number of radars available for merging, the number of common pixel points between the single radar HSDP fields can fluctuate. When there are multiple data points representing a single pixel, the choice is made to use the maximum value. The choice of this method is first based upon the simplicity of this approach. An alternative to this is to apply a mean method to the common pixels. However for this particular day of data, a comparison between the mean and max was done and there was very minimal difference between the two techniques, and that the maximum showed less bias and lower normalized standard error in regards to the mean approach. However these

results are based upon one day of data for May 15, 2014, and were only considering a domain that occurs within a complex terrain locale. In the Figures 7.7 - 7.9, this shows the HSDP for KGSP, KRMX and NPOL, respectively, after combining the single radar tilts following the previous stated procedure for this. In each of the single radar HSDP fields, blockage is visible in azimuth angles that scan over the mountaineous regions, which is located approximately midway between the KGSP and KMRX and spans from the southwest to the northeast. These images show both the rainrate and reflectivity fields that occured during a single five minute window in which a convective cell was moving in parallel to the mountain range. In Figure 7.10, the merged radar image is presented for this particular time frame by combining the three HSDP from KGSP, KRMS and NPOL.

7.4.2. Timing Issues in Merging

The merging of single radar HSDP scans into a mosaic has to account for both differences in the timing and the availability of the single radar combined scans. The radar scans to be merged is assumed to be un-synchronized in time, but only need to occur within a time span. The simple approach used to handle this variability is to establish a timing window. The time frame selected initially is a five minute window which is loosely based upon the typical interval for a NEXRAD WSR-88DP to complete a full volume scan operating in precipitation mode. So for each five minute time frame, the HSDP that occur from each radar are grouped. If there is a missing radar hybrid scan, the merge is accomplished with what is available. In the case that two HSDP fields from the same radar appear in the same timing window, the radar HSDP field with the earliest time stamp is applied in the mosaic for that particular time window. This is done as a simple first concept, where the assumption is that the storm movement is slow to moderate. An alternative would be to either shorten

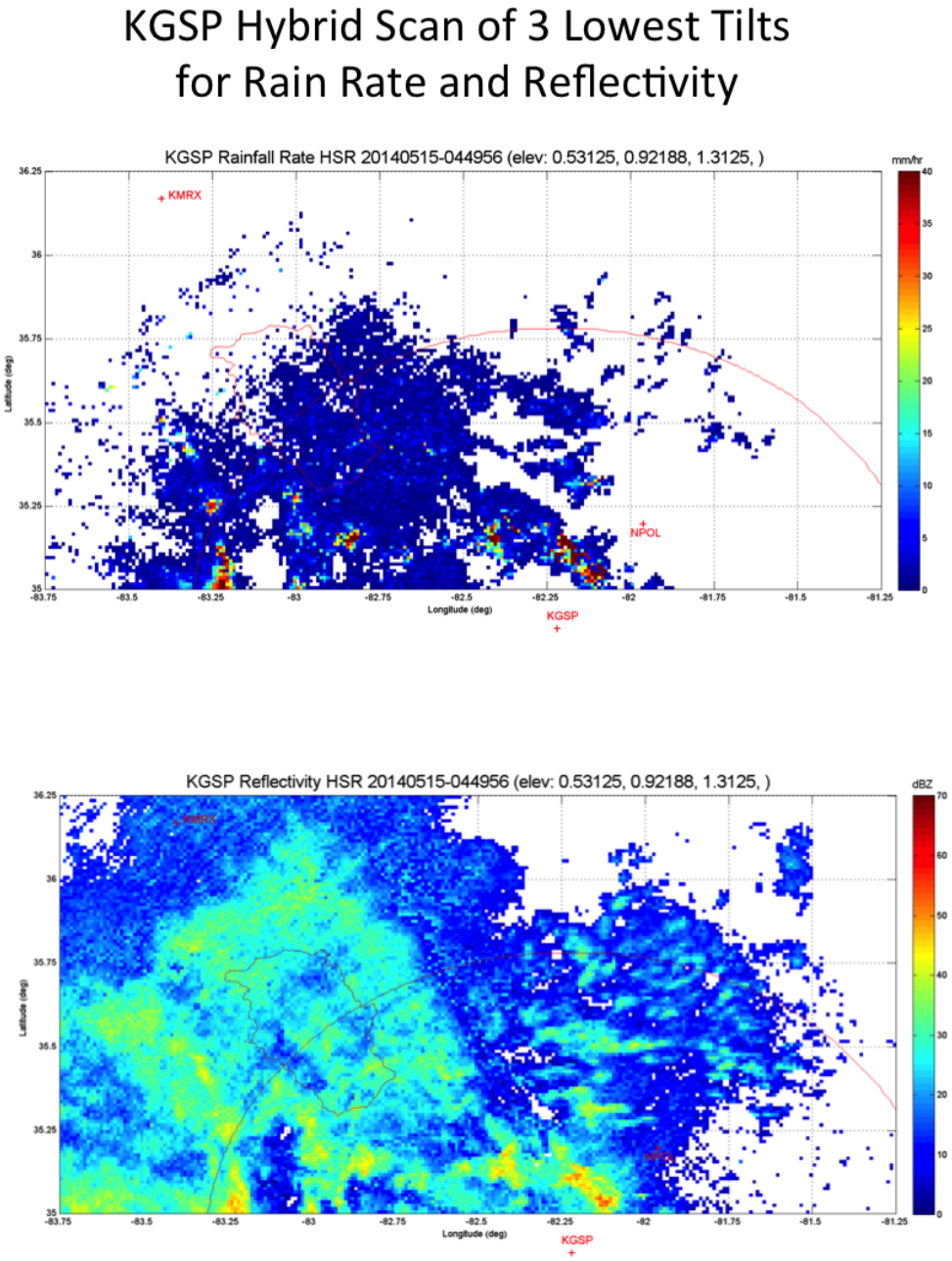

FIGURE 7.7. KGSP final HSDP field created from the lowest tilts.

the timing window or average the fields. In the event that there are no HSDP fields occurring for a particulate timing window, the merged is skipped and the process continues onto the

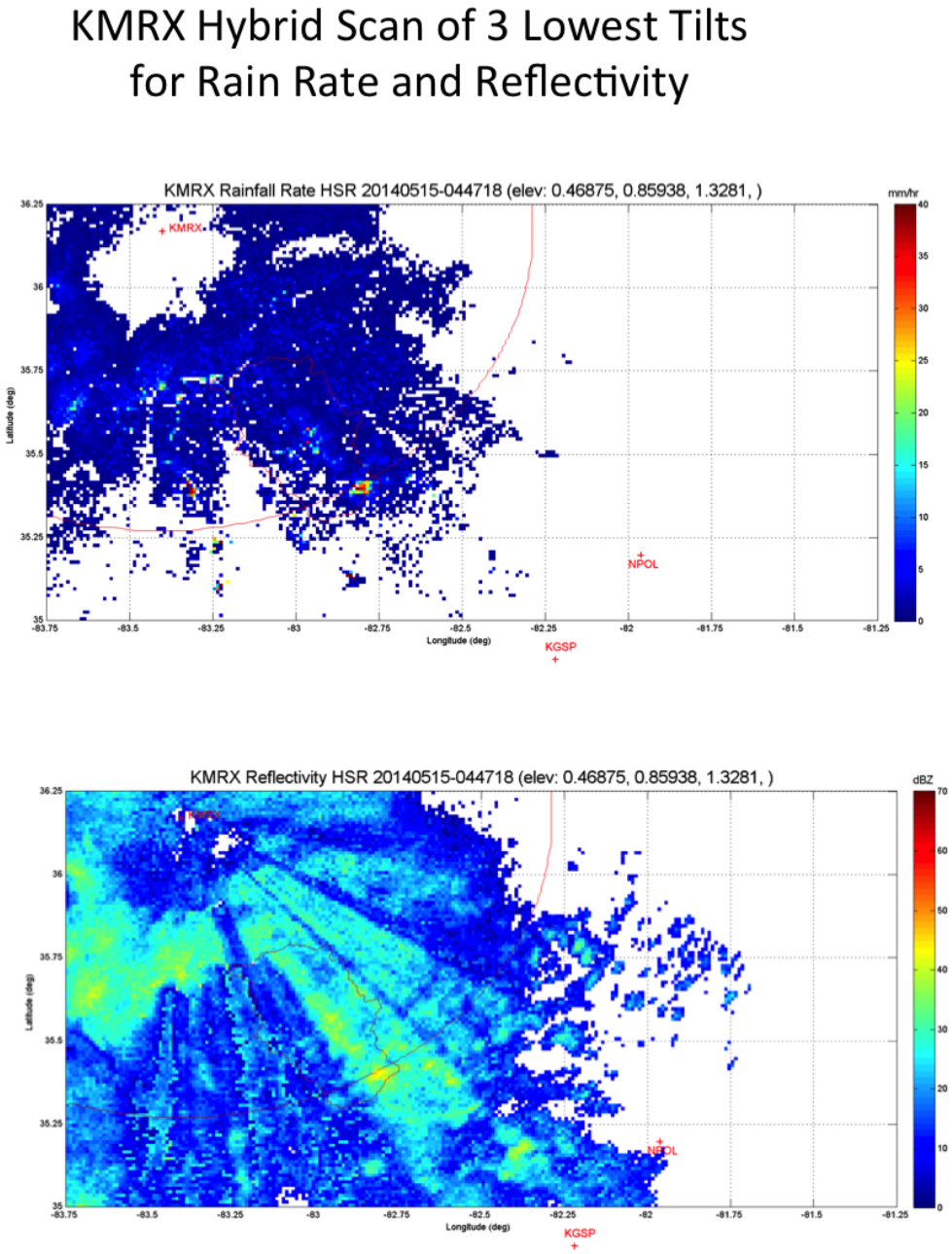

FIGURE 7.8. KMRX final HSDP field created from the lowest tilts.

next five minute time frame. Therefore producing mosaicked rain rate fields in five minute time intervals.

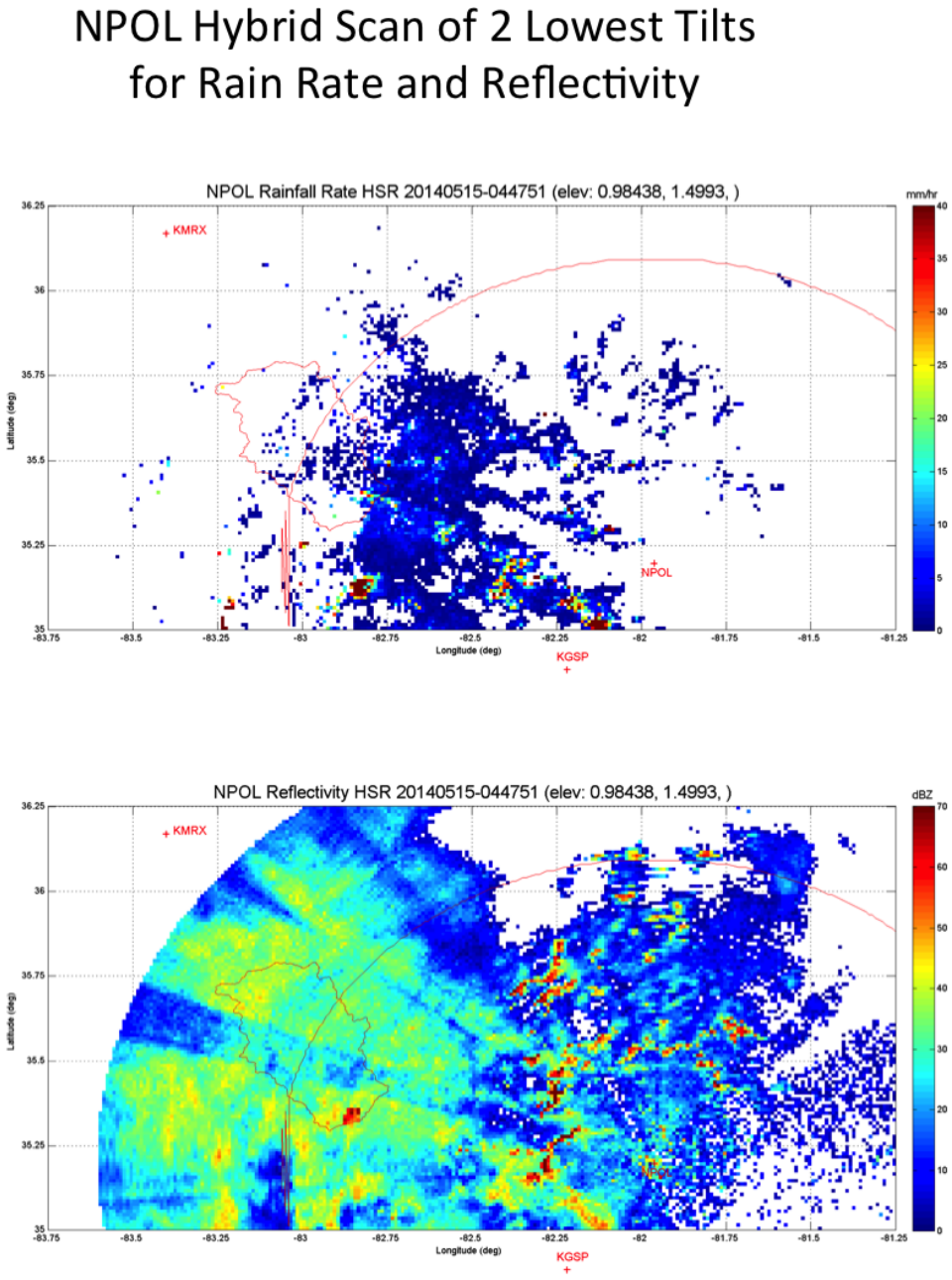

FIGURE 7.9. NPOL final HSDP field created from the lowest tilts.

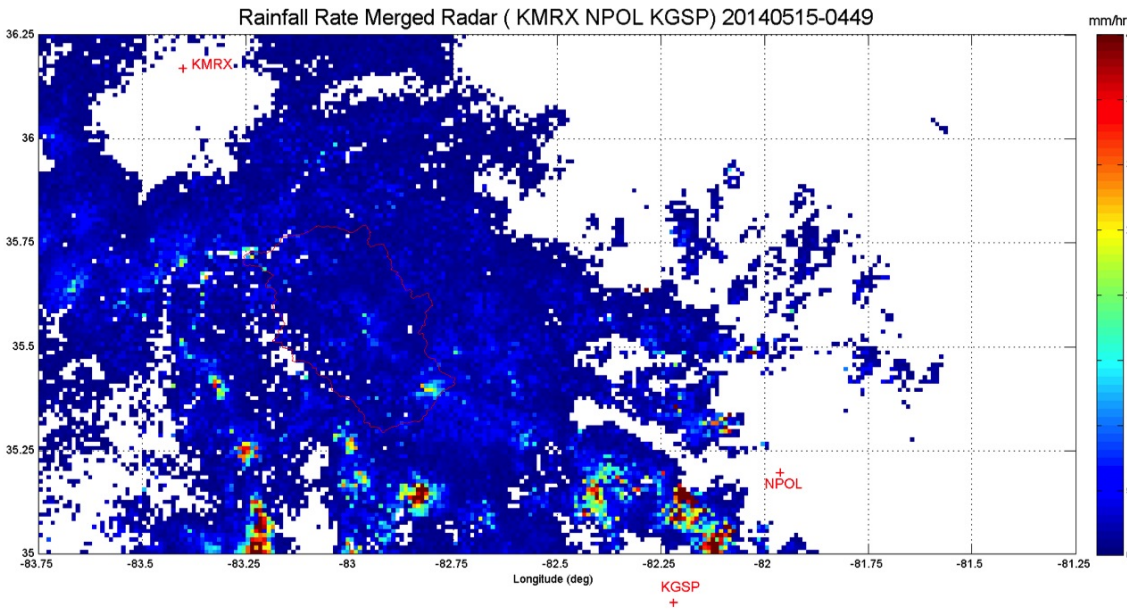

FIGURE 7.10. Mosaicked rain rate fields from KGSP, KMRX and NPOL radars.

CHAPTER 8

Evaluation of RAMS QPE over Pigeon River Basin within NOAA HMT-Southeast Domain

The NOAA Hydrometeorology Testbed (HMT) is established to allow for further research into unique weather conditions pertaining to regions of interest, where severe or continuous rainfall can generate flooding. It also strives to increase the science of climatology with the goal of transitioning these ideas into better forecasting. In this particular region, NOAA HMT has five principle areas of activity, which are:

(1) Quantitative Precipitation Estimates: Developing and prototyping 21st Century methods for observing precipitation.
(2) Quantitative Precipitation Forecasting: Addressing the challenge of extreme precipitation forecasting by identifying gaps to developing new tools.
(3) Snow Information: Characterizing snow to address uncertainty in forecasting, flood control, and water management.
(4) Hydrologic Applications: Evaluating advanced observations of rain and snow, temperature, and soil moisture to provide best possible "forcings" for river prediction.
(5) Decision Support: Developing better tools for forecasters and end users in regards to extreme precipitation forecasts.

Furthermore to advance the impact of NOAA HMT research and techniques in regards to orographic precipitation in diverse environments especially in complex terrains, NOAA has decided to conduct operations in the southeastern part of the U.S. referred to as the Southeast Pilot Study (HMT-SEP hereafter). This study is primarily focused on quantitative

precipitation estimation, which falls under one of the five major areas of study, but to also pursue opportunities that address the other areas of interest in the goals for HMT.

HMT-SEP area of interest is located in western North Carolina in several basins that are within the Appalachian Mountain range. NOAA along with other agencies has deployed numerous weather detecting instruments, where the majority of this equipment was committed to the areas of complex terrain within this region. The basins of primary interest are the Pigeon River basin and the Upper Catawba River basin (Figure 8.1) near Ashville, NC.

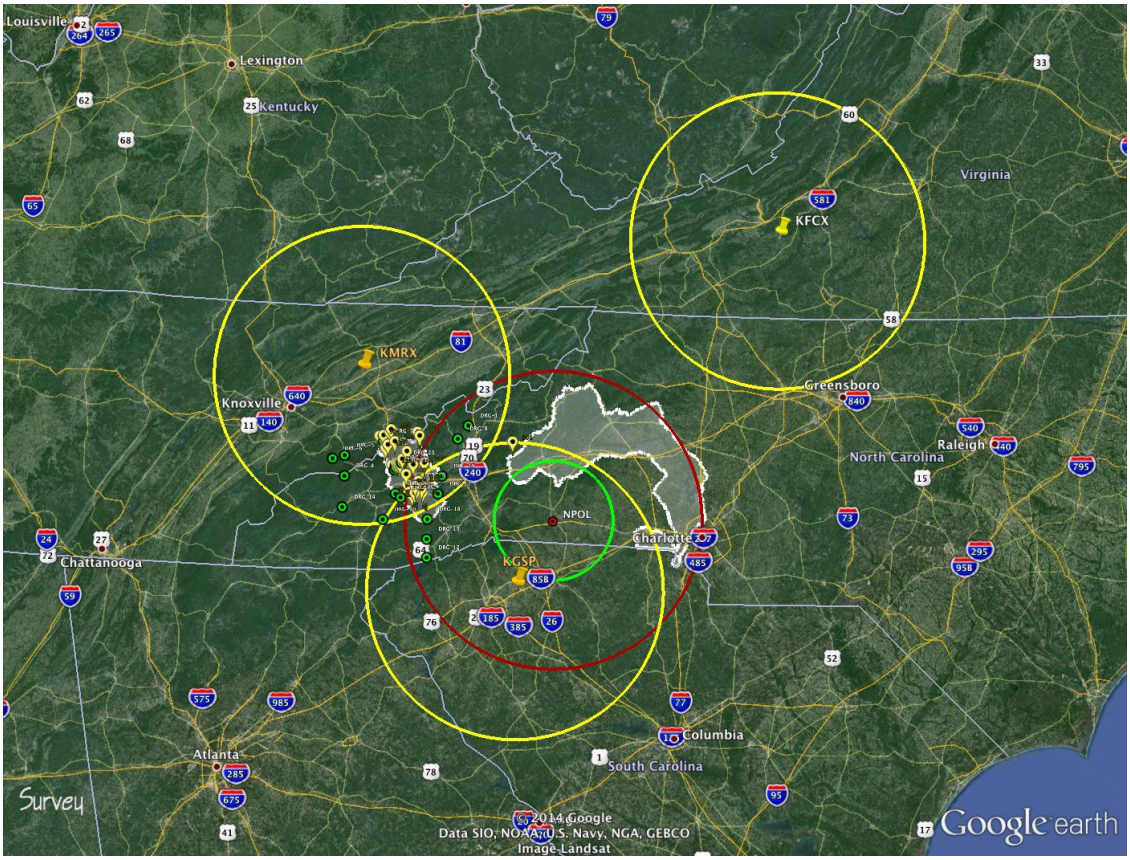

FIGURE 8.1. Map of NOAA HMT-SEP area of interest showing local NEXRAD radars (yellow 100 km range rings), NASA NPOL radar (red 100 km range ring) and NASA D3R radar (green 40 km range ring). The Pigeon River Watershed and Catawba River watershed are shaded in white.

This effort by NOAA complements the interest by NASA to validate precipitation retrieval algorithms in the same region of North Carolina for the Global Precipitation Measurement (GPM) satellite ground validation mission. The NASA field campaign is known as the GPM Integrated Precipitation and Hydrology Experiment (IPHEX). One of the factors of NASA's decision to conduct a field experiments in this location is the desire to partner with NOAA HMT in precipitation research energies.

IPHEX has two focused observational activities: 1) the long-term observing period (LOP) lasting from October 2013 through October 2014 involving an extended rain gauge network of 60 stations, where half of these gauges will be equipped with multiple rain gauge platforms. In addition to the fixed regional observing system, a disdrometer network consisting of twenty separate clusters, and two mobile profiling facilities including Micro Rain Radars (MRRs), and 2) an intense observing period (IOP) occurring from May through July of 2014, which is post GPM satellite launch. This IOP is focusing on four dimensional (4-D) mapping of precipitation structure during which NASA's NPOL S-band scanning dual-polarization radar, the dual-frequency Ka-Ku, dual polarized, Doppler radar (D3R), four additional MRRs, and an X-band radar was deployed in addition to the long-term fixed instrumentation.

8.1. Description of HMT Southeast Domain

This area of interest is positioned over the Southern Appalachians and can be characterized by complex relief but moderate orography with maximum elevation around 2000 m (Prat and Barros 2010). The region also is subject to humid continental climate with strong orographic effects and experiences precipitation patterns that are both tropical, extra tropical synoptic-scale systems, and smaller scale features such as: cold air damming, wedge

fronts and lee troughs. The HMT-SEP field study is structured to analyze QPE in regions of complex terrain and moderate orography (height less than 2000 m). The influences for choosing this region include:

- It is a region where known QPE and QPF bias occur.
- A variety of precipitation regimes occur in the region.
- There exists an infrastructure of precipitation and hydrologic instrumentation to leverage for examination of orographic hydrologic processes.

The climate for the study area also experiences moisture rich winds from the Gulf of Mexico and westerly mesoscale convective systems in the warm season, whereas westerly and northwesterly flows govern most of winter weather activities. Previous research has shown that the orographic rainfall enhancement is very strong, on the order of 60% at ridge locations compared to in the valley (Prat and Barros 2010). The extratropical synoptic-scale systems tend to approach from the west, northwest, or south directions, while the tropical hurricanes regularly move in from the south or east. Whenever these systems encroach into the southern Appalachian Mountains, the interaction of the moist low-level flow associated with the system and the terrain produces precipitation intensity usually in the far southwest portion of North Carolina. If there are an easterly component of the low-level winds, the orographic precipitation is seen farther to the east in the Catawba River basin (Figure 8.2). There are also mesoscale convective systems (MCSs) and warm season cold fronts that enter the region from the west (Moore et al. 2011). These varied types of precipitation provide considerable observational challenges and provides the motivation for investigating rainfall in this complex region.

Given that the primary focus of the HMT-SEP study is to emphasis QPE, the objectives for NOAA in this plan are to:

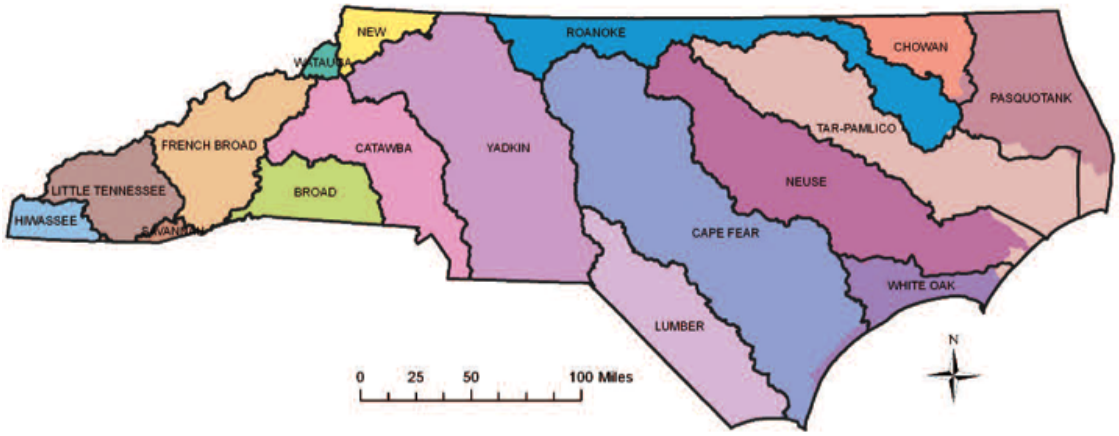

FIGURE 8.2. Map showing the 17 river basins in North Carolina. The Pigeon River watershed is within the French Broad river basin and the Catawba River watershed is located in the Catawba River basin.

- Support the National Weather Service (NWS) adaptation and use of polarimetric algorithms for the upgrade to the WSR-88D network, such as to evaluate the radar-rainfall algorithms.
- Evaluate and improve QPE systems (Multi-sensor Precipitation Estimation (MPE), Multi-Radar Multi-Sensor (MRMS), Stage IV and others as appropriate) in complex terrain extending from the Appalachian Mountains to the Piedmont to the coastal plain. In this effort to research these topics:
  - Intelligent integration of multi-sensor QPE information of gauges, radars, and satellites.

- Infrared (IR) and microwave satellite QPE products (CMORPH, SCaMPR, Hydro-Estimator, TRMM 2A25 And 3B42) with ground-based QPE.
- 4-D structure of precipitation and variability of the drop size distribution (DSD) with the resulting impact on QPE systems.
- Impact of gap-filling radars on QPE systems.

The domain defined for this area will encompass the fore mentioned basins and will provide a wide enough coverage to allow for flexibility in the various combinations of measuring input for QPE. The limits of the domain will extend from 33.50 degree to 38.50 degree latitude and 79.50 degree to 84.50 degreee longitude (Figure 8.3).

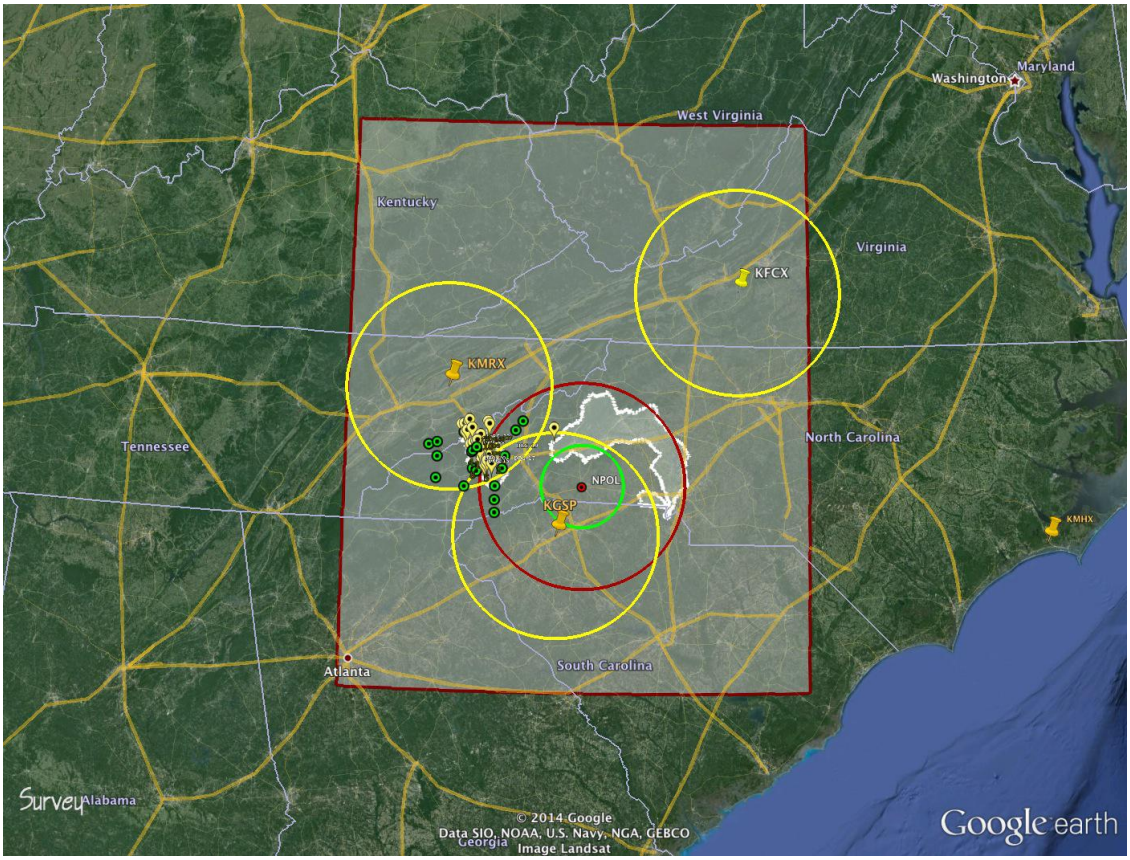

FIGURE 8.3. Map of the HMT-SEP domain covering the watersheds of interest. Domain is shaded in white. The yellow and red rings indicate the 100 km range rings of the local radars.

8.2. Radar Coverage

The radar coverage over this domain is comprised of the existing three NEXRAD WSR-88DP radars (KGSP, KMRX, and KFCX) as well as the NASA dual polarization field deployable radar (NPOL) and the NASA dual-frequency dual polarized (D3R) radar. These radar locations are shown in Figure 8.4 with 100 km (yellow and red) and 40 km (green) radar rings respectively. The location of the Pigeon River watershed with respect to NEXRAD and NPOL radars is at far distance from the radars and results in poor radar coverage. In addition to these stationary radars, NOAA has also deployed the mobile X-band Polarimetric Radar referred to as NOXP as a gap filling radar within the pigeon basin, and this will provide additional scanning capabilites in the mountainous locale. All of these radars are capable of recording dual polarization parameters.

The principal scientific use of NASA NPOL in IPHEX has been targeted toward providing high quality, relatively unattenuated, dual polarized rain mapping as well as observations of microphysical processes occurring in the vertical column. Use of NPOL in this effort seeks to meet the expectation of the NASA GPM integrated hydrologic and physical validation scientific objectives that place a premium on quality regional rainfall products for benchmarking satellite retrievals and hydrologic models, diagnosing distributions of particle size, shape, and phase in the vertical and providing an unattenuated reflectivity reference for studies of path integrated attenuation at Ka/Ku frequencies (e.g., those available from the GPM DPR and/or the D3R). NPOL performed sector volume and range height indicator (RHI) scans as well as plan-position indicator (PPI) scanning. NPOL operated in conjunction with the collocated D3R radar. Primary emphases for NPOL scanning has been geared towards: a) high quality rain mapping scans performed at lowest elevation angles, interspersed with b) rapid, high resolution sampling of the vertical structure of precipitation as desired and

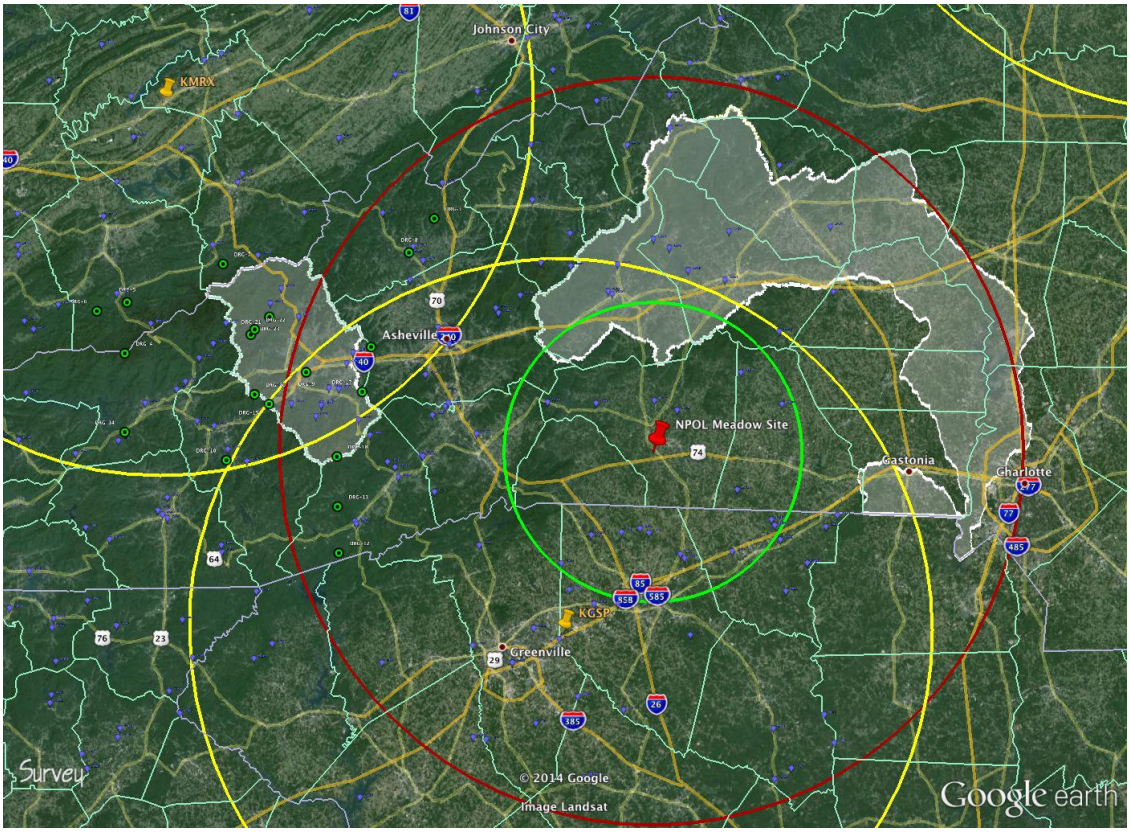

FIGURE 8.4. Radar coverage over the Pigeon River watershed. Yellow and red circles are the 100 km range rings for NEXRAD and NPOL, respectively. The 40 km range ring for the D3R radar is in green. Light purple dots are the NOAA HADS rain gauges, and the green dots are the NASA dual-tipping bucket rain gauges.

coordinated with aircraft scanning operations and/or satellite overpasses in the sampling domain.

The scanning strategies employed by the NPOL and NOAA radars are to enable joint studies of the vertical structure of precipitation processes, rain and DSD variability (decorrelation length, times), path integrated attenuation impacts and mitigation of GPM dual-frequency radar retrieval algorithms, and the coincident mapping of associated storm kinematics. Vertically pointing scans are conducted on a targeted basis in light stratiform precipitation to facilitate calibration of differential reflectivity (Zdr).

8.2.1. NEXRAD WSR-88DP

The three NEXRAD radars: KGSP, KMRX, and KFCX are the nearest in proximity to the basins of interest and the domain of the study. In considering the distance between the radars and the Pigeon River and Catawba River basins, the KFCX radar scanning data will have minimal influence on the QPE derived due to the distance weighting, but it is included since it is within proximity.

The physical location of the KGSP and KMRX are such that these radars are positioned on either side of the Appalachian mountain range, however due to the height and terrain considerations there is considerable blockage over the area of interest (Pigeon River basin). The coverage maps showing blockage can be seen for KGSP in the Figure 8.5 and for KMRX in Figure 8.6.

The NEXRAD WSR-88DP operates at S-band frequency and is capable of measuring dual polarization variables. The effective range is up to 230 km, and the scan strategies for precipitation and other types of events are listed in Table 2.1. The primary mode of operation for rain is VCP 21 and VCP 31.

8.2.2. NASA NPOL

NASA's dual-polarimetric (NPOL) radar (Gerlach and Petersen 2011) is positioned about 30 km north of Spartanburg, North Carolina at 35.196N (latitude), -81.963W (longitude). The radar normally operated 24 hours a day during the campaign and is managed by one radar engineer and a minimum of one radar scientist at all times. The NPOL radar is a 0.93 degree scanning dual polarized S-band radar. It is capable of operating in PPI sector, full volume scan mode, RHI mode, and vertically pointing mode. Dual polarized moments can be collected in either simultaneous transmit and receive (STAR) mode, or in an alternating

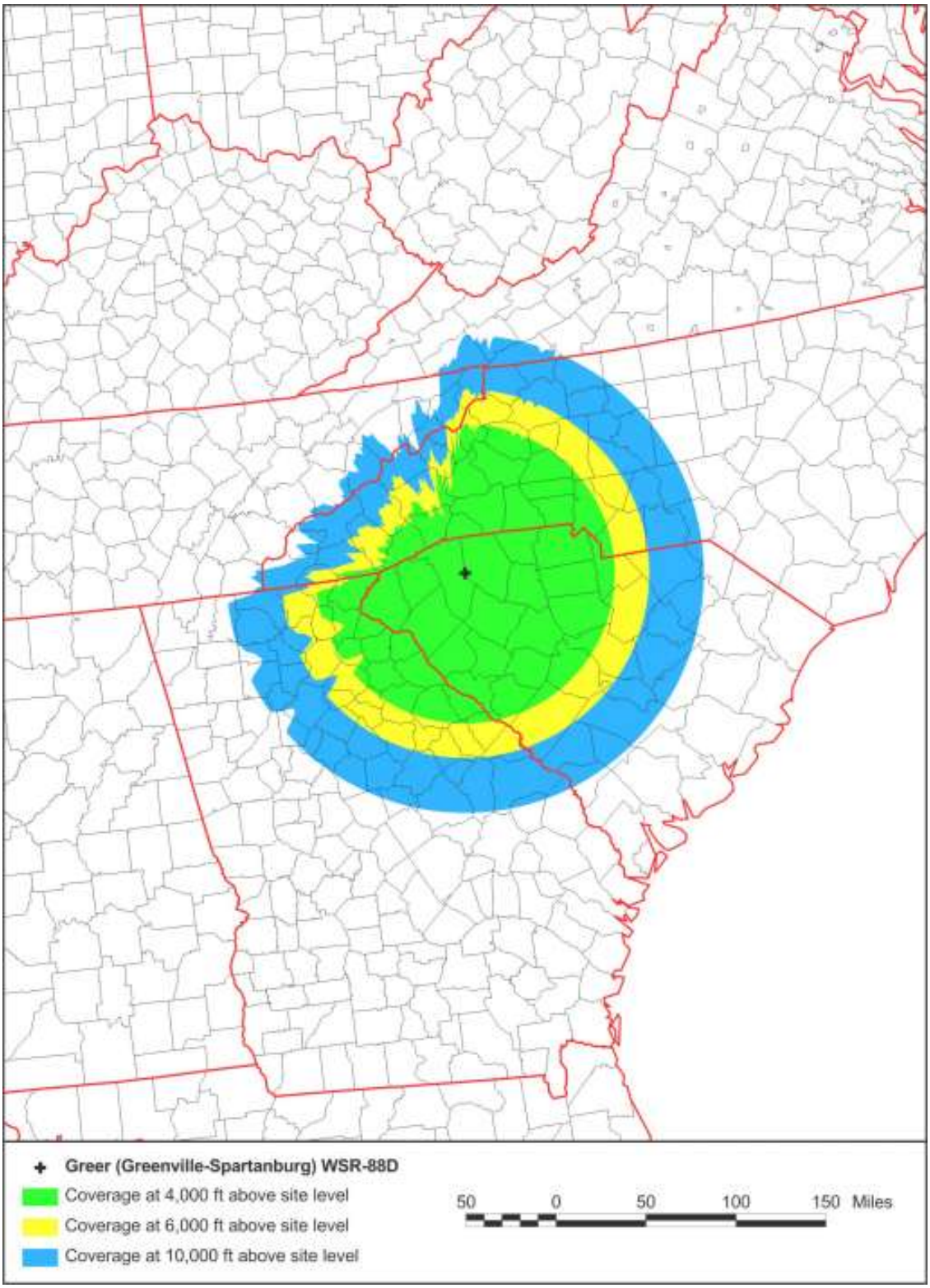

FIGURE 8.5. KGSP NEXRAD radar coverage map showing blockage towards the northwest direction in the region of the Pigeon River watershed.

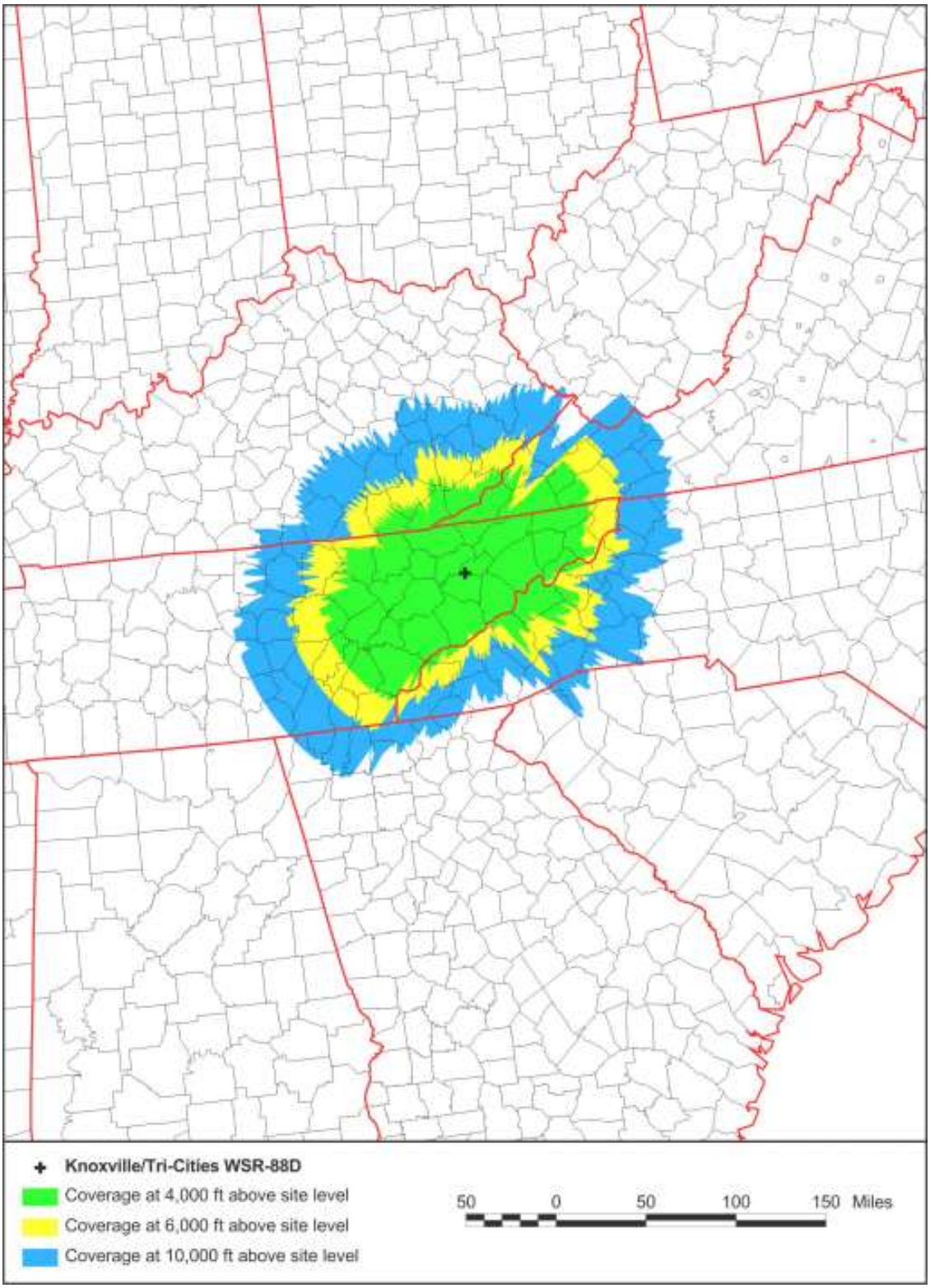

FIGURE 8.6. KMRX NEXRAD radar coverage map showing blockage towards the southeast direction in the region of the Pigeon River watershed.

Horizontal/Vertical (H/V) mode using a fast mechanical switch. The primary operational mode for NPOL is STAR, which is used in order to allow for more rapid scanning. The radar is controlled using Vaisala Sigmet Interactive Radar Information System (IRIS) radar software, and the data are processed with an RVP900 signal processor. Table 8.1 provides a description of the radar transmitter, antenna, receiver, and a summary of the science data that can be collected.

FIGURE 8.7. Picture of the NASA NPOL and D3R radars located in North Carolina participating in the IPHEX Campaign.

A near real-time data system was employed to provide updated imagery of several data fields of interest, which are reflectivity, differential reflectivity, rain rate, specific differential phase, co-polar correlation and hydrometeor identification. Additionally, two drop size distribution (DSD) fields will be retrieved. The DSD parameters recoreded are the Nw (normalized intercept) and the D_0 (median drop diameter). Depending upon the internet communication bandwidth, the raw data can be transmitted over this connection. If not, then data is copied to portable media on site and then hand delivered to NASA for further

TABLE 8.1. NASA S-Band Dual Polarimetric Radar (NPOL) Characteristics

Transmitter	
Transmitter Type	Coaxial Magnetron
Modulator Type	Solid State
Operating Frequency	2700-2900 MHz Tunable
Polarization	Horizontal, Vertical, Simultaneous, Alternating
Peak Pulse Power Output (STAR)	425 KW (H), 425 KW (V)
Peak Pulse Power Output (H & V)	425 KW (H), 425 KW (V)
Pulse Width	0.8 or 2.0 sec, selectable
PRF	250 to 1200 Hz
Antenna	
Reflector Type	8.5m Prime-Focus Parabolic
Beamwidth	0.93 at ±3dB (H), 0.94 at ±3dB (V)
Pedestal Type	Elevation over Azimuth
Type of Scan Patterns	PPI, RHI, Full Volume, Sector
Azimuth Angular Velocity	1 deg/sec to 20 deg/sec
Azimuth Angular Acceleration	20 deg/s^2
Azimuth Angular Accuracy	0.1 deg
Receiver	
Dual Receiver	Independent Receivers for H/V signals
Operating Frequencies	2700 MHz to 2900 MHz
Digital Receiver	Vaisala RVP900 / IFDR
Data	
Moments	Pulse Pair Processing
	T (Total Reflectivity) Z (Reflectivity) V (Doppler Mean Velocity) W (Doppler Spectrum Width) SQI (Signal Quality Index) ZDR (Differential Reflectivity) KDP (Specific Differential Phase) PhiDP (Differential Phase) RhoHV (Cross Channel Correlation Coefficient) LDR (Depolarization Ratio) I & Q (Time Series)

NASA NPOL S-Band radar Characteristics and Data Products

processing. During this particular field operation, NPOL was operational and prepared for data collection approximately one week prior to the official start of the IPHEX campaign, which provided additional time so as to assess terrain blockage as well as deal with other

unexpected hardware complications. Once the radar was operational, scan blockage was assessed, so that a set of near real-time blockage and hybrid scan algorithms could be applied prior to processing of the data during the official observational period.

Given the complex terrain over the radar domain, significant effort has been made towards optimizing suitable scanning strategies for NPOL and D3R. Pre-campaign estimates indicated considerable blockage at the lower elevation scanning angles. Work by Dr. Timothy Lang (NASA Marshall Space Flight Center) provided estimates of the blockage over the Pigeon and Catawba River watersheds. Figure 8.8 illustrates the blockage at 0.5 degree elevation, Figure 8.9 shows the 1.0 degree elevation blockage, and the 1.5 degree elevation blockage is shown in Figure 8.10. From these generated blockage maps, it is evident that there is much blockage (greater than 80%) over the Pigeon River watershed, and less so but still considerable blockage (greater than 20%) over the Catawba River basin. However at 1.5 degree elevation angle scans, there is only minimal blockage over Pigeon River basin and basically none over Catawba River basin.

NPOL used two scanning modes to handle storm events that occur close to the radar (within 50 km) and a far scanning mode for storms outside of the 50 km range. The near scanning mode operation is listed in Table 8.2, and the far scanning mode is listed in Table 8.3. The radar has the flexibility to deviate from this should the need arise and is left to the discretion of the research scientist on duty.

8.2.3. NASA D3R

The NASA Ka-Ku band deployable Dual-Frequency Dual-Polarimetric Doppler-Scanning Radar (D3R; Chandrasekar et al. 2012) was co-located with the NPOL radar during the IPHEX campaign (Figure 8.11), which was similar to its placement during Iowa Flood Studies

Table 8.2. NASA NPOL Near Scans

Sweep Number	Elevation (degrees)	Elevation Step (degrees)	Elapsed Time (seconds)	Max Height (km)	Range Intercept (km)
1	1.00	1.432	25.5	0.8	40.0
2	2.43	1.431	33.5	1.8	40.0
3	3.86	1.429	41.5	2.8	40.1
4	5.29	1.426	49.5	3.8	40.2
5	6.72	1.422	57.6	4.8	40.3
6	8.14	1.418	65.5	5.8	40.5
7	9.56	1.412	73.5	6.7	40.6
8	10.97	1.406	81.5	7.7	40.7
9	12.38	1.399	89.5	8.7	41.0
10	13.77	1.391	97.5	9.6	41.2
11	15.17	1.382	105.5	10.6	41.4
12	16.55	1.373	113.5	11.5	41.7
13	17.92	1.469	121.5	12.4	39.0
14	19.39	1.585	129.5	13.4	36.1
15	20.97	1.709	137.5	14.4	33.5
16	22.68	1.841	145.5	15.5	31.1
17	24.52	1.981	153.5	16.7	28.9
18	26.50	1.130	161.5	17.9	26.9
19	28.63	1.287	169.5	19.3	25.0
20	30.92	1.452	177.5	20.6	23.4

NPOL optimized near scan sequence, applied when precipitation events occur within 50 km of the radar.

Table 8.3. NASA NPOL Far Scans

Sweep Number	Elevation (degrees)	Elevation Step (degrees)	Elapsed Time (seconds)	Max Height (km)	Range Intercept (km)
1	1.00	0.537	28.5	2.3	100.0
2	1.57	0.537	39.5	3.3	100.0
3	2.15	0.537	50.5	4.3	100.1
4	2.72	0.572	61.5	5.3	100.1
5	3.29	0.572	72.6	6.3	100.2
6	3.86	0.572	83.5	7.3	100.2
7	4.43	0.571	94.5	8.3	100.3
8	5.01	0.571	105.5	9.3	100.4
9	5.58	0.570	116.5	10.3	100.5
10	6.15	0.570	127.5	11.3	100.6
11	6.72	0.558	138.5	12.3	102.6
12	7.27	0.605	149.5	13.3	94.8
13	7.88	0.654	160.5	14.3	87.5
14	8.53	0.708	171.5	15.4	80.9

NPOL optimized far scan sequence, applied when precipitation occurs at a distance greater than 50 km from the radar.

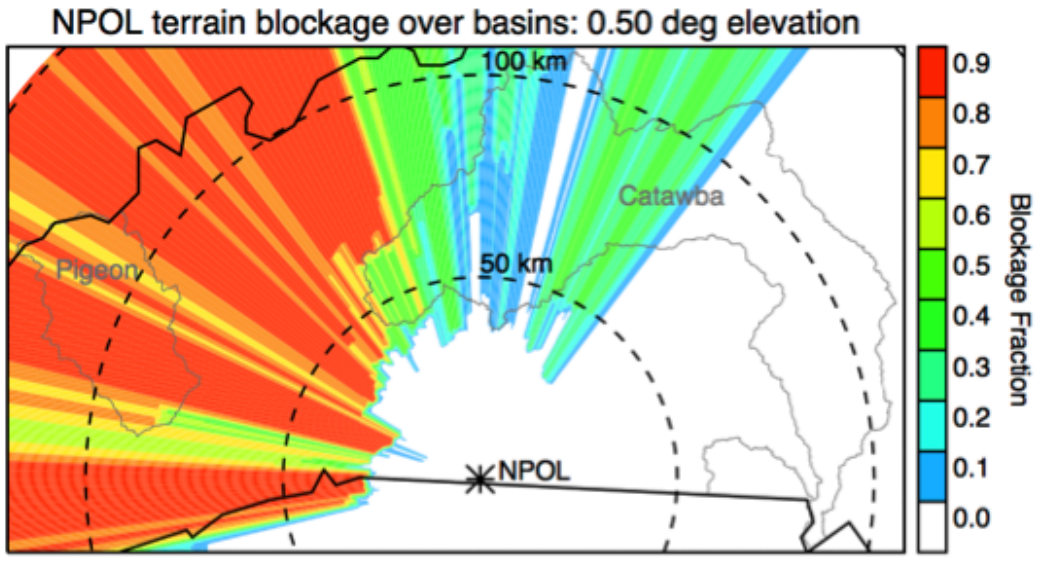

FIGURE 8.8. NASA NPOL terrain blockage at 0.5 degree elevation angle. The beam is blocked 70% to 90% in the direction of the Pigeon River watershed.

(IFLOODS) campaign that occured during the summer of 2013. D3R delivers a ground-based means to a) bridge observations of cloud and precipitation water in liquid and solid forms using frequencies consistent with the GPM Dual- Frequency Precipitation Radar (DPR); and b) provide a frequency consistent test platform for development and testing of DPR retrieval algorithms. The D3R is also used for scanning in coordination with the adjacent NPOL radar to test GPM dual-frequency path integrated attenuation (PIA), rain rate, DSD, and hydrometeor identification (e.g. liquid, melting, solid) retrievals. Engineering specifications for the D3R are provided in Table 8.4.

The position of the D3R during deployment was situated directly west and adjacent to the NPOL radar and therefore was beam blocked in azimuth by the NPOL physical structure approximately from 10 degree to about 170 degree. Therefore, the D3R scanning had

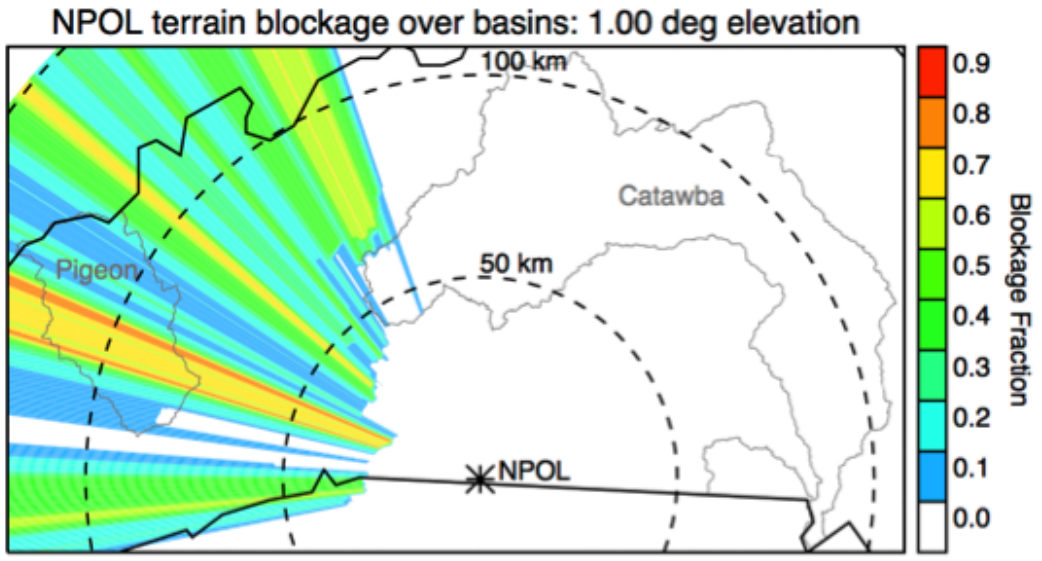

FIGURE 8.9. NASA NPOL terrain blockage at 1.0 degree elevation angle. The majority of beam is blocked between 30% to 70% in the direction of the Pigeon River watershed.

to concentrate its efforts on sampling to the northwest, which in coordination with NPOL provides triple frequency observations whenever possible over several gauges and disdrometers in that direction. D3R scanning also emphasized a portion of its RHI mode scans at approximately 298 degree azimuth to provide measurement over the nearby two-dimensional video disdrometer (2DVD) located at the Polk County Social Services Department and the Green Creek VFD. The D3R dual frequencies are such that they coincide with the GPM core satellite frequencies (Ku: 13.91 GHz±25 MHz and Ka: 35.56 GHz±25 MHz), and provide unique opportunities for precipitation observations during NASA GPM satellite overpasses.

The D3R scanning tasks will operate within these parameters:

- Simultaneous Transmit and Receive

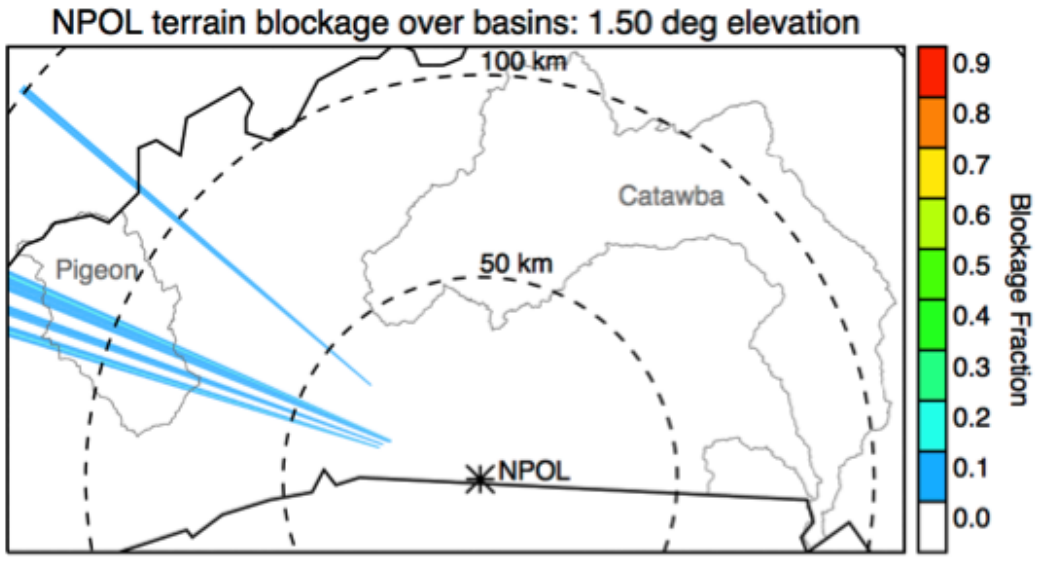

FIGURE 8.10. NASA NPOL terrain blockage at 1.5 degree elevation angle. The beam is minimally blocked in the direction of the Pigeon River watershed, but the height of beam at 100 km is approximately 4 km.

- Staggered PRT 400µs/600µs (500µs uniform PRT possible)
- Clutter filtering off
- Max range: 39.75 km
- Range Gate Spacing: 150 m
- 128 pulse integration
- Operational Azimuth limits: TBD (Limited by location at IPHEx site)
- Operational Elevation limits: 0 degrees to 90 degrees

Scan priority

(1) GPM Core satellite overpass

(2) Aircraft (RHI volume)

FIGURE 8.11. NASA D3R Ku/Ka band radar operating duing the IFLOODS campaign in Iowa.

(3) Coordinate with NPOL if target in range

(4) Surveillance and disdrometer scans

(5) Freelance targets of opportunity

Several disdrometers (2DVD) are situated along the radial at 298 degree in azimuth, therefore the planned RHI scan to coincide with these disdrometers is centered on this radial. Modifications to azimuth limits and elevation limits can be determined by the radar engineer based upon situational analysis. This was required during the campaign due to unxexpected

Table 8.4. NASA Ka/Ku Band D3R Characteristics

System	
Frequency	Ku:13.91 GHz ±25 MHz; Ka:35.56 GHz ±25 MHz
Minimum Setctable Signal	-8 dBZ, -2 dBZ noise equivalent at 15 km at 150m range resolution
Minimum Operational Range	450 m
Maximum Range	30 km (nominal)
Angular Coverage	0-360 deg Az, -0.5 to 90 deg Elev (full hemisphere)
Antenna	
Parabolic Reflector Diameter	6 ft (72 in.) (Ku), 28 in. (Ka)
Gain	45.6 dBi (Ku), 44.3 dBi (Ka)
HPBW	0.89 deg (Ku), 0.90 deg (Ka)
Polarization (Ku,Ka)	Dual linear simultaneous and alternating (H & V)
Maximum Side-Lobe Level (Ku,Ka)	$\sim$ -25 dB
Cross-Polarization Isolation (on axis)	$<$ -30 dB
Ka-Ku Beam Alignment	Within 0.1 degree
Scan Capability	0-24 deg/sec Az, 0-12 deg/s Elev
Scan Types	PPI sector, RHI, Surveillance, Vertical Pointing
Transmitter/Receiver	
Transmitter Architecture	Solid State Power Amplifiers Modules
Peak Power/Duty Cycle	200 W (Ku), 40 W (Ka) per H & V channel, max duty cycle 30%
Receiver Noise Figure	4.8 (Ku), 6.3 (Ka)
Receiver Dynamic Range (Ku,Ka)	$\sim$ 90 dB
Clutter Suppression	GMAP
Data Products	
Standard Products	- Equivalent reflectivity factor (Z_h) (Ku,Ka) - Doppler velocity (unambiguous: 26 m/s)
Dual-Polarization Products	- Differential reflectivity (Z_{dr}) (Ku,Ka) - Differential propagation phase (ϕ_{dp}) (Ku,Ka) - Copolar correlation coefficient (ρ_{hv}) (Ku,Ka) - Linear depolarization ratio (LDR_h,LDR_v) (Ku,Ka) (in alternate mode of operation)
Data Format	NETCDF

Characteristics of the D3R radar and data products. D3R is mobile dual-frequency (Ka/Ku), dual-polarization, Doppler radar built and operated by NASA Goddard Space Flight Center.

changes in the aircraft fly over patterns and storm evolution. Once the radar was configured and calibrated, the planned scanning modes applied are listed in Table 8.5.

8.2.4. NOAA X-band Polarimetric Radar (NOXP)

The NOAA NOXP radar (Schuur et al. 2014) shown in Figure 8.12 is positioned within the Pigeon River watershed at Lookout Mountain on a ridge that borders the basin, its

Table 8.5. NASA Ka/Ku Band D3R Scans

Scan Name	Scan Mode	Azimuth	Elevation	Scan Rate (deg/s)	Est. Time (sec)
iphex_surveillance	PPI	max limits assume 145 deg	1.0, 2.0, 3.0 (3 elevations)	7.5	64
iphex_90Near	PPI	X to X+90	see note 1 (20 elevations)	7.5	264
iphex_45Near	PPI	X to X+45	see note 1 (20 elevations)	7.5	132
iphex_rhi_disdrometer	RHI	X + -5 to 5 by 2.5 (5 azimuths)	0 to 45	6	41
iphex_rhi_aircraft	RHI	X + -2 to 2 by 1.0 (5 azimuths)	0 to 45	6	41
iphex_birdbath	PPI	0 to 359	90	12	33
iphex_gpmcore	1) PPI 2) RHI 3) PPI	1) max limits or overpass extent 2) see below (22 azimuths) 3) max limits or overpass extent	1) see below (20 elevations) 2) 0 to 75 3) see below (20 elevations)	10 6 10	900

Note 1: 20 scan PPI sector (NEAR) elevations are: {1.00, 2.43, 3.86, 5.29, 6.72, 8.14, 9.56, 10.97, 12.38, 13.77, 15.17, 16.55, 17.92, 19.39, 20.97, 22.68, 24.52, 26.50, 28.63, 30.92}

D3R scan strategy for IPHEX campaign.

coordinates are 35.564N (latitude), -82.910W (longitude). In prior campaigns, the mobility of NOXP has been instrumental, such as campaigns like the Verification of the Origins of Rotation in Tornadoes Experiment II (VORTEX-II) in 2009 to study tornado genesis, which required a radar with the ability to physically move with the storms. It has also been deployed in the desert regions of Arizona during the summers of 2012-2013 to study thunderstorms, microbursts, and dust storms. NOXP has also been transported abroad to France for the Hydrological cycle in the Mediterranean Experiment during the autumn of 2012 (HyMeX) (Ducrocq et al. 2013). For IPHEx, the NOXP radar will provide event based volume scans of precipitation over the ridge and valley system over the Pigeon River watershed with the idea of scanning above the dense networks of surface instrumentation in regions where NEXRAD and NPOL coverage is blocked. In unison with aircraft fly over operations above the Pigeon River watershed, the NOXP was able to collect both sector

volume and RHI scans in addition to its rain mapping VCP. The characteristics of this radar are listed in Table 8.6.

FIGURE 8.12. NOAA NOXP mobile radar on Lookout Mountain overlooking the Pigeon River watershed.

NOXP was primarily operated in a volume coverage mode in order to maximize its hydrologic potential. A frequently used volume coverage pattern (VCP) for this radar is shown below in Figure 8.13, where an additional tilt has been added at 0.1 degree. This low angle was put in place, since this radar has the advantage of being located on a ridge and has an unobstructed scanning view over the basin. Operationally, a birdbath scan at vertical incidence (90 degree) is done at least once every hour when rain is occuring at the site in order for calibration of Zdr. NOXP operates the Vaisala Sigmet RVP8 processor, since it provides a great deal of flexibility in scanning modes (volume coverages, RHIs, sector scans), pulse

TABLE 8.6. NOAA X-Band Polarimetric Radar Characteristics

System	
Wavelength	3.22 cm
Mobile/Transportable/Fixed	mobile (0.88 deg half-power beamwidth)
Scanning/Profiler	scanning (1.0 deg resolution)
Conventional/Doppler/Polarimetric	dual-polarimetric (STAR) and H-only mode
Scan capabilities	30 deg/s in azimuth; 0-90 deg in elevation; RHI capable
Range	Max range defined by selectable PRF; previous deployment used 1350 pulses/s which equates to 111 km
Communication capabilities	Voice: VHF radio, cell phone; data: USA cell-based wireless; 918 MHz radio
Antenna	
Width	8.5 ft (259 cm)
Height	14 ft (427 cm)
Weight	26,000 lbs (11,793 kg)
Gain	45.5 dBi
-3dB antenna aperture	0.9 deg
Relative gain at horizon	45.5 dBi
Polarization	Dual Linear
Rotation speed (rpm) (min and max)	0-5 RPM (min & max)
Transmitter/Receiver	
Frequency	9410 MHz
Peak power at antenna port	47 dBW
Equivalent Isotropically Radiated Power (EIRP)	47 dBW
Modulation type	Pulse
Modulation Characteristics (e.g. sweep period, sweep rate,)	None
Data Products	
Standard Products	- Equivalent reflectivity factor (Z_h) (Ku,Ka) - Doppler velocity (unambiguous: 26 m/s)
Dual-Polarization Products	- Differential reflectivity (Z_{dr}) (Ku,Ka) - Differential propagation phase (ϕ_{dp}) (Ku,Ka) - Copolar correlation coefficient (ρ_{hv}) (Ku,Ka) - Linear depolarization ratio (LDR_h,LDR_v) (Ku,Ka) (in alternate mode of operation)
Data Format	NETCDF

Characteristics of the NOAA NOXP radar and data products. NOXP is an X-band dual-polarization radar built and operated by NOAA HMT ESRL.

widths and pulse repetition frequencies (PRF). During IPHEX, radar engineers operated the radar mainly in VCP-12 mode (plus the 0.1 degree elevation angle) and in short pulse mode (0.5 µs) with a PRF of 1350 s^{-1}. These settings resulted in a maximum range of 111 km

and range gate spacing of 75 m. The VCP-12 is structured to allow the radar to complete all scans in less than 5 min.

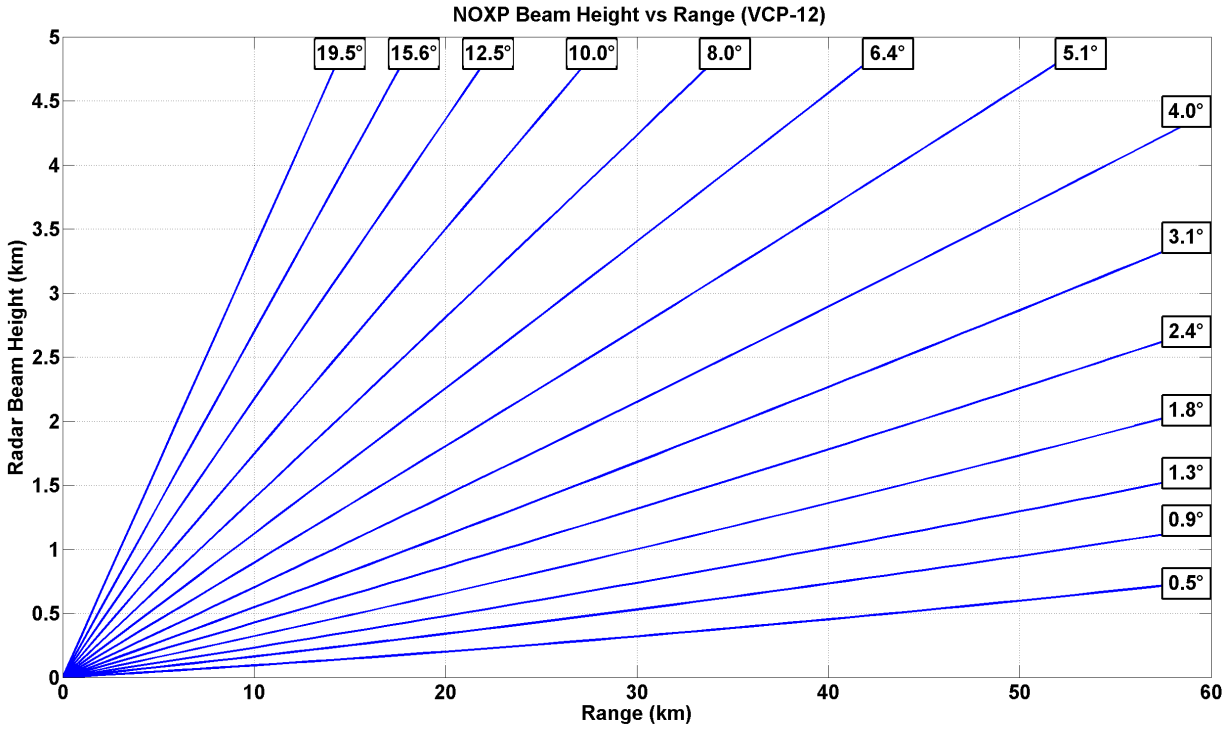

FIGURE 8.13. NOAA NOXP scanning angles to be used during the IPHEX campaign.

The amount of NXOP beam blockage can be seen in Figure 8.14, where the heights are in reference to above ground level (AGL). The radar is positioned, such that it is situated on a ridge location with an altitude of 1172 meters (3858 ft). This image is constructed from the digital elevation map (DEM)-250 topography layout, where the height indicated is the lowest tilt available that clears the obstructions, and the Pigeon River watershed is outlined in red.

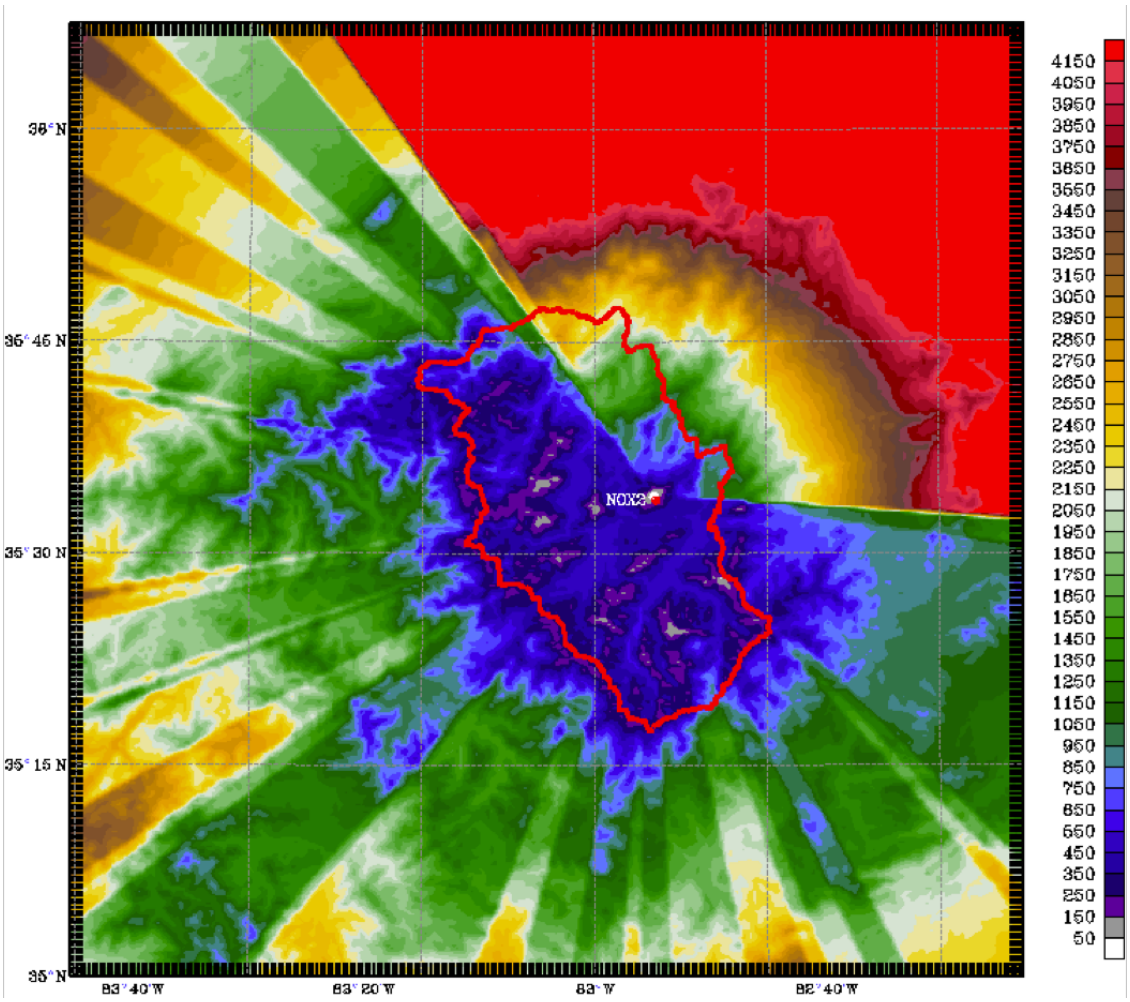

FIGURE 8.14. NOXP radar indicating the blockage in elevation in feet.

8.3. Micro Rain Radar (MRR)

Two NASA Micro Rain Radars (K-band: 24.25 GHz, CW) are deployed within the domain of observation around the Pigeon River watershed. These radars provide a low level vertical profile of precipitation of the doppler spectra that is integrated to provide profiles of radar reflectivity, precipitation rate, and DSD. These radars are set to read data at 60 m range gates up to an altitude of 1800 m above ground level. In addition, two additional MRRs were deployed by Duke University and were positioned along the 2DVD scanning azimuth and within scanning range of the NPOL and D3R radars (Figure 8.15). The other two are

collocated with microwave radiometers located within the Duke network of the Pigeon River watershed and at the intersection of the NPOL and XPOL system on the eastern ridges.

FIGURE 8.15. Micro Rain Radar pictured around Purchase Knob in the Great Smoky Mountains National Park, is a vertical profiler radar that delivers information about vertical structure in the atmospheric column and provides an estimation to the vertical distribution of rainfall. It can operate 24/7.

The profile of reflectivities from previous year MRR measurements taken near and in the Pigeon River watershed is shown in Figure 8.16. These measurements show a profile expected from warm rain processes, where the reflectivity increases with decreasing height (Wilson and Barros 2014). The freezing layer appears to be around 3 km in height.

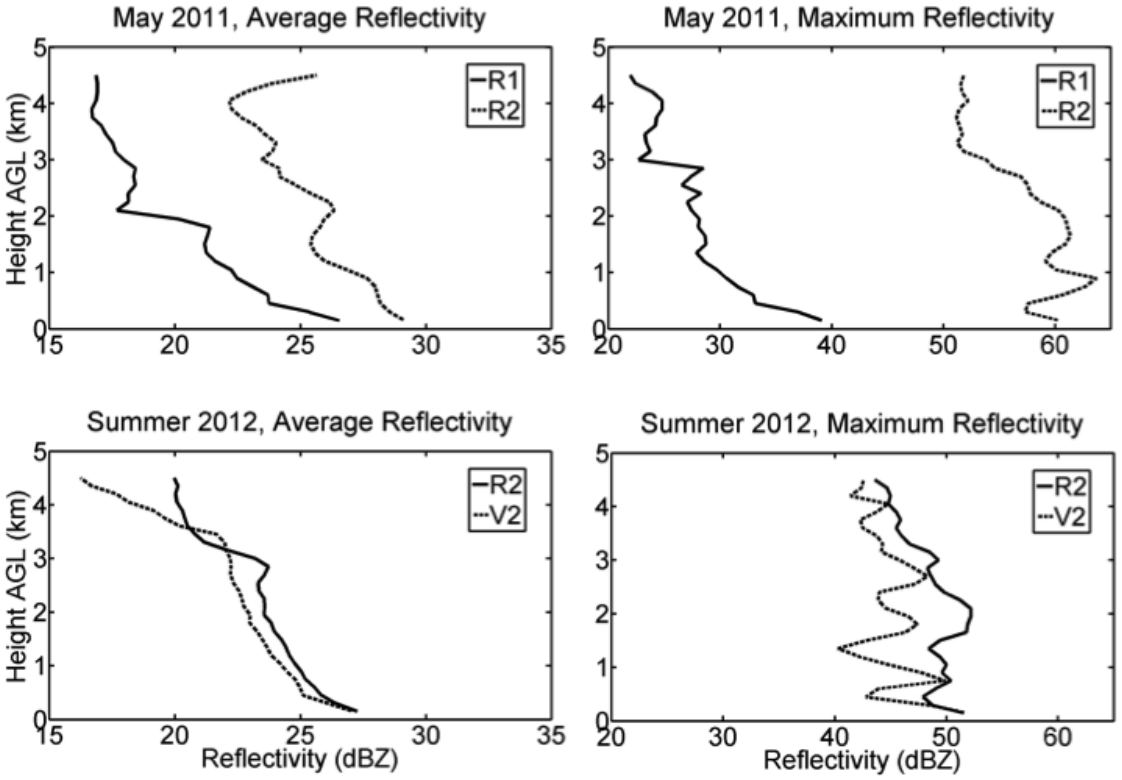

FIGURE 8.16. VPR taken by MRR in 2011 and 2012 during the summer season showing the vertical profile of reflectivity seen over the Pigeon River basin (from Wilson and Barros 2014).

8.4. Rain Gauge Networks within IPHEX Domain

There are several rain gauge networks that already reside within the Pigeon basin as well as the surrounding areas that can be used to provide ground validation of rainfall amounts. The rain gauge networks that occur within the Pigeon River watershed region are the U.S. Geological Survey sites, hydrometeorological automated data system (HADS), Duke University Great Smokey Mountain National Park (GSMNP) high-resolution rain gauge network, and a network of 20 NASA telemetered dual-gauge platforms, designed by University of Iowa. A picture of the dual tipping bucket is displayed in Figure 8.17. This platform allows this type of gauge to self validate the rainfall amounts to insure that the measurements are consistent and accurate.

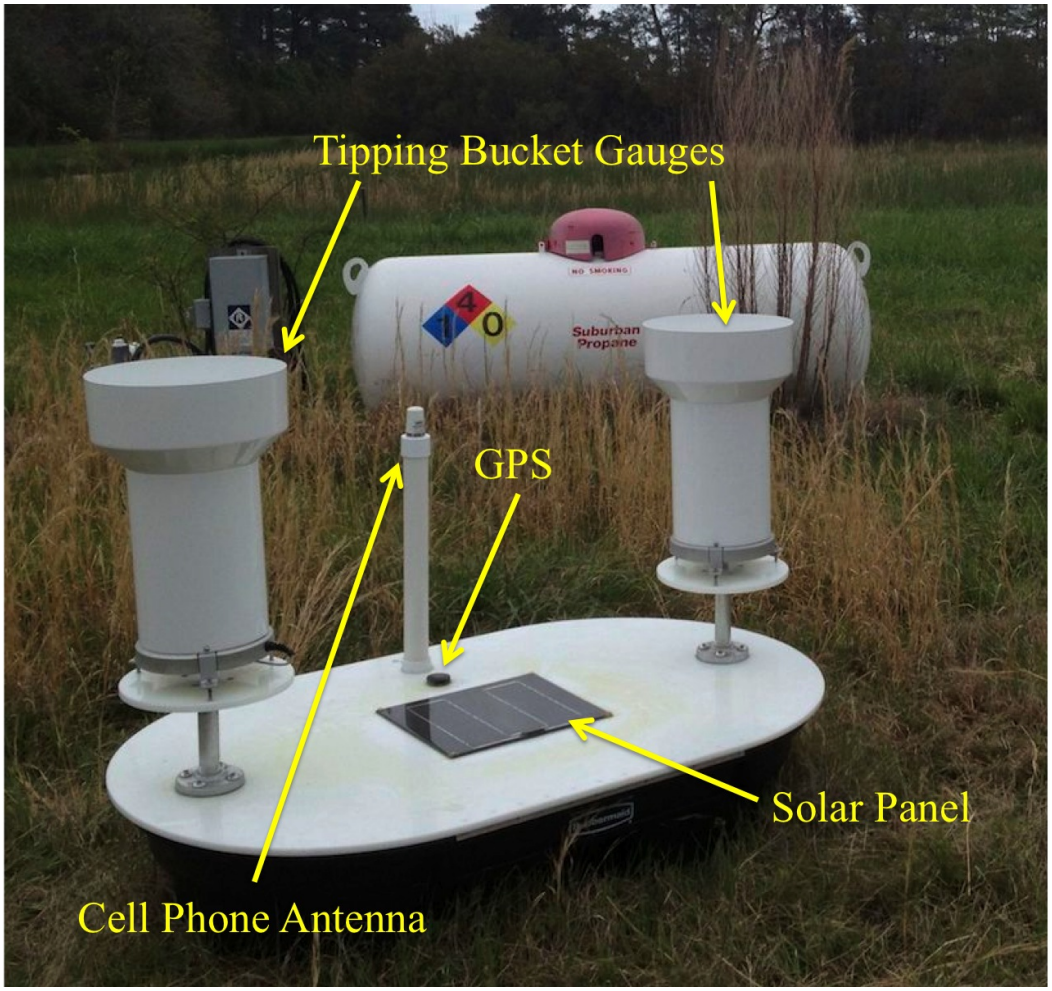

FIGURE 8.17. NASA Dual Tipping Bucket designed by Univeristy of Iowa.

The IPHEX rain gauges deployed by NASA specifically for this intense observation campaign are the dual tipping bucket gauges developed from the University of Iowa. Figure 8.17 shows an automated gauge platform deployed near Nassawadox, Virginia. The gauges are a self contained units that rely upon solar power. The various components of these dual gauge platforms are: 1) Two tipping bucket gauges (0.01 inch per tip); 2) Cell phone antenna; 3) Solar panel; and 4) GPS system. The gauges are configured to send packets via cellular to a collection server located at NASA GSFC every 15 minutes, where is provides an update on system health information includeing battery levels, cell signal strength, GPS location, and

tips from each gauge. This gauge data is made available on a NASA website that displays this information.

8.4.1. Validation Gauges for QPE Analysis

Validation of RAMS QPE and MRMS QPE systems are performed against the NOAA Hydrometeorological Automated Data System. This gauge set was selected, since they are spatially widespread over the radar coverage area, where the elevation of the gauges was not available in the data. However given the location of the gauges within this terrain, these gauges do provide a diverse combination of elevation and distance from the radars based upon the geographic locations. As an alternative, the application of the GSMNP for validation would give a better indication of orographic rainfall within this area, but these guages do not provide much information beyond the park boundaries. As another consideration, the use of the NASA gauges allows for a larger coverage area that includes parts of the Catawba River watershed, but is still focused on the mountaineous regions. The choice of the HADS gauges for validation provides a more diverse perspective that includes both the flat regions as well as some mountaneous areas.

8.5. RAMS QPE Evaluation

The results from the RAMS QPE takes into account the two NEXRAD radars KGSP and KMRX for radar input into the system. The validation gauge set is comprised of the NOAA Hydrometeorological Automated Data System. The radar data is retrieved for one day of rainfall events that occurred on May 15, 2014, since this is the best rainfall case that occurred during the NASA GPM Ground Validation campaign. The location of the gauges are spatially diverse and appear within the mountains that make up the southeastern portion of the Appalachian mountains that include the Pigeon River basin, the Catawba

River basin and other mountaineous areas adjacent to these two watersheds as well as in the lower unobstructed terrain around the NEXRAD radars. The Figure 8.18 shows the location of the gauges used for the validation of the QPE systems with respect to the NEXRAD 100 km range rings (red) and the Pigeon River basin (outlined in red).

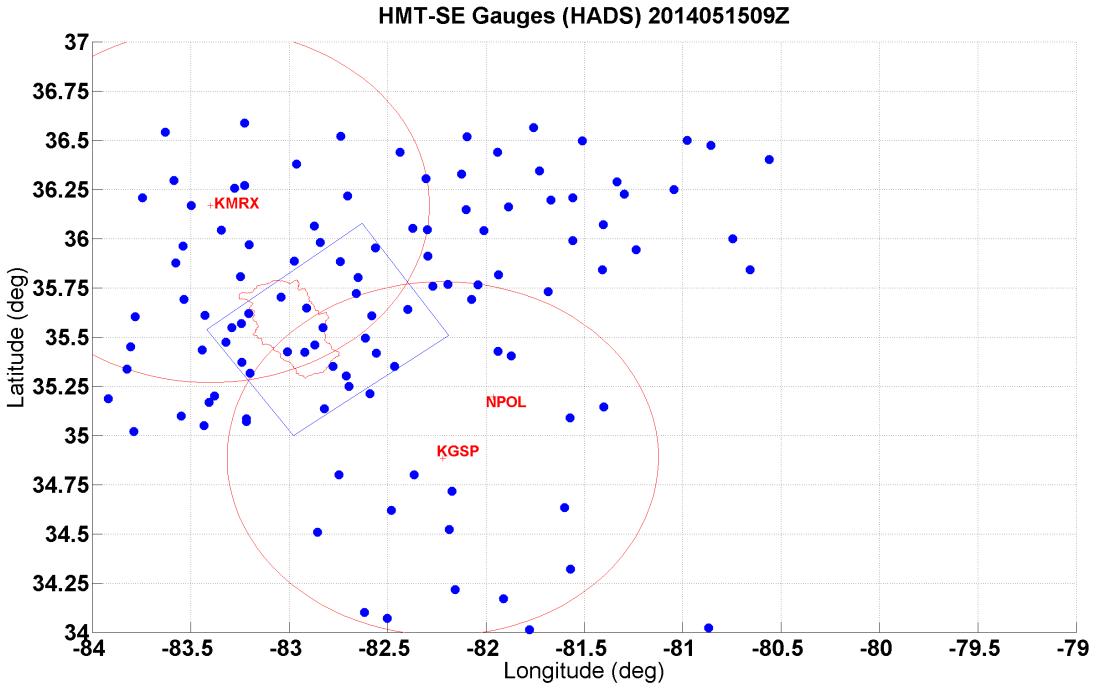

FIGURE 8.18. Validation gauges consisting of NOAA HADS gauges that surround the area of interest and provide measurements at various ranges and elevations from the radars. The Pigeon River basin is outlined in red, and the red rings are the 100 km range of the NEXRAD radars.

The RAMS QPE is evaluated using two radar scenarios. The first is to consider only the NEXRAD radars for input, and the second is to consider both NEXRAD and NPOL as radar inputs. In the development of the HSDP for the NEXRAD radars, the first lowest tilt is withheld from the hybrid scan due to its poor performance in the single radar analysis for this region (see Figures 6.12 and 6.13). All the scans for the NPOL radar are used in the HSDP since they have good performance. Even though NPOL is available, the scope of the QPE analysis for this study will only consider the NEXRAD only radar input. This is

done in order to equivalently evaluate the RAMS QPE system with the MRMS QPE system, where MRMS is only using NEXRAD radar input.

8.5.1. DFW Radar-Only QPE

An example of the ability of radar using CSU DROPS for rainfall estimation is shown by Chen and Chandrasekar (2015), this QPE is also derived using the CSU dual polarization methods for rain rate estimation. This study was performed over the Dallas-Fort Worth metropolitan area, which has NEXRAD coverage from KFWS as well as X-band radars provided by the CASA and the North Central Texas Council of Governments (NCTCOG) network. The QPE performance from the singe KFWS radar is illustrated in Figure 8.19, which shows the one hour rainfall radar QPE versus the one hour rain gauge data. These results give an indication as to the precision that is achievable for WSR-88D by applying this type of QPE methodology. For this case, the NSE is 15% using gauges that are located within 40 km range of the radar site. It should be noted that this locale is relatively flat and is not hindered by beam blockage due to high mountains. For a multiple radar senario, the X-band radars provided by the NCTCOG network was then merged with the KFWS radar data in order to further improve QPE. The addition of this particular network of X-band radars provides higher resolution and allows scanning much closer to the surface of the earth. This merged radar QPE is shown in Figure 8.20, where the NSE was slight improved to 14.8%. This data set consisted of four rainfall events that occured over the radar common coverage area.

8.5.2. Radar-Only QPE over HMT SE Domain

In the area of the HMT-SEP, the location of mountains does impose challenges to good QPE measurements. In order to evaluate QPE performance of different methods in this

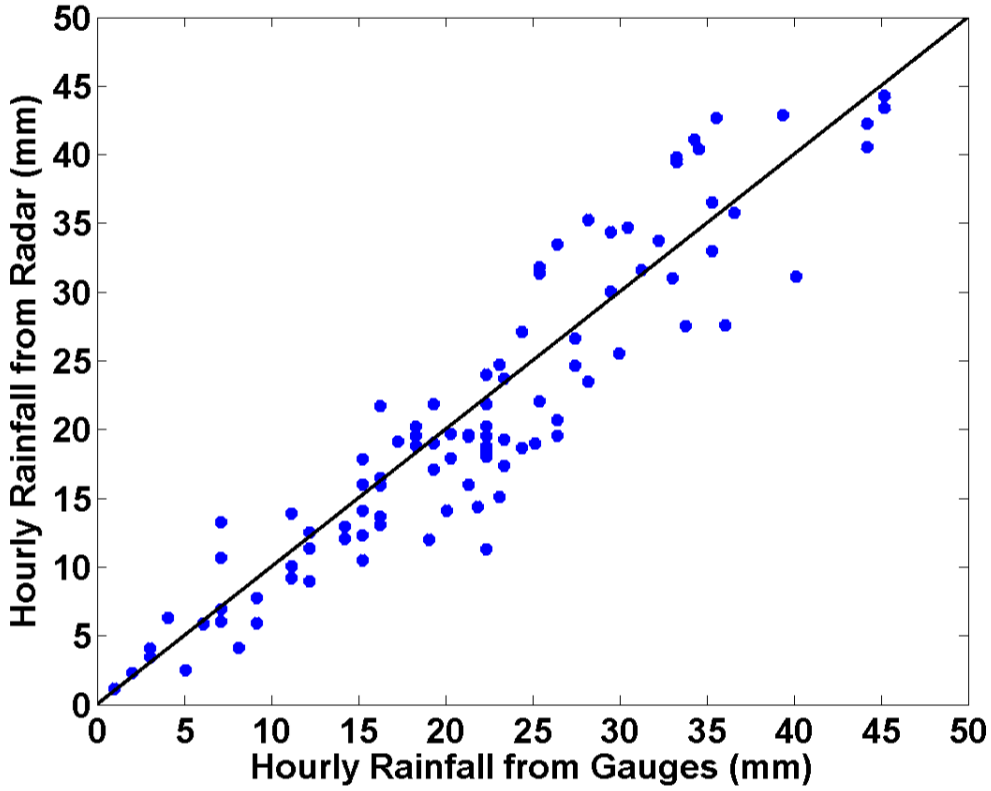

FIGURE 8.19. Scatter plot showing the DFW QPE using NEXRAD KFWS radar near Dallas, TX. The NSE for this data set is 15% using hourly rainfall amounts for ranges less than 40 km from the radar site (from Chen and Chandrasekar 2015).

locale, rainfall estimates were taken from the MRMS radar-only QPE product and from the QPE derived from KGSP using the CSU DROPS technique.

First of all, the MRMS QPE system configured by NSSL for application in the IPHEX campaign was done using much larger domain boundaries in comparison to the RAMS QPE domain, however the MRMS system was modified to coincide with the domain coordinates given previously for the RAMS QPE system where the coverage of the domain includes the Pigeon River basin and Catawba River basin. This was done to allow for comparison between the two QPE systems in the region.

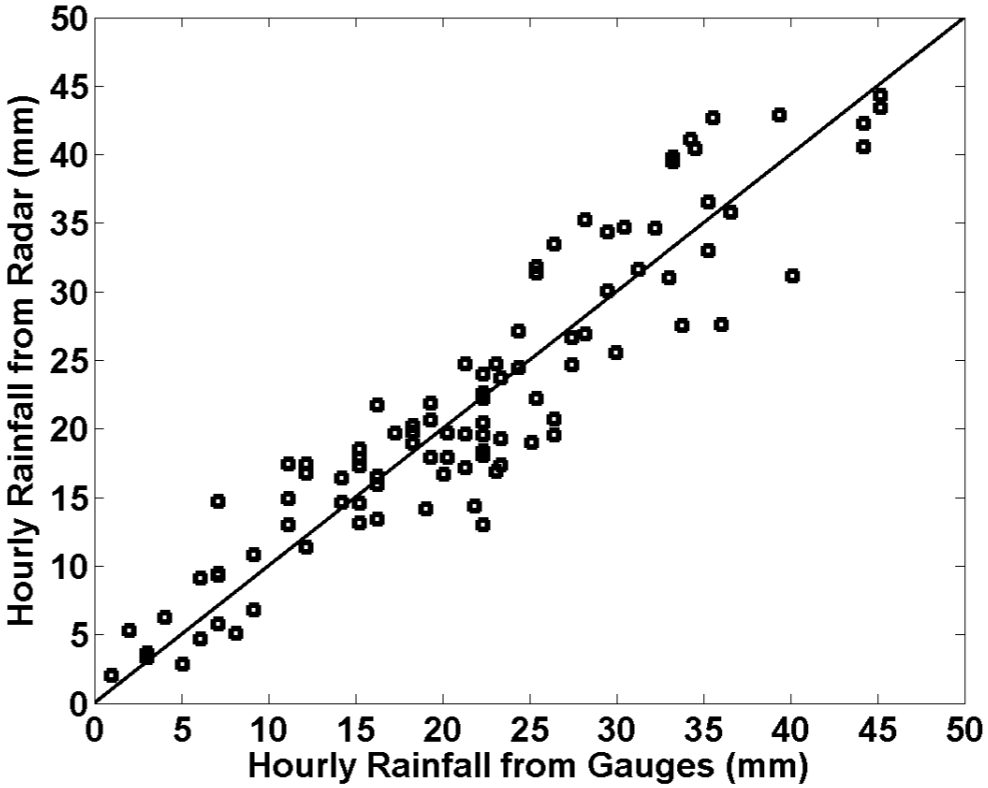

FIGURE 8.20. Scatter plot showing the DFW Merged QPE using NEXRAD KFWS with local X-band radars near Dallas, TX. The NSE for this data set is 14.8% using hourly rainfall amounts for ranges less than 40 km from the radar site (from Chen and Chandrasekar 2015).

The radar input into MRMS initially consists of the surrounding three NEXRAD radars (KGSP, KMRX, KFCX), where the level 2 radar data input is ingested. The rainfall events that occurred on May 15, 2014 during the IPHEX campaign is considered for this data analysis. The use of NPOL and D3R radar data was not included as input into MRMS, since the system was configured and executed by NSSL for this campaign, and the ability to integrate non-NEXRAD radars was not considered. It is also unknown as to which gauges were ingested by MRMS for use in the gauge correction algorithm.

MRMS QPE product of interest for evaluation in this study is the radar-only with VPR correction applied. In these results the radar inputs to MRMS processing are comprised of

the three surrounding NEXRADs, where the gauge input is not specified. Several MRMS products were made available as part of the IPHEX campaign, and the results are taken as is. Results for this particular MRMS product considering this one day event are shown in Table 8.7. Here the NSE is 47.6% and the normalized bias is -36.8%, with the hourly rainfall amounts below 1 mm removed from both the radar rainfall amounts and the gauge accumulations.

Next to gain perspective on the performance of a single NEXRAD radar using the CSU DROPS methodology, the rainfall estimates were derived for the KGSP radar, which is located near Greensville-Spartenburg, NC . The plot is shown in Figure 8.21. Here the results show good performance with respect to the validation gauges, and the NSE is 22.7%, which is within the neighborhood of the NSE of 15% from KFWS (Figure 8.19). In this analysis, the gauges considered are located within 60 km of the KGSP radar and the elevation angle is 1.36 degree. As it was shown in the previous chapter, as the range increase the performance tends to decrease due to effects of beam broadening and possible non-uniform beam filling, but these results do indicate good comparison around this radar.

In terms of the RAMS QPE results, the two NEXRAD radars are processed and then merged to create a mosaicked radar-only QPE product. The statistical results are shown in Table 8.7. The NSE for RAMS QPE is 42.7% and the normalized bias is -19.1%, where the instances of hourly radar rainfall amounts and hourly gauge amounts that are below 1 mm are removed in order to focus on substantial rainfall amounts. In this case, there are instances of partial beam blockage within a complex terrrain environment. However, the application of CSU DROPS methodology to the NEXRAD radar data along with RAMS QPE merging techinique does show better performance over the MRMS radar-only with VPR correction product. Since this is an intitial concept, it is assumed that the use of

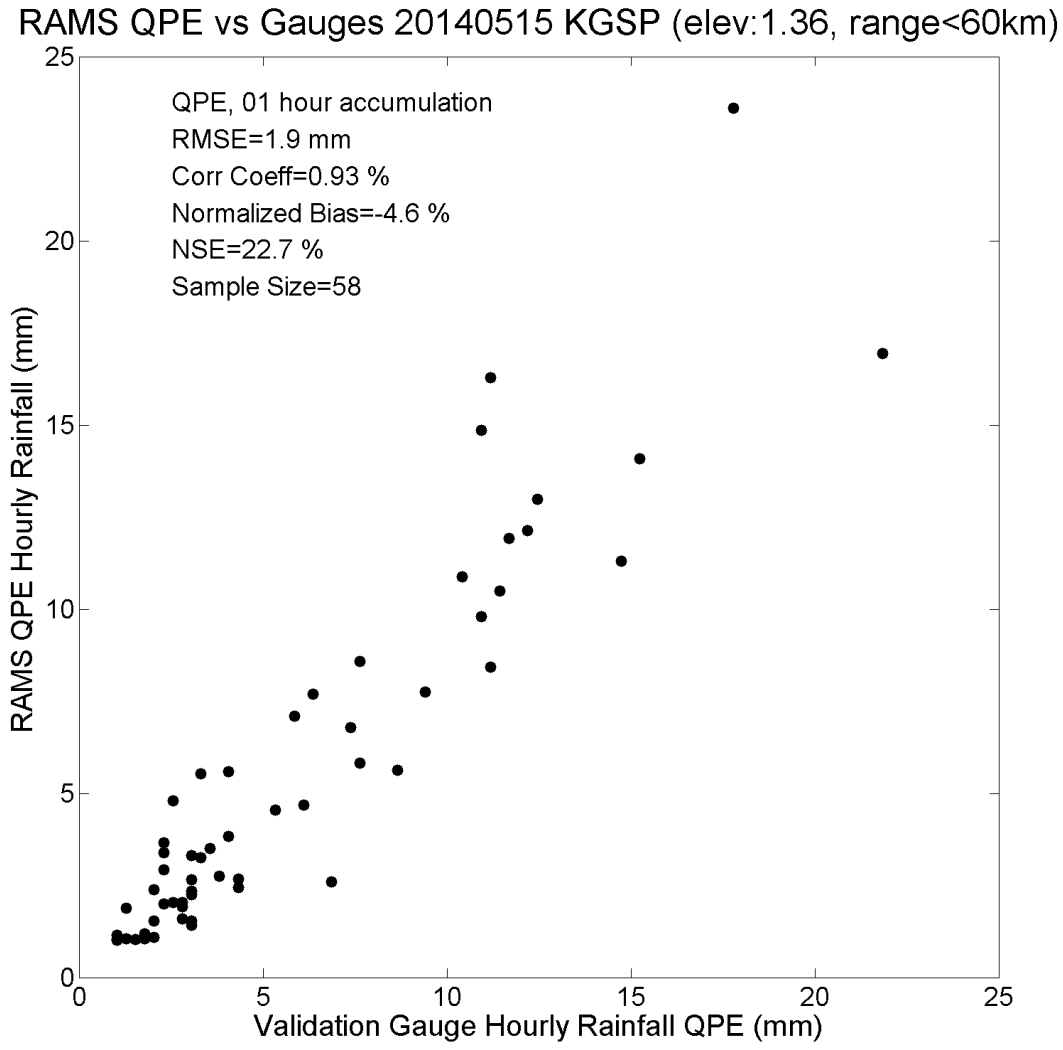

FIGURE 8.21. Scatter plot showing the KGSP DROPS QPE versus the validation gauges over the HMT-SEP domain. NSE for this radar was 22.7% for ranges less than 60 km and an elevation angle of 1.36 degree.

DROPS is the primary factor in regards to the improvement, where the RAMS QPE hybrid and mosaic methodology has yet to be fully assessed. The performance for the single KGSP radar for gauges within 60 km is better, but at ranges farther out, higher elevation scans are needed to clear the blockage. It has been shown that the NSE can be as low as 15% by applying DROPS QPE technique to NEXRAD dual polarization measurements (Chen and Chandrasekar 2015). With further refinement, RAMS QPE performance can improve.

Table 8.7. RAMS and MRMS Statistics

Parameter	RAMS QPE	MRMS QPE
RMSE	3.55 mm	4.02 mm
Corr Coeff	0.67%	0.69%
Normalized Bias	-19.14%	-36.75%
Normalized Standard Error	42.74%	47.61%

Validation gauges are taken from the NOAA HADS gauge set.

CHAPTER 9

Summary and Future Work

9.1. Summary

QPE in mountainous terrain is a multi-faceted challenge involving limitations of radar physical scanning measurements as well as local storm dynamics and evolution. It is the desire to incorporate the advancements made in dual polarization methodologies into effective QPE products. However there are still the issues of beam blockage that require higher scanning into the atmosphere to clear obstacles, such that the use of gap filling radars provides a direct way to obtain reliable QPE. It will take further research efforts to understand unique local environmental conditions, so that adjustments and corrections can be made to give reliable rainfall estimates using NEXRAD radars at far distances. Since all NEXRAD radars have been upgraded dual polarization measurement capabilities, it is of interest to pursue these new techniques, so that it can further the goal of obtaining accurate rainfall estimation.

In the assessment of the NSSL MRMS QPE system over Russian River basin, there were several outcomes of interest. In regards to the MRMS products of radar-only and radar with VPR correction, these products in this region did not provide very reliable rainfall estimates especially when compared to the non-NEXRAD gap filling KPIX radar-only QPE. However, MRMS does give the best overall performance of QPE when gauge correction is applied to the VPR corrected reflectivity. The other notable result from this study are the radar inputs. The results indicate that MRMS QPE products show similar performance, regardless of which radar input is applied where the three scenarios considered were NEXRAD only, KPIX only, and NEXRAD with KPIX. These give a conclusion that radar input for MRMS

is not a major contributor to the best QPE product. Again MRMS was initially developed as a reflectivity-based system, which entails very elaborate and intelligent quality control and VPR correction methods and is what was applied for the Russian River analysis. The current version of MRMS does have dual pole capabilities, but was not available for this study. Overall this system is designed to work in conjunction with the NWS WSR-88D radars and is intended to provide QPE over the entire continental United States, so when applied to a smaller domain in complex terrain, such as the Russian River basin, it performance is degraded, and it requires adaptation to the unique regional conditions. For this case, modifications to the rain rate relations and VPR correction is needed to improve the QPE results.

To address the need for a customizable regional QPE system with the ability to merge multiple radar scans, the RAMS QPE system was implemented. This is a system that draws upon the dual polarization rainfall estimation relations and the hydrometeor identification methods developed from the Colorado State University Radar Research Group. The RAMS QPE system is designed to be open architecture, so as to allow for ongoing enhancements and developments from interested individuals. The ingest of radar data should consider all types of dual polarization capable systems as long as the data is verified to contain reliable measurements. In regards to performance of rainfall estimation, the NEXRAD radar KGSP (located near Greenville, NC) was evaluated individually with another NEXRAD radar KFWS (located near Dallas, TX) using only the CSU DROPS technique. These results indicated good agreement between these similar radars using the same dual pole rain rate estimation in different parts of the country. Evaluation of the RAMS QPE and the MRMS QPE system was performed simultaneously using the same NEXRAD radar inputs as well as over the same domain. This area was located near Asheville, NC and contains a

combination of complex terrain and flat unobstructed radar views. The results show that the mosaic of the RAMS QPE out performed the MRMS radar with VPR correction product, however this only considers one day of rain events that occurred on May 15, 2014. Additional data will help to improve the statistics. RAMS QPE still needs to be further evaluated with additional data sets as well as assessment in other types of regions. It would be desirable to apply NOXP as gap filling radar in the IPHEX domain and determine if it can enhance QPE performance in an orographic region.

9.2. Furture Work

This is a list of initial items that can be addressed to improve upon and add some flexibility to the RAMS QPE System

- Some of the process steps can be modularized; so as newer techniques are developed or changes occur, they can be applied more readily. The option to switch between different methods should be possible as well as an option to revert to an older version.
- In regards to the gridding, it is desirable for the system to have its own gridding process. If this can be done internally without having to rely upon external code, it allows for application of various gridding and weighting techniques. Currently the method is applying a linear approach. Some basic concepts would be to add in a method that uses the nearest neighbor while the pixel within the beam width and then linearly interpolate pixels with the adjacent beams if they occur outside of the beam.

- In mosaicking, a weighting scheme can be implemented to allow for the closest radar to have more weight with the option to only use the closest radar within a certain range and weight values from each radar if pixels are outside of a range threshold.
- Allow for flexibility in the time scale to merge HSDP, it currently set to 5 min, but this should be adjustable from 1 min to 10 min.
- Currently the QPE is accumulated in one hour time frames at the top of the hour, this can be modified to accumulate an hourly QPE every five minutes as well as being adjustable. It would also be desirable to allow for an adjustable QPE accumulation time interval, so that QPE can be accumulated in smaller timeframes like 5 minutes and with the ability to expand to 24 hour or more if desired, where the higher time periods can be aggregated from the one hour QPE amounts.
- It is also suitable to have DROPS ingest NetCDF files directly as well as have it write files in NetCDF format, and therefore eliminating the reliance upon the universal file format.

9.2.1. RAMS QPE Gauge Correction

Gauges are useful in providing ground validation of rainfall amounts. There are other techniques that are worth consideration such as the PRISM (Schaake et al. 2004), which has been shown to give good results in mountaineous terrain. Another possible gauge correction scheme is the mean field bias approach (Seo et al. 1999). However, the approach used by Ware (2005) is simple and performs well against more computationally intensive methods, it is chosen as a first approach to create a gauge-only QPE product. The equations used in this inverse distance weighting are as follows (Simanton and Osborn 1980):

$$F(x,y) = \sum_{i=1}^{n} w_i f_i \tag{41}$$

$$w_i = \frac{\frac{1}{d_i^b}}{\sum_{i=1}^{n} \frac{1}{d_i^b}} \tag{42}$$

where f_i = gauge value, b = power parameter, d = distance from interpolation point to gauge, and i is the gauge number. If there is a sparse network, the extrapolation of a single gauge value within the radius of influence is constant. To lessen this effect, an exponential weighting will also be applied with the maximum at the gauge point and then tapering off as a function of distance from the gauge. This will reduce the influence a single isolated gauge has on the overall QPE. For dense networks the exponential will also be applied, but will have less of an influence on QPE, since the neighboring gauges also are additive. The values of the parameters are set to $b = 2$, and d=2 km, where the value of $b > 2$ does not change the overall values by much and a 10 km radius of influence is reasonable in terms of range. It can be larger if the events are known to be stratiform, but in convective cases, it may be better to reduce to a smaller value.

The format for the gauge QPE will follow the MDF file format so as to be able to share a common format with other QPE systems such as MRMS. Gauge data is generated by numerous agencies, and one of the greatest tasks is to locate regional data. Once the gauge data is established, the major undertaking in creating the MDF is formatting the data to a common structure and time scale. The majority of gauges report with an hourly time

schedule. One of the widely available gauge data repositories is the HADS gauge database, which is updated as gauges report.

Bibliography

Beard, K. V., and C. Chuang, 1987: A new model for the equilibrium shape of raindrops. *Journal of the Atmospheric Sciences*, **44 (11)**, 1509–1524.

Benjamin, S. G., and Coauthors, 2004: An hourly assimilation–forecast cycle: The ruc. *Monthly Weather Review*, **132 (2)**, 495–518.

Bringi, V. N., and V. Chandrasekar, 2001: *Polarimetric Doppler Weather Radar: Principles and Applications*. Cambridge University Press, New York.

Bringi, V. N., L. Liu, P. C. Kennedy, V. Chandrasekar, and S. A. Rutledge, 1996: Dual multiparameter radar observations of intense convective storms: The 24 june 1992 case study. *Meteorology and Atmospheric Physics*, **59 (1-2)**, 3–31.

Chandrasekar, V., and Coauthors, 2012: Dual-frequency dual-polarized doppler radar (d3r) system for gpm ground validation: Update and recent field observations. *Geoscience and Remote Sensing Symposium (IGARSS), 2012 IEEE International*, 346–349.

Chen, H., and V. Chandrasekar, 2015: The quantitative precipitation estimation system for dallas-fort worth (dfw) urban remote sensing network, manuscript submitted for publication.

Cifelli, R., and V. Chandrasekar, 2013: *Dual-Polarization Radar Rainfall Estimation*, 105–125. American Geophysical Union, Washington, D. C.

Cifelli, R., V. Chandrasekar, S. Lim, P. C. Kennedy, Y. Wang, and S. A. Rutledge, 2011: A new dual-polarization radar rainfall algorithm: Application in colorado precipitation events. *Journal of Atmospheric and Oceanic Technology*, **28 (3)**, 352–364.

Crum, T. D., and R. L. Alberty, 1993: The wsr-88d and the wsr-88d operational support facility. *Bulletin of the American Meteorological Society*, **74 (9)**, 1669–1687.

Doviak, R. J., and D. S. Zrnic, 1993: *Doppler Radar and Weather Observations*. 2nd ed., Academic Press, Inc, 1250 Sixth Avenue, San Diego, California.

Ducrocq, V., and Coauthors, 2013: Hymex-sop1: The field campaign dedicated to heavy precipitation and flash flooding in the northwestern mediterranean. *Bulletin of the American Meteorological Society*, **95 (7)**, 1083–1100.

Fulton, R. A., J. P. Breidenbach, D.-J. Seo, D. A. Miller, and T. O'Bannon, 1998: The wsr-88d rainfall algorithm. *Weather and Forecasting*, **13 (2)**, 377–395.

Gerlach, J., and W. Petersen, 2011: Npol : The nasa transportable s-band dual-polarimetric radar. antenna system upgrades, performance and deployment during mc3e. *35th Conference on Radar Meteorology*, Pittsburgh, PA.

Grecu, M., and W. F. Krajewski, 2000: An efficient methodology for detection of anomalous propagation echoes in radar reflectivity data using neural networks. *Journal of Atmospheric and Oceanic Technology*, **17 (2)**, 121–129.

Greene, D. R., and R. A. Clark, 1972: Vertically integrated liquid water—a new analysis tool. *Monthly Weather Review*, **100 (7)**, 548–552.

Jorgensen, D. P., P. H. Hildebrand, and C. L. Frush, 1983: Feasibility test of an airborne pulse-doppler meteorological radar. *Journal of Climate and Applied Meteorology*, **22 (5)**, 744–757.

Joss, J., and R. Lee, 1995: The application of radargauge comparisons to operational precipitation profile corrections. *Journal of Applied Meteorology*, **34 (12)**, 2612–2630.

Kessinger, C., S. Ellis, and J. Van Andel, 2003: The radar echo classifier: A fuzzy logic algorithm for the wsr-88d. *Third Conf. on Artificial Applications to the Environmental Sciences*, Long Beach, CA, American Meteorological Society.

Kitchen, M., R. Brown, and A. Davies, 1994: Real-time correction of weather radar data for the effects of bright band, range and orographic growth in widespread precipitation. *Quarterly Journal of the Royal Meteorological Society*, **120 (519)**, 1231–1254.

Kitzmiller, D., and Coauthors, 2011: Evolving multisensor precipitation estimation methods: Their impacts on flow prediction using a distributed hydrologic model. *Journal of Hydrometeorology*, **12 (6)**, 1414–1431.

Kucera, P. A., W. F. Krajewski, and C. B. Young, 2004: Radar beam occultation studies using gis and dem technology: An example study of guam. *Journal of Atmospheric and Oceanic Technology*, **21 (7)**, 995–1006.

Lakshmanan, V., 2001: A hierarchical, multiscale texture segmentation algorithm for real-world scenes. Ph.D. thesis, University of Oklahoma, Norman, OK.

Lakshmanan, V., A. Fritz, T. Smith, K. Hondl, and G. Stumpf, 2007: An automated technique to quality control radar reflectivity data. *Journal of Applied Meteorology and Climatology*, **46 (3)**, 288–305.

Lakshmanan, V., R. Rabin, and V. DeBrunner, 2003: Multiscale storm identification and forecast. *Atmospheric Research*, **67–68 (0)**, 367–380.

Lakshmanan, V., J. Zhang, and K. Howard, 2009: A technique to censor biological echoes in radar reflectivity data. *Journal of Applied Meteorology and Climatology*, **49 (3)**, 453–462.

Lawrence, B. A., M. I. Shebsovich, M. J. Glaudemans, and P. S. Tilles, 2003: Enhancing precipitation estimation capabilities at national weather service field offices using multisensor precipitation data mosaics. *19th Conference on Interactive Information Processing Systems (IIPS)*, Long Beach, CA, American Meteorological Society.

Lim, S., V. Chandrasekar, and V. N. Bringi, 2005: Hydrometeor classification system using dual-polarization radar measurements: model improvements and in situ verification. *Geoscience and Remote Sensing, IEEE Transactions on*, **43 (4)**, 792–801.

Liu, H., and V. Chandrasekar, 2000: Classification of hydrometeors based on polarimetric radar measurements: Development of fuzzy logic and neuro-fuzzy systems, and in situ verification. *Journal of Atmospheric and Oceanic Technology*, **17 (2)**, 140–164.

Liu, Y., Y. Wang, V. Chandrasekar, and V. Bringi, 2007: Real-time three-dimensional radar mosaic in casa ip1 testbed. *International Geoscience and Remote Sensing Symposium*, Barcelona, Spain, IEEE International, 2754-2757.

Maddox, R. A., J. Zhang, J. J. Gourley, and K. W. Howard, 2002: Weather radar coverage over the contiguous united states. *Weather and Forecasting*, **17 (4)**, 927–934.

Martner, B. E., S. E. Yuter, A. B. White, S. Y. Matrosov, D. E. Kingsmill, and F. M. Ralph, 2008: Raindrop size distributions and rain characteristics in california coastal rainfall for periods with and without a radar bright band. *Journal of Hydrometeorology*, **9 (3)**, 408–425.

Matrosov, S. Y., F. M. Ralph, P. J. Neiman, and A. B. White, 2014: Quantitative assessment of operational weather radar rainfall estimates over california's northern sonoma county using hmt-west data. *Journal of Hydrometeorology*, **15 (1)**, 393–410.

McLaughlin, D., and Coauthors, 2009: Short-wavelength technology and the potential for distributed networks of small radar systems. *Bulletin of the American Meteorological Society*, **90 (12)**, 1797–1817.

McLaughlin, D. J., and Coauthors, 2005: Distributed collaborative adaptive sensing (dcas) for improved detection, understanding, and prediction of atmospheric hazards. *Ninth Symposium on Integrated Observing and Assimilation Systems for the Atmosphere, Oceans, and Land Surface (IOAS-AOLS)*, San Diego, CA, American Meteorological Society.

Moore, B. J., P. J. Neiman, F. M. Ralph, and F. E. Barthold, 2011: Physical processes associated with heavy flooding rainfall in nashville, tennessee, and vicinity during 1–2 may 2010: The role of an atmospheric river and mesoscale convective systems. *Monthly Weather Review*, **140 (2)**, 358–378.

O'Bannon, T., 1997: Using a 'terrain-based' hybrid scan to improve wsr-88d precipitation estimates. *28th International Conference on Radar Meteorology*, Austin, TX, American Meteorological Society, 506–507.

Petersen, W. A., and Coauthors, 1999: Mesoscale and radar observations of the fort collins flash flood of 28 july 1997. *Bulletin of the American Meteorological Society*, **80 (2)**, 191–216.

Prat, O. P., and A. P. Barros, 2010: Ground observations to characterize the spatial gradients and vertical structure of orographic precipitation –experiments in the inner region of the great smoky mountains. *Journal of Hydrology*, **391 (1–2)**, 141–156.

Riedmiller, M., and H. Braun, 1993: A direct adaptive method for faster backpropagation learning: the rprop algorithm. *Neural Networks, 1993., IEEE International Conference on*, 586–591 vol.1.

Ryzhkov, A., and D. S. Zrnic, 1995: Precipitation and attenuation measurements at a 10-cm wavelength. *Journal of Applied Meteorology*, **34 (10)**, 2121–2134.

Ryzhkov, A. V., S. E. Giangrande, and T. J. Schuur, 2005: Rainfall estimation with a polarimetric prototype of wsr-88d. *Journal of Applied Meteorology*, **44 (4)**, 502–515.

Saxion, D., and R. Ice, 2012: New science for the wsr-88d: Status of the dual polarization upgrade. *28th Conference on Interactive Information Processing Systems (IIPS)*, New Orleans, LA, American Meteorological Society.

Schaake, J. A., A. Henkel, and S. Cong, 2004: Application of prism climatologies for hydrologic modeling and forecasting in the western u.s. *18th Conference on Hydrology*, Seattle, WA, American Meteorological Society.

Schuur, T., A. Ryzhkov, D. Forsyth, P. Zhang, and H. Reeves, 2014: Precipitation observations with nssl's x-band polarimetric radar during the snow-v10 campaign. *Pure Appl. Geophys.*, **171 (1-2)**, 95–112.

Seliga, T. A., and V. N. Bringi, 1976: Potential use of radar differential reflectivity measurements at orthogonal polarizations for measuring precipitation. *Journal of Applied Meteorology*, **15 (1)**, 69–76.

Seo, D., R. Siddique, and P. Ahnert, 2014: Objective reduction of rain gauge network via geostatistical analysis of uncertainty in radar-gauge precipitation estimation. *Journal of Hydrologic Engineering*, **20 (4)**, 04014 050.

Seo, D. J., J. P. Breidenbach, and E. R. Johnson, 1999: Real-time estimation of mean field bias in radar rainfall data. *Journal of Hydrology*, **223 (3–4)**, 131–147.

Seo, D.-J., A. Seed, and G. Delrieu, 2013: *Radar and Multisensor Rainfall Estimation for Hydrologic Applications*, 79–104. American Geophysical Union, Washington, D. C.

Shapiro, A., P. Robinson, J. Wurman, and J. Gao, 2003: Single-doppler velocity retrieval with rapid-scan radar data. *Journal of Atmospheric and Oceanic Technology*, **20 (12)**, 1758–1775.

Simanton, J. R., and H. B. Osborn, 1980: Reciprocal-distance estimate of point rainfall. *Journal of the Hydraulics Division*, **106 (7)**, 1242–1246.

Steiner, M., and J. A. Smith, 2002: Use of three-dimensional reflectivity structure for automated detection and removal of nonprecipitating echoes in radar data. *Journal of Atmospheric and Oceanic Technology*, **19 (5)**, 673–686.

Vasiloff, S. V., and Coauthors, 2007: Improving qpe and very short term qpf: An initiative for a community-wide integrated approach. *Bulletin of the American Meteorological Society*, **88 (12)**, 1899–1911.

Vignal, B., G. Galli, J. Joss, and U. Germann, 2000: Three methods to determine profiles of reflectivity from volumetric radar data to correct precipitation estimates. *Journal of Applied Meteorology*, **39 (10)**, 1715–1726.

Vignal, B., and W. F. Krajewski, 2001: Large-sample evaluation of two methods to correct range-dependent error for wsr-88d rainfall estimates. *Journal of Hydrometeorology*, **2 (5)**, 490–504.

Wang, Y., and V. Chandrasekar, 2009: Algorithm for estimation of the specific differential phase. *Journal of Atmospheric and Oceanic Technology*, **26 (12)**, 2565–2578.

Wang, Y., and V. Chandrasekar, 2010: Quantitative precipitation estimation in the casa x-band dual-polarization radar network. *Journal of Atmospheric and Oceanic Technology*, **27 (10)**, 1665–1676.

Ware, E. C., 2005: Corrections to radar-estimated precipitation using observed rain gauge data. M.S. thesis, Cornell University, Ithaca, NY.

Weygandt, S. S., A. Shapiro, and K. K. Droegemeier, 2002: Retrieval of model initial fields from single-doppler observations of a supercell thunderstorm. part i: Single-doppler velocity retrieval. *Monthly Weather Review*, **130 (3)**, 433–453.

White, A. B., P. J. Neiman, F. M. Ralph, D. E. Kingsmill, and P. O. G. Persson, 2003: Coastal orographic rainfall processes observed by radar during the california land-falling jets experiment. *Journal of Hydrometeorology*, **4 (2)**, 264–282.

Willie, D., H. Chen, V. Chandrasekar, R. Cifelli, C. Campbell, D. Reynolds, S. Matrosov, and Y. Zhang, 2014: Evaluation of multisensor quantitative precipitation estimation in the russian river basin. *International Weather Radar and Hydrology Symposium*, Reston, VA, American Society of Civil Engineers.

Wilson, A. M., and A. P. Barros, 2014: An investigation of warm rainfall microphysics in the southern appalachians: Orographic enhancement via low-level seeder–feeder interactions. *Journal of the Atmospheric Sciences*, **71**, 1783–1805.

Xu, X., K. Howard, and J. Zhang, 2008: An automated radar technique for the identification of tropical precipitation. *Journal of Hydrometeorology*, **9 (5)**, 885–902.

Zhang, J., K. Howard, and J. J. Gourley, 2005: Constructing three-dimensional multiple-radar reflectivity mosaics: Examples of convective storms and stratiform rain echoes. *Journal of Atmospheric and Oceanic Technology*, **22 (1)**, 30–42.

Zhang, J., C. Langston, and K. Howard, 2008: Brightband identification based on vertical profiles of reflectivity from the wsr-88d. *Journal of Atmospheric and Oceanic Technology*, **25 (10)**, 1859–1872.

Zhang, J., and Y. Qi, 2010: A real-time algorithm for the correction of brightband effects in radar-derived qpe. *Journal of Hydrometeorology*, **11 (5)**, 1157–1171.

Zhang, J., Y. Qi, D. Kingsmill, and K. Howard, 2012: Radar-based quantitative precipitation estimation for the cool season in complex terrain: Case studies from the noaa hydrometeorology testbed. *Journal of Hydrometeorology*, **13 (6)**, 1836–1854.

Zhang, J., and Coauthors, 2011: National mosaic and multi-sensor qpe (nmq) system: Description, results, and future plans. *Bulletin of the American Meteorological Society*, **92 (10)**, 1321–1338.

Zrnić, D. S., A. Ryzhkov, J. Straka, Y. Liu, and J. Vivekanandan, 2001: Testing a procedure for automatic classification of hydrometeor types. *Journal of Atmospheric and Oceanic Technology*, **18 (6)**, 892–913.